Chem Soc Rev

REVIEW ARTICLE

View Article Online
View Journal | View Issue

Cite this: *Chem. Soc. Rev.*, 2023, **52**, 601

Fluorescent probes for the detection of chemical warfare agents

Wen-Qi Meng, †*[a] Adam C. Sedgwick, †[f] Nahyun Kwon, [c] Mingxue Sun, [a] Kai Xiao, *[a] Xiao-Peng He, *[bhi] Eric V. Anslyn, *[g] Tony D. James *[de] and Juyoung Yoon *[c]

Chemical warfare agents (CWAs) are toxic chemicals that have been intentionally developed for targeted and deadly use on humans. Although intended for military targets, the use of CWAs more often than not results in mass civilian casualties. To prevent further atrocities from occurring during conflicts, a global ban was implemented through the chemical weapons convention, with the aim of eliminating the development, stockpiling, and use of CWAs. Unfortunately, because of their relatively low cost, ease of manufacture and effectiveness on mass populations, CWAs still exist in today's world. CWAs have been used in several recent terrorist-related incidents and conflicts (*e.g.*, Syria). Therefore, they continue to remain serious threats to public health and safety and to global peace and stability. Analytical methods that can accurately detect CWAs are essential to global security measures and for forensic analysis. Small molecule fluorescent probes have emerged as attractive chemical tools for CWA detection, due to their simplicity, ease of use, excellent selectivity and high sensitivity, as well as their ability to be translated into handheld devices. This includes the ability to non-invasively image CWA distribution within living systems (*in vitro* and *in vivo*) to permit in-depth evaluation of their biological interactions and allow potential identification of therapeutic countermeasures. In this review, we provide an overview of the various reported fluorescent probes that have been designed for the detection of CWAs. The mechanism for CWA detection, change in optical output and application for each fluorescent probe are described in detail. The limitations and challenges of currently developed fluorescent probes are discussed providing insight into the future development of this research area. We hope the information provided in this review will give readers a clear understanding of how to design a fluorescent probe for the detection of a specific CWA. We anticipate that this will advance our security systems and provide new tools for environmental and toxicology monitoring.

Received 30th July 2022

DOI: 10.1039/d2cs00650b

rsc.li/chem-soc-rev

1. Introduction

The topic of chemical warfare agents (CWAs) continuously re-emerges in various media outlets due to their frequent use in assassinations and during warfare.[1–5] CWAs are toxic chemicals that have been designed to incapacitate and kill an enemy during conflict. Chemical warfare has a long history that can date back to *circa* 600 B.C. with toxic Hellebore roots being used during the siege of Kirrha.[6] Other "primitive" CWAs include the use of arsenic smoke in the Song Dynasty, the use of "Greek fire" in Byzantium, the use of pitch and sulfur by the Spartans, and the use of mandrake roots by the Carthaginians.[6,7] The rise of the chemical industry in the mid-19th century saw the first CWAs being developed, and the use of "modern" CWAs was

[a] *Department of Protective Medicine Against Chemical Agents, Faculty of Naval Medicine, Naval Medical University, 800 Xiangying Rd., Shanghai 200433, China. E-mail: wenqimeng@smmu.edu.cn, kaixiaocn@163.com*
[b] *Key Laboratory for Advanced Materials and Joint International Research Laboratory of Precision Chemistry and Molecular Engineering, Feringa Nobel Prize Scientist Joint Research Center, Frontiers Center for Materiobiology and Dynamic Chemistry, School of Chemistry and Molecular Engineering, East China University of Science and Technology, 130 Meilong Rd., Shanghai 200237, China. E-mail: xphe@ecust.edu.cn*
[c] *Department of Chemistry and Nanoscience, Ewha Womans University, Seoul 120-750, Korea. E-mail: jyoon@ewha.ac.kr*
[d] *Department of Chemistry, University of Bath, Bath, BA2 7AY, UK. E-mail: t.d.james@bath.ac.uk*
[e] *School of Chemistry and Chemical Engineering, Henan Normal University, Xinxiang 453007, China*
[f] *Chemistry Research Laboratory, University of Oxford, Mansfield Road, OX1 3TA, UK*
[g] *Department of Chemistry, The University of Texas at Austin, Austin, Texas 78712-1224, USA. E-mail: anslyn@austin.utexas.edu*
[h] *The International Cooperation Laboratory on Signal Transduction, Eastern Hepatobiliary Surgery Hospital, Shanghai 200438, China*
[i] *National Center for Liver Cancer, Shanghai 200438, China*
† Equal contribution.

seen for the first time during World War I (WWI). Notably, before WWI, the Hague Declaration of 1899 and the Hague Convention of 1907 prohibited the use of poisonous gases. Despite these best efforts, more than 125 000 tons of CWAs, including chlorine, phosgene, diphosgene, cyanide, and sulfur mustard (SM), were produced and used in WWI, which led to

Wen-Qi Meng

Wen-Qi Meng is a lecturer at Naval Medical University. He received his PhD from Nanjing Tech University. His research interest focuses on the development new fluorescent probes for CWAs.

Adam C. Sedgwick

Adam C. Sedgwick received his PhD in 2018 at the University of Bath with Prof. Tony D. James and obtained his postdoctoral research experience with Prof. Jonathan L. Sessler (2018–2021). He is now a Glasstone Research Fellow at the University of Oxford and is a Junior Research Fellow at Jesus College.

Nahyun Kwon

Nahyun Kwon is a postdoctoral researcher in Princess Margaret Cancer Centre, University Health Network in the laboratory of Prof. Gang Zheng. She received her PhD in Chemistry and Nanoscience from Ewha Womans Universiy in 2020 under the guidance of Professor Juyoung Yoon. Her research focuses on the development of nano-system for photo- and radio-dyanmic therapy and imaging-guided drug delivery system. Her long-term research plan is to use multifunctional nanosystems to simultaneously diagnose and treat tumors and develop treatments with fewer side effects.

Mingxue Sun

Ming-Xue Sun is an associate professor at Naval Medical University. She obtained her BSc (2003) and PhD (2000) from The Second Military Medical University. She has been devoted to the research on medical protection of chemical weapons.

Kai Xiao

Kai Xiao is a professor at Naval Medical University. He obtained his BSc (1994) and MASc (1997) from The Second Military Medical University and PhD (2000) from Shanghai Institute of Materia Medica, Chinese Academy of Sciences. He is a nominated Organisation for the Prohibition of Chemical Weapons (OPCW) instructor and qualified expert for the United Nations Secretary-General's Mechanism (UNSGM) for the investigation of alleged use of chemical biological and toxin weapons.

Xiao-Peng He

Xiao-Peng He is professor at the Feringa Nobel Prize Scientists Joint Research Center, School of Chemistry and Molecular Engineering, ECUST, and a Guest Research Fellow at the National Center for Liver Cancer. He was awarded the 2020–2021 Most Cited Chinese Researchers, the Thieme Chemistry Journal Award (2020), the Chinese Chemical Society Prize for Young Scientists (2018) and the Chinese Chemical Society Prize for Young Scientists in Chemical Biology (2018). His research interests include chemical glycobiology, fluorescent probes and supramolecular theranostic materials.

over one million casualties.[5,7] The devastation seen from these CWAs led to the Geneva Protocol being signed in 1925 to prohibit the use of chemical and biological weapons. In WWII, even though CWAs were not used on European battlefields, the Japanese military employed them in Chinese battlefields and the German military used CWAs in their concentration camps. Significant stockpiling of CWAs was also reported by the Axis and Allied powers. After WWII, more potent CWAs were developed, including Novichok, saxitoxin and VX.[1,8] Efforts to improve the storage and ability to transport CWAs resulted in the development of binary chemical weapons, which consist of chemical precursors that are less toxic than a CWA. Upon activation, these precursors are designed to react and form the highly toxic CWA. Such examples include VX and sarin (GB).[6] CWAs have recently been used during the Egyptian intervention in Yemen (1960s), the American intervention in Vietnam (1955–1975) and the Iran-Iraq war (1980–1988). Due to their persistent use and civilian casualties the international community fashioned and signed the arms treaty known as the Chemical Weapons Convention (CWC) in 1993 to prohibit their development, stockpiling and use. These efforts were led by the Organization for the Prohibition of Chemical Warfare (OPCW). In 2013, OPCW was awarded the Nobel Peace Prize for its contribution to the control of chemical weapons. Although 193 states have signed the treaty, the use of CWAs in terrorist attacks and asymmetric conflicts have continued *e.g.*, the conflict in Syria (from 2013 to the present, potentially including SM, sarin, and chlorine)[4] and the assassinations in Malaysia-Kuala Lumpur (2017, VX) and UK-Salisbury (2018, Novichok).[5,9,10] Research on CWAs therefore needs to remain active to allow security and forensics to be vigilant and ready for any potential future attacks.

CWAs can be classified according to their different properties; the organs they target, the severity of damage, and mechanism of toxicity.[11] From a toxicology perspective, CWAs are divided into seven classes: blister agents, nerve agents, blood agents, choking agents, incapacitating agents, riot control agents, and antiplant agents.[12] Large amounts of antiplant agents were used during the Vietnam War (agent orange), which had a considerable impact on the local environment (*i.e.*, deforestation) and its use has now been linked to several serious health problems that still affect the Vietnamese population.[13] Despite these serious health issues, antiplant agents are not currently listed as CWAs due to their low toxicity, and since the Vietnam War, antiplant agents have not been routinely used. In addition, riot control agents, such as *o*-chlorobenzylidene malonitrile (CS) were previously used in chemical warfare; while currently these agents are only used by law enforcement agencies for crowd control purposes.

Due to this continuous threat from CWAs, efforts are being devoted to the development of new analytical methods that can improve our detection capabilities. These methods include ion mobility spectrometry (IMS), infrared/Raman/laser/terahertz spectroscopy, photoionization/flame photometry-gas chromatography, surface acoustic waves (SAWs), and chemical colourimetry.[14–16] (1) At present Ion Mobility Spectrometry (IMS) is predominately used for field detection of CWAs. An IMS detector has low LOD and rapid analytical response. Furthermore, an IMS detector is easy to operate and maintain.[17,18] However, IMS is susceptible to contamination, which requires long clearance

Eric V. Anslyn

Eric V. Anslyn is the Welch Regents Chair of Chemistry at the University of Texas at Austin. His research interests encompass sensor development, functional materials, and mechanistic organic chemistry. He has won several research awards in the areas of supramolecular chemistry and physical organic chemistry, as well as many teaching awards from Univ. Texas at Austin. His H-index is 99 (Google Scholar).

Tony D. James

Tony D. James is Professor at the University of Bath and Fellow of the Royal Society of Chemistry. He was a Royal Society University Research Fellow (1995–2000), Wolfson Research Merit Award holder (2017–2022) and was awarded the Daiwa-Adrian Prize (2013), the CASE Prize (2015), the MSMLG Czarnik Award (2018) and Frontiers in Chemistry Diversity Award. (2020). His research interests include many aspects of Supramolecular chemistry, including probes for redox imbalance and theranostic systems. His h-index is 79 (Google Scholar).

Juyoung Yoon

Juyoung Yoon is a distinguished professor at the Department of Chemistry and Nanoscience, Ewha Womans University. His research interests include investigations of fluorescent chemosensors, activatable photosensitizers theranostics, and organic functional materials. He was listed as a highly cited researcher in chemistry for 2014–2021.

times for cycling the drift tube.[18] Furthermore, IMS also shows poor selectivity and is prone to false alarms.[19] Currently, numerous portable field detectors based on IMS have been developed. Most of them exhibited similar capabilities for CWAs detection, including Chemical Warfare Agent Monitor (CAM-2), Advanced Portable Chemical Agent Detector (APD 2000), ICAM, GID-3 (also known as ACADA), SABRE 4000, Lightweight Chemical detector (LCD 3.3), Rapid Alarm and Identification Device-Monitor (RAID-M100Plus), IMS-2000, and Chempro 100. (2) Flame Photometry Detectors (FPDs), equipped with a specific optical filter for sulfur and phosphorus, are highly sensitive (ppb to ppm) for sulfur and phosphorus compounds with low LODs. A major limitation associated with FPDs is that the detection scope is limited to sulfur and phosphorus. FPD is also prone to false positive results with samples containing sulfur and phosphorus.[19] AP2C is the first generation of FPD, with AP4C being the second generation. In addition, MiniCAMS, which is also based on flame photometry, is not hand-portable. (3) Theoretically, Infra-Red (IR) detectors can selectively detect all kinds of CWAs by careful selection of a wavelength for each CWA.[17,20] Currently, there are several different techniques that employ IR spectroscopy, including filter-based IR spectroscopy, photoacoustic IR spectroscopy and Fourier Transform IR spectroscopy. The major disadvantages of IR-based detectors are their high cost, complexity and bulkiness. Furthermore, IR-based detectors are not sensitive enough for CWAs at the acute exposure guideline level-1 (AEGL-1)/immediate danger to life and health (IDLH) levels. IR-Based detectors are generally employed in field applications that include remote and point sample detection.[17] Remote detectors, based on IR radiation changes in the background, include the M21 detector and the Joint Service Lightweight Standoff Chemical Agent Detector (JSLSCAD). MIRAN SapphIRe, TravelIR HCI, and HazMat ID are man-portable detectors. (4) Raman spectroscopy is a relatively new technique for CWAs detection, which is based on light scattering.[19] Raman spectroscopy is able to non-destructively detect CWAs in a glass container. However, it cannot be used for sensing CWAs in munitions since the technique requires a window to let light through. Furthermore, Raman spectroscopy is not capable of detecting CWAs if a mixture contains only 10% of CWAs and 90% of other materials.[19] Only two handheld Raman-based detectors are available for CWAs, which are FirstDefender Detector and Joint Contaminated Surface Detector (JCSD). (5) Flame Ionization Detectors (FIDs) and Photoionization Ionization Detectors (PIDs) are commonly used for GC systems in laboratory environments. ppbRAE, MiniRAE Classic, MiniRAE 3000 are handheld portable detectors based on this technique, which employ 10.6 eV UV light as ionization source. TVA 1000B employs both FID and PID to further improve the detection performance. Detectors employing FID/PID are expensive and complicated, and the CWA selectivity is limited.[20] (6) Surface Acoustic Wave (SAW) detectors can be manufactured at low cost with good sensitivity.[19] The major limitation of SAW detectors is their susceptibility to damage from highly reactive vapors, and the performance of SAW detectors is also impacted by humidity and temperature variations.[20] There are some SAW-based detectors currently available for field detection, including the SAW MiniCAD mk II, HAZMATCAD, the Joint Chemical Agent Detector, and CW sentry Plus. (7) Colorimetric detectors are easy-to-use and cheap.[17] However, referring to a color change for the detection of CWAs might generate problems because the naked-eye perception to colors may vary between observers. A variety of colorimetric detectors have been developed, *e.g.* M8/M9 detection paper, Three-Way CWA Liquid Detection Paper, M256A1/M18A3/M272 Chemical Agent Detection Kit and Colorimetric Detection Tubes. However, the intrinsic color of a real-world sample could cause false reporting. This approach results in a substantial delay in obtaining meaningful data, which makes it unsuitable for fast response times and security setups (Table 1).

Over the years, small molecule fluorescent probes have been demonstrated as indispensable chemical tools for the detection of analytes.[21–23] The design of fluorescent probes for the detection of CWAs is particularly attractive due to their ease of synthesis, high sensitivity, excellent selectivity, low cost and proven translation into handheld devices.[15,24] The biocompatibility and noninvasiveness of fluorescent probes allows the real-time detection of CWAs *in vitro* and *in vivo* for medical diagnostic and toxicology studies.[24] These advantages, have led to several research groups including those of Anslyn, Churchill, Dasgupta, Banks, and Yoon pursuing fluorescent probes for CWA detection.[25–34] This review serves to highlight the design of fluorescent probes for the detection of each type of CWA. This was achieved by breaking this review into five sections based on the CWA classification: (1) fluorescent probes for the

Table 1 Detection performance of available CWAs detectors

	Detected agents	LOD	Response time	Portability & weight	Operational life
IMS based detectors (PAD 2000/Chempro 100)	All kinds of CWAs	ppb	Immediate	Hand-held, weight <3 kg	9–14 h
FPD based detectors (AP2C)	Sulfur mustard and nerve agents	10–400 μg m^{-3}	Less than 2 s	Hand-held, weight <2.5 kg	12 h
IR based detectors (MIRAN SapphIRe/TravelIR HCI)	Blister agents and nerve agents	1–5 mg m^{-3}	Less than 20 s	Man-portable, weight <12 kg	NR
Raman based detectors (FirstDefender)	All kinds of CWAs	NR	analysis time <15 s	Hand-held, weight <1.5 kg	5 h
SAW based detectors (SAW MiniCAD mk II/HAZMATCAD/JCAD)	All kinds of CWAs	ppm	Response time from 20 to 120 s	Hand-held	5–12 h
Colorimetric based detectors (M8/9 paper)	Nerve agents and blister agents	100 μ drops	Response time <30 s	Hand-held	3 years shelf life

detection of vesicants; (2) fluorescent probes for the detection of nerve agents; (3) fluorescent probes for the detection of blood agents; (4) fluorescent probes for the detection of choking agents; and (5) fluorescent probes for the enzymes and metabolite targets of CWAs. The ordering of CWAs in this manuscript is based on the military significance and characteristics of CWAs. In each section, before we discuss each reported fluorescent probe, we include background information on the target CWA, including the mode of action, example CW agent, history, and recent use. Then, we outline the design strategies for each fluorescent probe. This outline is designed to help readers at all career stages gain a full understanding of the significance of CWA detection, the various design strategies for fluorescent probes, and their applications in the fields of chemical biology, environmental science, and medicine.

2. Design strategies involving fluorescent probes for the detection of CWAs

For a general overview on the types of fluorophores and the fluorescent mechanisms used for the design of a fluorescent probe, the reader can be directed to some excellent reviews.[23] An alternative approach is to exploit the fluorescent properties of the resulting product from a nonfluorescent compound reacting with a CWA. Since each type of CWA displays different types of reactivities, the design of a fluorescent probe for each type of CWA often varies to a considerable extent. Researchers therefore need to have a broad understanding of fluorescent probe design and the different types of CWA reactivity. The reader will see throughout the review that common synthetic transformations have been used as strategies for the detection of CWAs (*i.e.*, Michael addition). For example, SM, which is an example of a vesicant agent, mainly reacts with biological nucleophiles *via* S_N2 alkylation *e.g.*, amino and sulfhydryl functional groups found on proteins and amino acids.[35–37] As a result, thioketones and thioamides have been exploited as recognition units for SM detection due to their high reactivity and good selectivity. Nerve agents are strong electrophiles, which means fluorescent probes designed for their detection consist of nucleophiles such as hydroxyl or amino functional groups. These functionalities are designed to react with the electrophilic phosphorus unit and provide a concomitant change in fluorescence emission. Since nerve agents such as sarin, soman, and tabun usually contain the leaving groups, fluoride ion, cyanide ion or a thiol moiety, another design strategy is to indirectly detect CWA *via* monitoring the release of fluoride, cyanides, or thiols. Phosgene, a representative choking agent, consists of a carbonyl group and two chlorine atoms. This unique structure leads to the selective carbonylation of amino or hydroxyl units found on proteins and potential protein cross-linking reactions. Therefore, fluorescent probes designed for the detection of phosgene consist of single amino groups or contain more than one nucleophilic unit, which leads to subsequent ring formation. Blood agents are usually fast-acting cyanide-based or arsenic-based CWAs, an example includes hydrogen cyanide (HCN). Numerous fluorescent probe strategies have been reported for the detection of cyanide, which incorporate indolium/pyridinium, dicyanovinyls, carbanyls, and salicylaldehyde groups. Cyanide-responsive fluorescent probes that exploit the known interactions between cyanides and metal complexes and boronic acid derivatives have also been reported.

Importantly, CWA-responsive fluorescent probes need to meet several specific requirements before they are deemed suitable for real-life situations. Rapid response times are a prerequisite, especially for the detection of nerve agents and blood agents since some CWAs can cause death in a short period (a few minutes). Substantial changes in fluorescence emission intensity should also be observed upon CWA recognition. This behaviour aids in on-the-spot rapid detection tests with the use of a handheld fluorescence detector or handheld ultraviolet (UV) lamp. Although fluorescence-based analysis offers greater sensitivity, a simultaneous change in colour would further aid the rapid naked-eye detection of a CWA. Throughout this review, we will summarize the design principals, syntheses of probes, and sensing performances including detection speed, mode of fluorescence change and limit of detection of fluorescent probes for a variety of different CWAs.

3. Fluorescent probes for vesicants

Vesicants, also called blister agents, are a type of CWA that can cause local inflammation and necrosis of the skin and mucous membranes. Systemic poisoning can also occur through their absorption through the skin, eyes, and respiratory tract.[38] Blister agents include SM, Lewisite, phosgene oxime, and nitrogen mustard (HN1, HN2 and HN3) (Fig. 1).[38] SM was used during several conflicts, including WWI, the Italian invasion of Abyssinia, the Japanese invasion of China, the Iran-Iraq war, and the civil war in Syria.[6] Lewisite was first synthesized in 1918 by US Army Captain W. L. Lewis.[39] There is no reliable report of its use on the battlefield. However, Lewisite was also manufactured and abandoned by Japan and Germany at various sites in China and around Europe, respectively. One of the most important applications of Lewisite is its ability to decrease the freezing point of SM (14 °C) in order to render them more suitable for use in low temperature zones.[40] Nitrogen mustard is a general name of three alkylating agents: HN1, HN2, and HN3. Nitrogen mustard was first synthesized after WWI, and was stockpiled during WWII. Whether nitrogen mustard had been used in wars remains debatable.[41,42] Notably, nitrogen mustard (HN2) was the first chemotherapeutic drug to be used in the clinic for the treatment of lymphoma.[43] Blister agents are primarily intended to injury rather than kill people, but exposure can also be fatal.[38] The AEGLs of vesicants were listed in Table 2. The IDLHs of sulfur mustard and Lewisite are 0.0004 and 0.0003 ppm, respectively. To date, the available fluorescent probes for the detection of blister agents are rather limited: 9 references for SM and 1 for Lewisite.[44–55] No report exists on a fluorescent probe that can detect either phosgene oxime or nitrogen mustard. Since blister agents are toxic and are

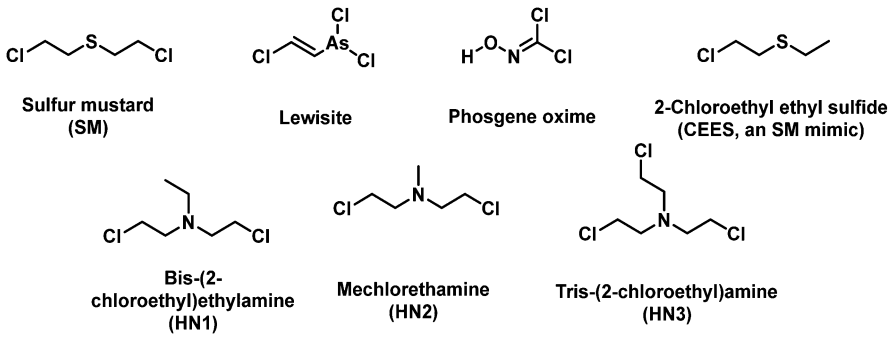

Fig. 1 Chemical structures of blister agents and their mimics.

Table 2 Acute exposure guideline levels of blister agents

		10 min	30 min	60 min	4 h	8 h
ppm (mg m^{-3})						
Sulfur mustard	AEGL 1	0.060 (0.40)	0.020 (0.13)	0.010 (0.067)	0.0030 (0.017)	0.0010 (0.0083)
	AEGL 2	0.090 (0.60)	0.030 (0.20)	0.020 (0.10)	0.0040 (0.025)	0.0020 (0.013)
	AEGL 3	0.59 (3.9)	0.41 (2.7)	0.32 (2.1)	0.080 (0.53)	0.040 (0.27)
mg m^{-3}						
Lewisite	AEGL 1	NR	NR	NR	NR	NR
	AEGL 2	1.3	0.47	0.25	0.070	0.037
	AEGL 3	3.9	1.4	0.74	0.21	0.11

NR = not recommended due to insufficient data.

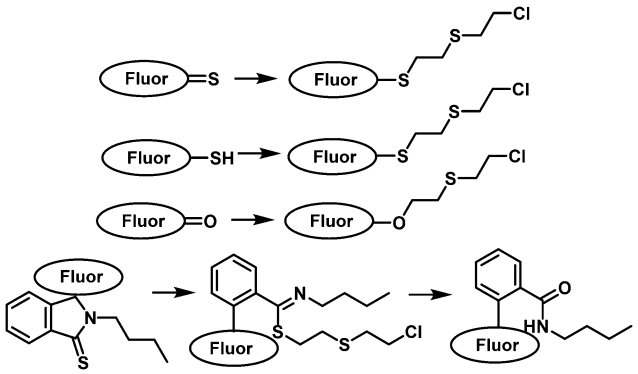

Fig. 2 Diagrammatic representation of the common strategies used to generate fluorescent probes for the detection of vesicants.

controlled substances, researchers use less-toxic blister agent mimics such as 2-chloroethyl ethyl sulfide (CEES) to evaluate the fluorescent probe. The most common design strategies for the detection of vesicants are given in Fig. 2. Due to the weak electrophilicity and absence of hydrogen-bond donor or acceptor groups, it is challenging to design a suitable receptor unit for vesicants. Most fluorescent probes for blister agents are based on thioamide, thione, and thiol. Probes suitable for the detection of blister agents are probes **1–21** (Fig. 3–5).

In 2013, Anslyn and Kumar developed the first fluorescent system (**1** and **1-a**) for the detection of SM,[44] which used a metal–ion indicator displacement assay (IDA) approach.[56] In this strategy, CEES reacted with a dithiol-species to form a podand-based product. The resultant podand product displayed a strong affinity for cadmium ions (Cd^{2+}) that were bound to a 4-methylesculetin fluorophore. The displacement of the Cd^{2+} ion in aqueous solution at pH 9 resulted in a clear increase in fluorescence emission intensity at 460 nm. The fluorescent system exhibited an excellent selectivity when evaluated against potential interferents including 2-chloroethyl ethyl ether, acetyl chloride and diethyl chlorophosphate (DEP). A fast response time (1 min) was observed with moderate sensitivity – LOD of 0.2 mM. Within this study, **1** was shown capable of detecting CEES on surfaces and in soil samples. Probes **2** and **3** were subsequently synthesized to improve the sensitivity of SM detection.[45,46] It is well known that the alkyl halide units on mustard gas are reactive to nucleophiles *e.g.*, thiols. Unfortunately, numerous fluorophores are unstable to these thiol containing species. For example, squaraines, such as SQ and SQ-OH, can also react with thiols. In the absence of SM, thiol **1** reacted with SQ/SQ-OH resulting in the bleaching of the dyes. However, in the presence of SM, the thiol reacts with SM resulting in the retention of the spectrographic properties of SQ/SQ-OH. In 2014, Goud *et al.* synthesized probe **4** for the detection of SM.[47] The fluorophore rhodamine 6G was masked with a thioamide functionality to quench the fluorescence emission and enable the selective detection of SM. The unmasking reaction involves *S*-alkylation and subsequent desulfurization of the thioamide unit. The high sensitivity of **4** enabled the naked-eye detection of 6.25 ppm of SM in the gas phase. In 2018, Kumar and co-workers reported 3,6-bis(dimethylamino)-9(10*H*)-acridine thione (**5**), a chromogenic and fluorogenic probe for the selective detection of SM.[48] Compound **5** displayed excellent sensitivity when viewed by the naked eye (0.04 mg mL^{-1}), UV spectroscopy (0.02 mg mL^{-1}), and fluorescence spectroscopy (0.005 mg mL^{-1}) in CH_2Cl_2. One particular limitation of **5** was

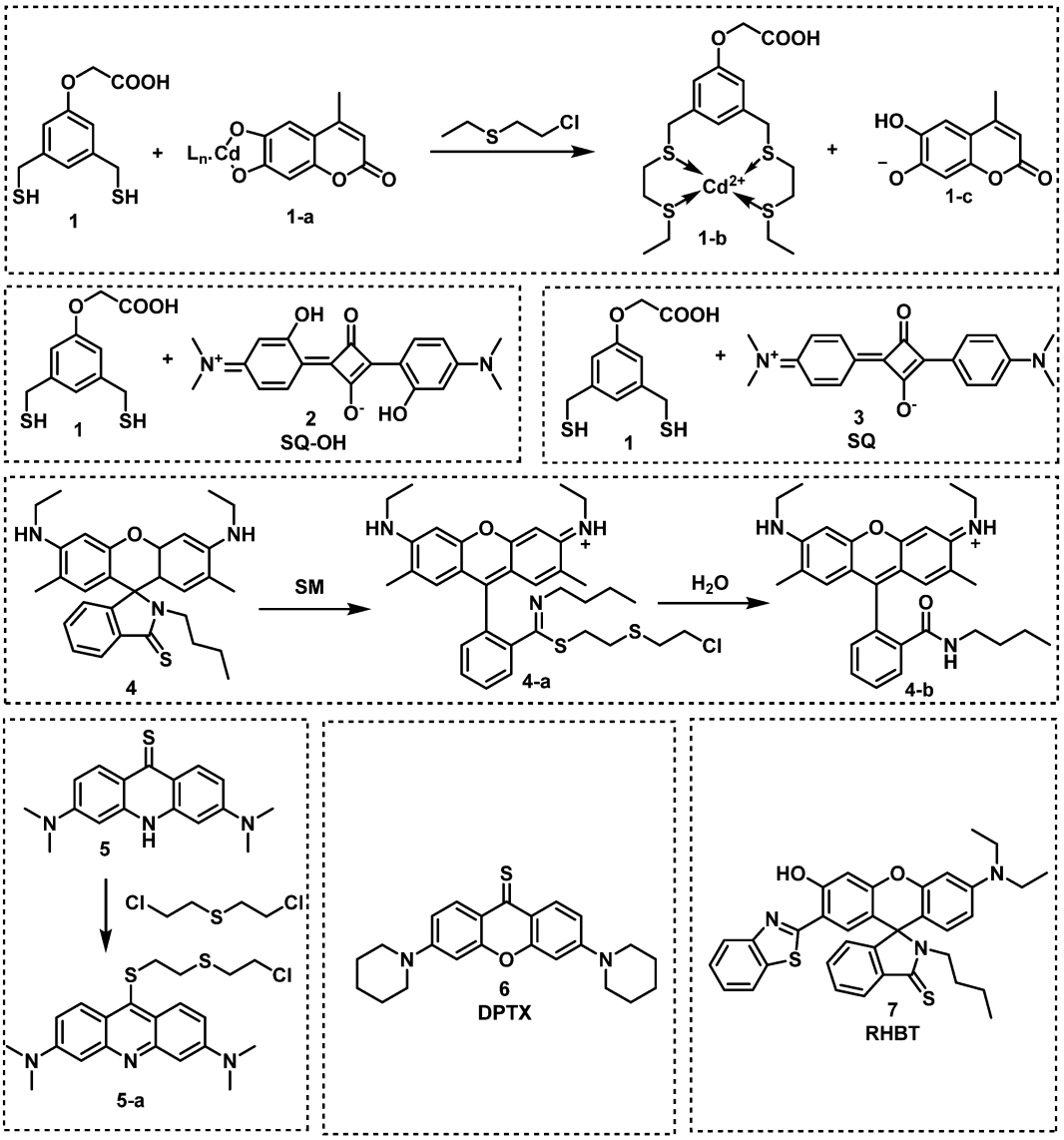

Fig. 3 Chemical structures of fluorescent probes **1–7** designed for the selective detection of sulfur mustard (SM).

the fact that it required a strong base as a catalyst. Based on a similar strategy, Zhang and co-workers reported the fluorescent probe, **DPTX** (**6**), which was capable of detecting SM at a concentration of 1.2 mM in solution and 0.5 ppm in the gas phase. A marked red-shift in the absorbance from 445 nm to 567 nm and an 850-fold increase in fluorescence intensity at 593 nm were observed without catalyst. These authors demonstrated the superior performances of **DPTX** to other previously reported probes. In 2018, Wang and co-workers reported the fluorescent probe **RHBT** (**7**) for SM/CEES detection.[49] **RHBT** consisted of a rhodol chromophore functionalized with a benzothiazole group, and the fluorescent framework was masked with the SM-reactive thioamide functional group. In the presence of SM, **7** exhibited a 10-fold enhancement in fluorescence intensity at 517 nm with an LOD of 3.19 mM in THF. Although these probes exhibited low LODs, the reaction conditions include the use of strong bases (KOH, pyridine) and organic solvents (THF, CH_2Cl_2, DMF) which limits their real-world application.

In 2019, Meng and co-workers reported the fluorescent probe **SM-Flu** (**8**), for the selective and sensitive detection of SM in living cells and jellyfish polyps.[50] The fluorescent probe **8** was also used for the evaluation of the concentration *versus* time profiles of SM in mouse brains after exposure to SM. Mice were exposed to SM (30 mg kg^{-1}) and the concentration of SM in brain tissue was found to increase over 6 h; subsequently, the concentration of SM decreased gradually over 48 h. Unfortunately, the response rate of **8** was slow ($\sim$30 min), so the authors synthesized a series of similar probes (**9–12**) to improve the ability to detect SM.[51] Amongst those probes, **SiNIR-SM** (**12**) exhibited a large ON–OFF change in emission intensity (90-fold), excellent sensitivity (0.8 μM), and a greater response time (10 min). The near-infrared (NIR) emission features of **12** permitted its use in live cell and *in vivo* imaging. Using **12**, SM was found to accumulate in the mitochondria of live HaCaT cells. **SiNIR-SM** was also applied for early diagnostic imaging of SM poisoning in

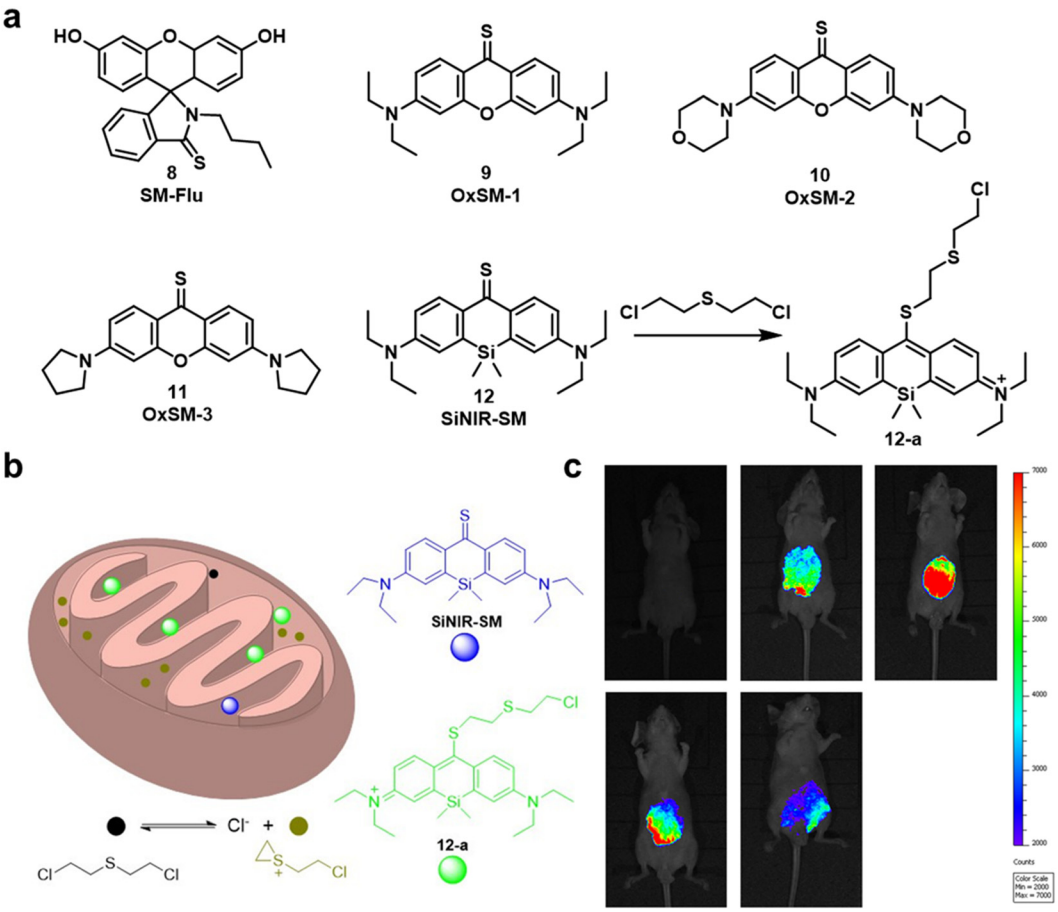

Fig. 4 (a) Chemical structures of fluorescent probes **8–12** that enabled the detection of SM. (b) Basic schematic of the potential sensing mechanism of SN in mitochondria. (c) Fluorescent images of living SKH-1 mice for visualizing sulfur mustard levels using **SiNIR-SM**. Reproduced with permission from ref. 51. Copyright (2019) American Chemical Society.

SKH-1 mice. It is important to note that the alkyl halide on SM is also reactive towards GSH, DNA and other biomolecules, therefore false positive signals may arise when using this strategy in biological samples. In 2021, Singh, Kumar and co-workers demonstrated that the combination of luminol and an ionic liquid (IL) (1-ethyl-3-methylimidazolium dicyanamide, [emim][DCA]) facilitated the rapid fluorescence-based detection of SM in aqueous media. Excellent sensitivity (LOD: 6 ppm) and selectivity (over nerve agents and alkylating agents) and a very fast response time (<1 min) were observed. Li and co-workers explored a similar strategy using fluorescent probe **SRB-NB** (**14**), and an IL (1-butyl-3-methylimidazolium dicyandiamide).[52] In the presence of SM, the **SRB-NB**/IL system exhibited a significant fluorescence increase at 583 nm, and an LOD of 3 μM was determined. The Song group designed and synthesized a series of probes (**15–20**) for the selective detection of SM.[53,57] The team were the first to employ quinoline-2-thiones as fluorescent probes **15–18** for the detection of SM.[53] In the presence of KOH, these probes were found to readily react with SM to form highly fluorescent quinoline-2-thioethers. In subsequent studies, the Song group developed two 4-mercaptocoumarin-based fluorescent probes, **Et-Cou-SE** (**19**) and **Pr-Cou-SE** (**20**), for the detection of SM and SM-based derivatives in ethanol.[57] **Et-Cou-SE** and **Pr-Cou-SE** reacted with SM *via* nucleophilic substitution reactions to generate fluorescent thioethers, which is likely ascribed to a strong ICT effect. **Pr-Cou-SE** displayed LODs of 16 nM for SM, 6.6 nM for CEES and 3.6 nM for NH1. Lee and co-workers developed the first fluorescent probe (**21**) for the detection of a Lewisite mimic ($AsCl_3$).[55] This probe exhibited a high selectivity for $AsCl_3$ compared with other metal ions. Upon contact with $AsCl_3$, the fluorescence emission intensity at 445 nm decreased considerably, with an LOD of 61.2 μmol kg^{-1}. The dithiol group on **21** captures thiophilic $AsCl_3$, resulting in fluorescence quenching owing to the heavy atom effect by As^{3+}.

Although these reported probes (probe **1–12**, **14–21**) employ thioamide, thione, and thiol units to facilitate the selective and sensitive detection of blister agents, they are prone to oxidation. Detection systems that are easy to store for longer periods of time are needed. As seen for non-thiol containing probes **13** and **14**, ionic liquids enhanced the nucleophilicity of these probes thus promoting the reactivity towards SM. Unfortunately, this strategy can be only applied to environmental situations. Considering that most recognition units for SM are unstable for long storage periods, the combination of probe **13** and an ionic liquid ([emim][DCA]) seems to be the optimal solution for SM

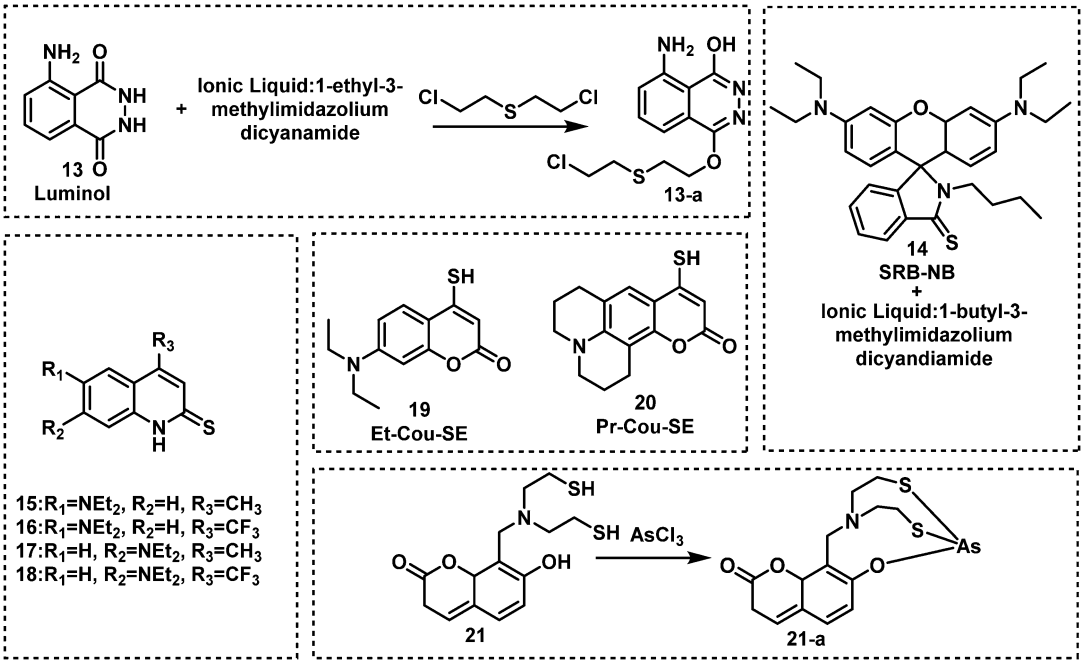

Fig. 5 Chemical structures of fluorescent probes for the detection of sulfur mustard and Lewisite simulants **13–21**.

detection in environmental samples. Probe **13** is stable in air, and the presence of ionic liquid further lowers its LOD and enhances reactivity. To the best of our knowledge, **SiNIR-SM** (**12**) appears to be one of the only reported systems that permits the detection of SM in biological samples and *in vivo* (Fig. 6).

4. Fluorescent probes for nerve agents

Nerve agents are highly toxic organophosphate-based compounds.[11,58] Nerve agent poisoning is characterized by the inhibition of acetylcholinesterase (AChE). A covalent reaction between a nerve agent and the serine residue of the active site of AChE[59] results in the accumulation of acetylcholine in the synaptic cleft and subsequent overstimulation of the cholinergic receptor resulting in respiratory depression, circulatory collapse, and death.[60,61] Similar reactions occur with butyrylcholinesterase (BuChE) and serum albumin present in blood.[59] As such, the measurement based on mass spectrometric analysis of HuBuChE's serine-198 residue being modified by nerve agents is a well-accepted means to characterize nerve agent exposure.[62] Nerve agents are generally divided into three classes, G-, V-, and A-type, which are based on their structural characteristics. Tabun (GA), the first nerve agent, was developed by Schrader in the 1930s for use as an insecticide. With the support of the German army, Schrader further developed GB, soman (GD) and cyclosarin (GF). V-Type nerve agents were first synthesized by the British scientist Ranajit Ghosh in the 1950s.[63] These types of nerve agents include VE, VG, VM, and VX. The dermal toxicity of VX was found to be one hundred-fold greater than that of GB.[64] From the 1970s to the 1990s, the former Soviet Union developed A-type nerve agents, of which little information has been published. In 2018, the former double-agent Sergei Skripal and his daughter Yulia Skripal were subjected to an assassination attempt with Novichok, an A-type nerve agent.[9] In 2019, A-type nerve agents were listed in the CWC. The AEGLs of nerve agents were listed in Table 3. The IDLHs of GA, GB, GD, GF and VX are 0.03, 0.03, 0.008, 0.03, and 0.002 ppm, respectively. There are a range of design strategies for fluorescent probes that detect nerve agents, those include *N*-activation, hydroxyl-activation, and metal ion chelation (Fig. 7).

A common strategy for nerve agent-based fluorescent probes exploits their ability to phosphorylate hydroxyl groups. An additional strategy aimed at improving the selectivity of a nerve agent selective fluorescent probe is to generate a cyclization reaction upon phosphorylation. Houten and co-workers reported the first fluorescent probe (**22**) for the detection of nerve agents in CH_2Cl_2.[65] This probe contained a heterocyclic-substituted platinum 1,2-enedithiolate with an appended alcohol arm. The ethyl-hydroxy group is highly nucleophilic toward phosphate esters because of its proximity to the intramolecular pyridine ring. Following phosphorylation, the activated phosphate ester acts as a leaving group for dihydropyrolidinium ring closure as shown in Fig. 8. In 2019, the same authors developed fluorescent probe **23** for the detection of nerve agents.[66] Compound **23** was designed to react with nerve agent simulants (DECP and DFP) that underwent subsequent cyclization to form a dihydroquinolizinium ring. This reaction was accompanied was a significant increase in fluorescence emission intensity at 515 nm. The probe has been functionalized with monomeric substituents to produce polymer film-coated filter paper test strips. Moreover, the inclusion of silicon dioxide into the polymer led to further improvements in selectivity by eliminating the influence of mineral acids on probe **23**. Utilizing the same

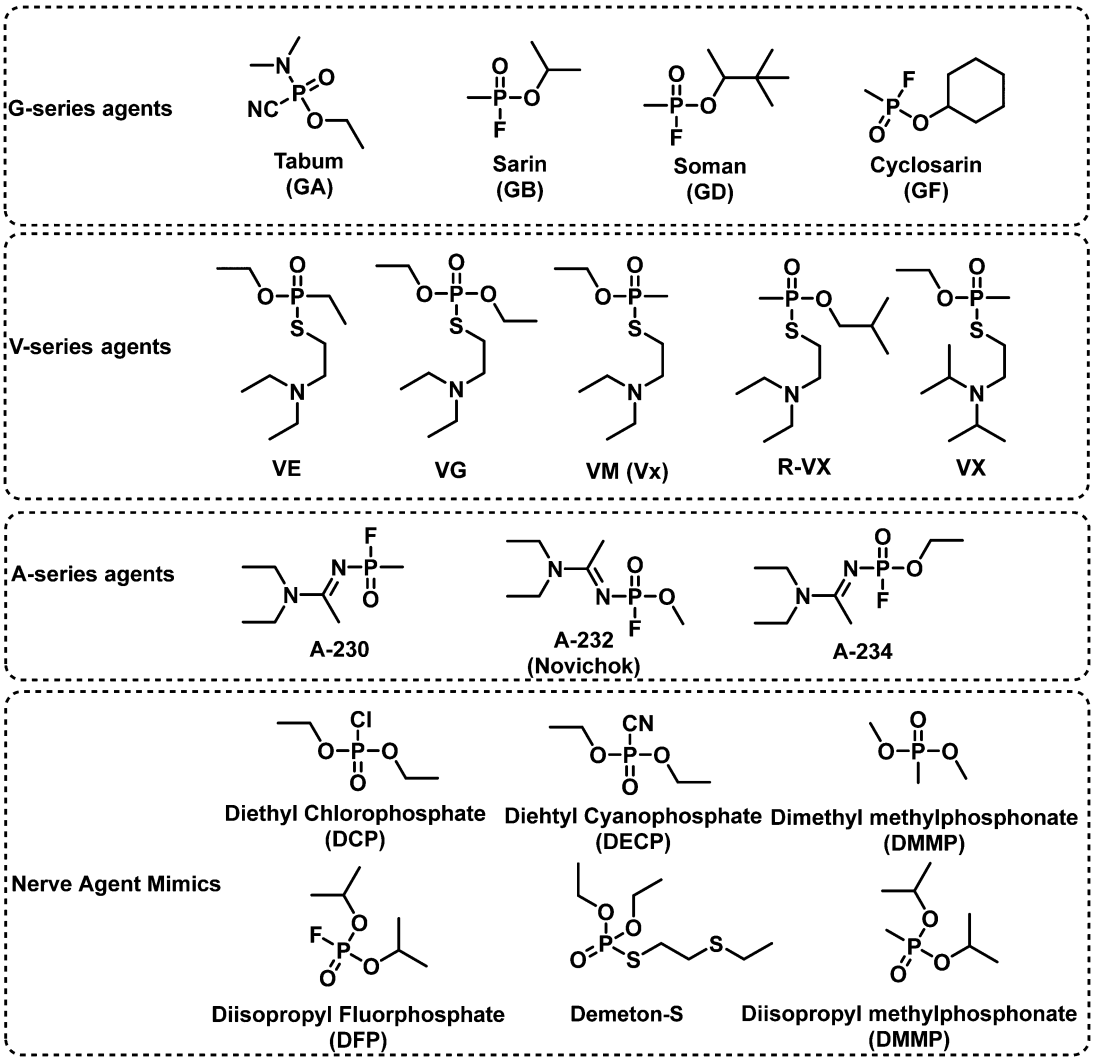

Fig. 6 Chemical structures of G-, V-, and A-type nerve agents and their mimics for research use.

Table 3 Acute exposure guideline levels of nerve agents

		10 min	30 min	60 min	4 h	8 h
ppm (mg m^{-3})						
Sarin	AEGL 1	0.0012 (0.0069)	0.00068 (0.0040)	0.00048 (0.0028)	0.00024 (0.0014)	0.00017 (0.0010)
	AEGL 2	0.015 (0.087)	0.0085 (0.050)	0.0060 (0.035)	0.0029 (0.017)	0.0022 (0.013)
	AEGL 3	0.064 (0.38)	0.032 (0.19)	0.022 (0.13)	0.012 (0.070)	0.0087 (0.051)
ppm (mg m^{-3})						
Tabun	AEGL 1	0.0010 (0.0069)	0.00060 (0.0040)	0.00042 (0.0028)	0.00021 (0.0014)	0.00015 (0.0010)
	AEGL 2	0.013 (0.087)	0.0075 (0.050)	0.0053 (0.035)	0.0026 (0.017)	0.0020 (0.013)
	AEGL 3	0.11 (0.76)	0.057 (0.38)	0.039 (0.26)	0.021 (0.14)	0.015 (0.10)
ppm (mg m^{-3})						
Soman	AEGL 1	0.0012 (0.0069)	0.00068 (0.0040)	0.00048 (0.0028)	0.00024 (0.0014)	0.00017 (0.0010)
	AEGL 2	0.015 (0.087)	0.0085 (0.050)	0.0060 (0.035)	0.0029 (0.017)	0.0022 (0.013)
	AEGL 3	0.064 (0.38)	0.032 (0.19)	0.022 (0.13)	0.012 (0.070)	0.0087 (0.051)

approach, Swager developed a series of fluorescent probes (**24–26**) for nerve agent detection.[67] Probe **26** was found to have the fastest response rate, and the lowest LOD. Rebek and co-workers developed a series of fluorescent probes **27–30** that used a similar strategy and incorporated pyrene into the framework (Fig. 8).[68] Because of photoinduced electron transfer (PeT), initially these probes exhibited weak fluorescence emission intensity at 378 nm. The reaction of **27** with DCP led to the sequential phosphorylation–cyclization reaction, which provided a concomitant 22-fold increase in fluorescence emission intensity and a fast response time (5 s). A similar strategy was used for BODIPY-based fluorescent probes **31–36**.[69–71] Reaction of these

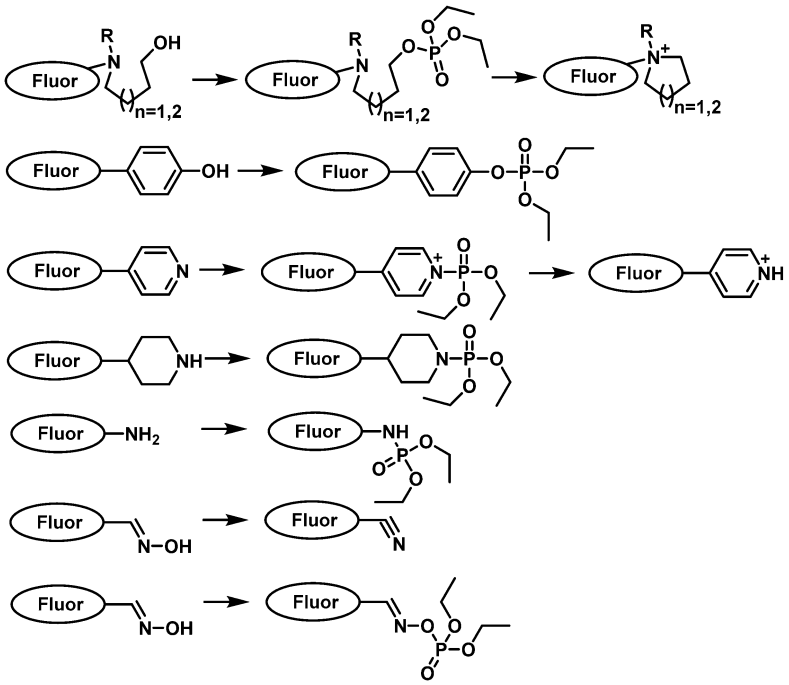

Fig. 7 Schematic representation of the common strategies used to generate fluorescent probes for the detection of nerve agents.

probes with a nerve agent simulant (DFP or DECP) resulted in the phosphorylation of the hydroxy unit and subsequent intramolecular *N*-alkylation to form the corresponding morpholino cations **32** and **33** or five-membered-ring quaternary ammonium salts. All these probes exhibited a fast response and excellent sensitivity for the nerve agent mimics evaluated.

The Han research group reported three rhodamine B-based fluorescent probes, **37**, **38** and **39** for the detection of nerve agents from 2010 to 2012.[72–74] Compound **37** utilized the Lossen rearrangement of rhodamine-hydroxamate for the detection of DCP, undergoing phosphorylation with DCP, followed by ring opening of the spirolactam *via* Lossen rearrangement to form **37-a**. In the presence of water, **37-a** is hydrolyzed to afford **37-b**, which is further decomposed to release **37-c**. While **38** and **39** could detect nerve agent mimics *via* phosphorylation-intramolecular cyclization in DMF. In 2019, a similar strategy was used by the Son group for the development of the rhodamine 6G-based fluorescent probe, **RDS** (**40**).[75] Sarkar and co-workers developed the rhodamine based fluorescent probe, **ARC** (**41**), for the detection of the nerve agent mimic DCP in catfish brains.[76] In the presence of DCP (1.1 μM), **ARC** gave a 100-fold increase in the fluorescence signal at 585 nm, a fast response time (a few seconds) and a low LOD (5.6 nM). In 2019, Li and co-workers reported **RB-CT** (**42**), a thiourea-functionalized rhodamine fluorescent probe, for the detection of nerve agents.[77] **RB-CT** readily reacted with DCP to induce the ring opening of the spirolactam of rhodamine and form a seven-membered heterocycle adduct. This reaction affords a substantial change in colour (colourless to pink) and a fluorescence increase at 583 nm. The response time was less than 5 min, and the LOD was found to be 2 mM. **RB-CT** was used for the detection of the nerve agent GD in both the liquid and gas phases (Fig. 9–11).

Jang *et al.* developed a coumarin-4-dimethyaminoaryl based fluorescent probe, **CoumNMe$_2$** (**43**), for the detection of the nerve agent simulant, DCP, in $CHCl_3$.[78] Compound **43** was shown to selectively detect DCP when evaluated against other relevant analytes, such as DECP and DEMP. DCP was shown to react with the benzyl alcohol motif on **43** to form a phosphoester, which then underwent intramolecular cyclization. This phosphorylation–cyclization induced a 10-fold increase in fluorescence emission intensity at 460 nm. This fluorescence increase was ascribed to the inhibition of PeT. Hu and co-workers designed and synthesized the near-infrared probe **44** for the sensitive detection of nerve agent simulants, DCP and DECP, in CH_3CN.[79] Compound **44** takes advantage of the activation of carboxylic acids by phosphorous-based reagents for amide coupling (in this case intramolecular amidation). This intramolecular amidation resulted in a redshift in absorption and a substantial increase in fluorescence emission at 807 nm. Low LODs were calculated for DECP (2.23 nM) and DCP (0.661 nM). Lei and Yang reported a ''covalent-assembly''-based fluorescent probe (**NA570**, **45**), for the detection of DCP in nonprotic solvents (dichloro-methane, dichloroethane, and nitrobenzene). Using the ''covalent-assembly'' approach the push–pull conjugative backbone of a fluorophore is split into two fragments (**NA570**). These two fragments of **NA570** are then covalently assembled to restore the dye, this in turn leads to significant fluorescence increase in emission at 573 nm with zero background.[80] **NA570** was shown to be able to detect GB mimics *via* an analogous Vilsmeier–Haack reaction. Mahapatra *et al.* reported the ratiometric fluorescent probe, **NTBT** (**46**), for DCP detection, which is based on a napthothiazolium–benzothiazole conjugate.[81] Compound **46** exhibited excellent

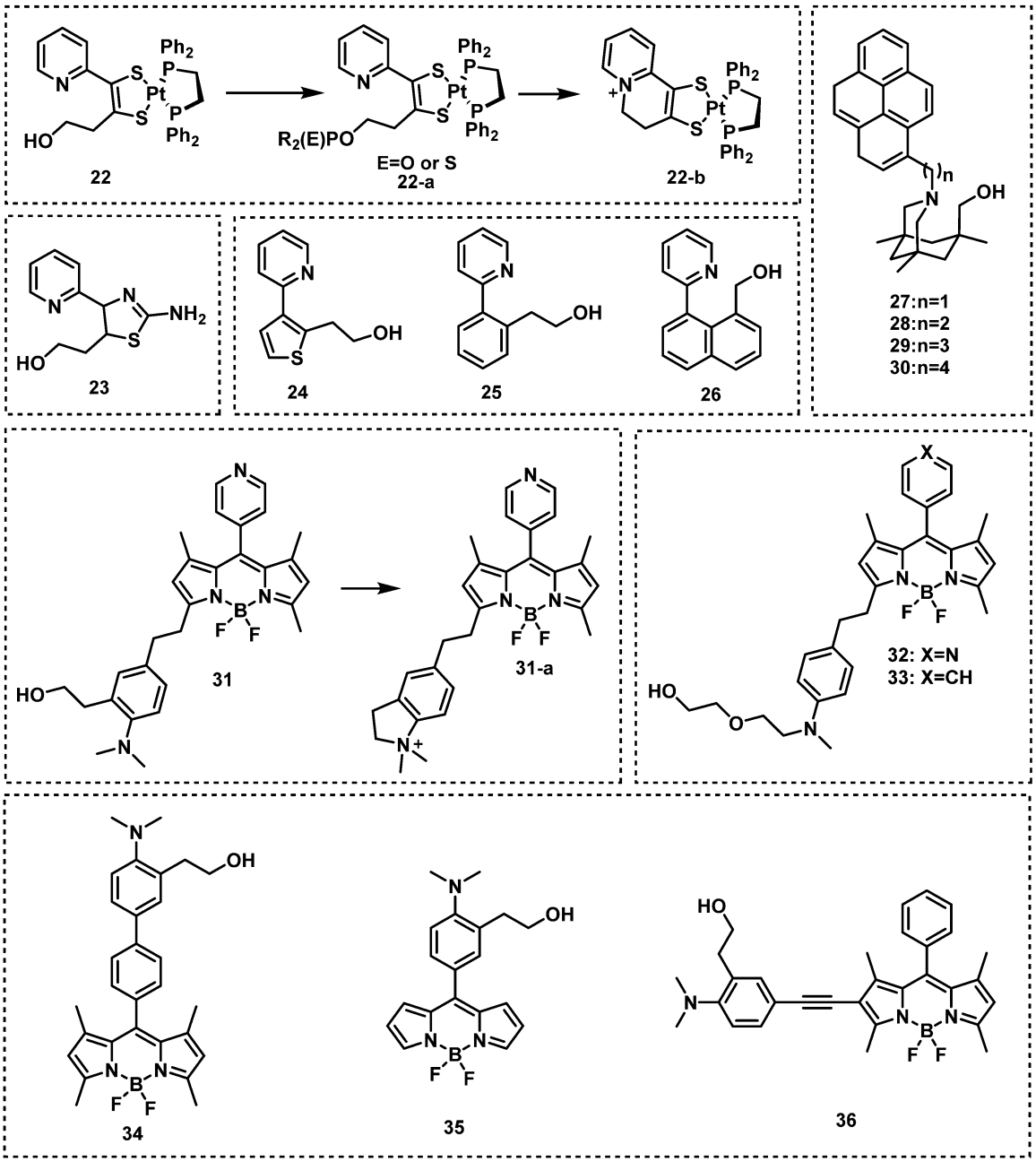

Fig. 8 Chemical structures of fluorescent nerve agent probes based on phosphorylation and subsequent cyclization **22–36**.

sensitivity (in the nanomolar range) and a large emission shift (135 nm) due to DCP-induced spiropyran ring opening. A similar strategy was used to develop the fluorescent probe **CYD** (**47**).[82] **CYD** had a fast response (1 min) and a low LOD (18.86 nM) for the detection of DCP in CH_3CN–H_2O. **NTBT** and **CYD** exhibited the ability to visualize nerve agent simulant DCP in living cells (Raw 264.7 and Hep-2 cells). The same group reported a fluorescent probe for nerve agent detection, **HNBM** (**48**),[83] which used a phenol functional group as the recognition unit. The phenol on **48** was shown to be phosphorylated by DCP, which then underwent intramolecular cyclization to afford a fluorescent phosphoester product. This reaction proceeded within 45 s and resulted in a significant increase in fluorescence emission at 503 nm.

Two fluorescent naphthalimide derivatives were developed and evaluated for their ability to detect DMMP.[84] **Naphthyl-Mono-AE** (**49**) was functionalized with one ethanolamine and **naphthyl-Di-AE** (**50**) was functionalized with two ethanolamine arms. These compounds were designed as recognition units for DMMP. Interestingly, **Naphthyl-Di-AE** exhibited a higher affinity for DMMP than **Naphthyl-Mono-AE** in toluene. Liu *et al.* synthesized the fluorescent probe 3,5-dibromosalicylidene-2,3,4,5,6-pentafluoroaniline (**DBPFA**) for the detection of DCP in iso-propanol solution. During this study, they identified

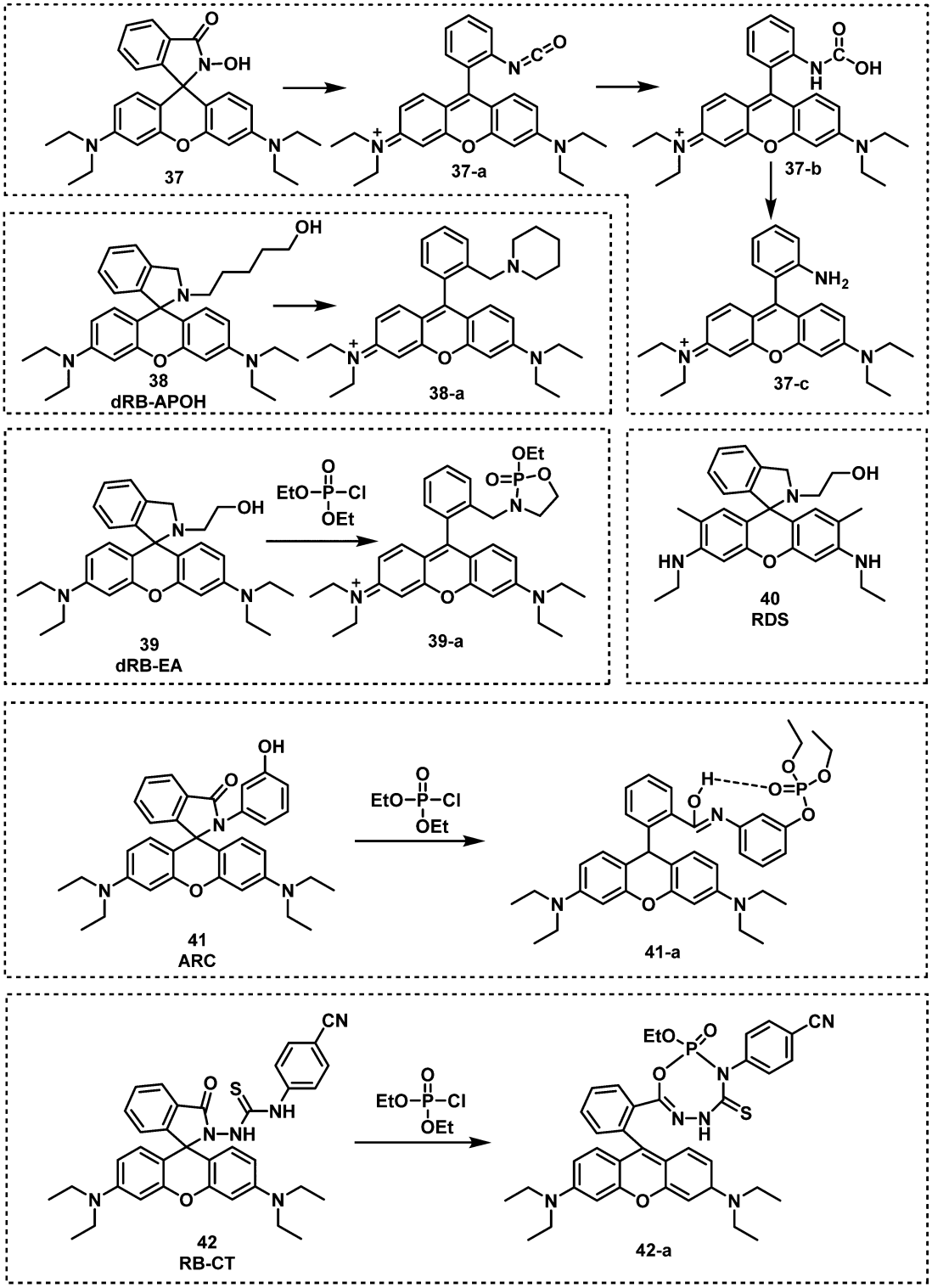

Fig. 9 Chemical structures of fluorescent probes **37–42** and their reaction mechanism for the detection of nerve agents.

DBPFA to have poor fluorescence emission in iso-propanol solution, but treatment with NaOH afforded the highly emissive phenolic species **DBPFA-I** (λ_{em} = 500 nm). They rationalised that the high nucleophilicity of **DBPFA-I** (**51**) would facilitate the detection of electrophilic nerve agents.[85] The LOD of **DBPFA-I** was 1.94 nM. **DBPFA-I** was also used to develop a paper strip device. Upon exposure to DCP, the green fluorescence of paper strips became non-fluorescent within 15 s.

Kim and co-workers reported the BODIPY-based fluorescent probe **52** in which a phenyl unit was functionalized with an

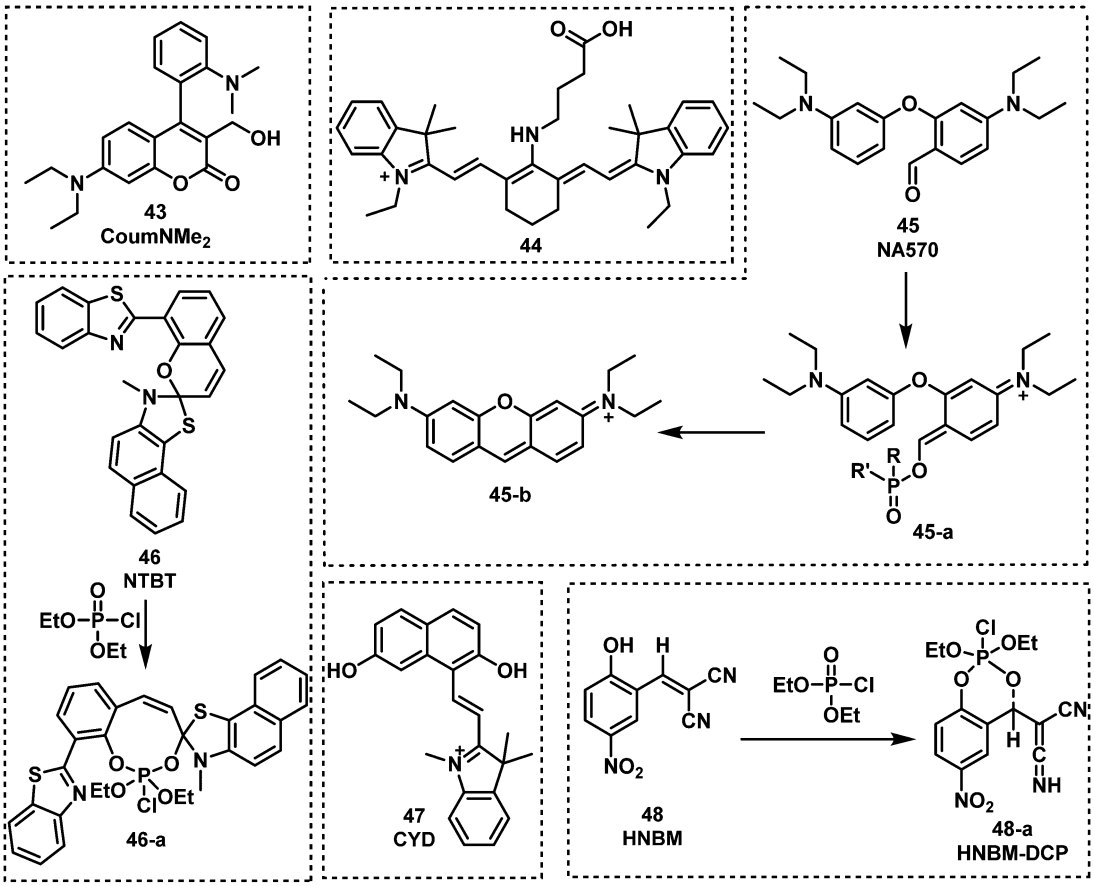

Fig. 10 Chemical structures of fluorescent probes **43–48** and their corresponding mechanism of detection for nerve agent mimic DCP.

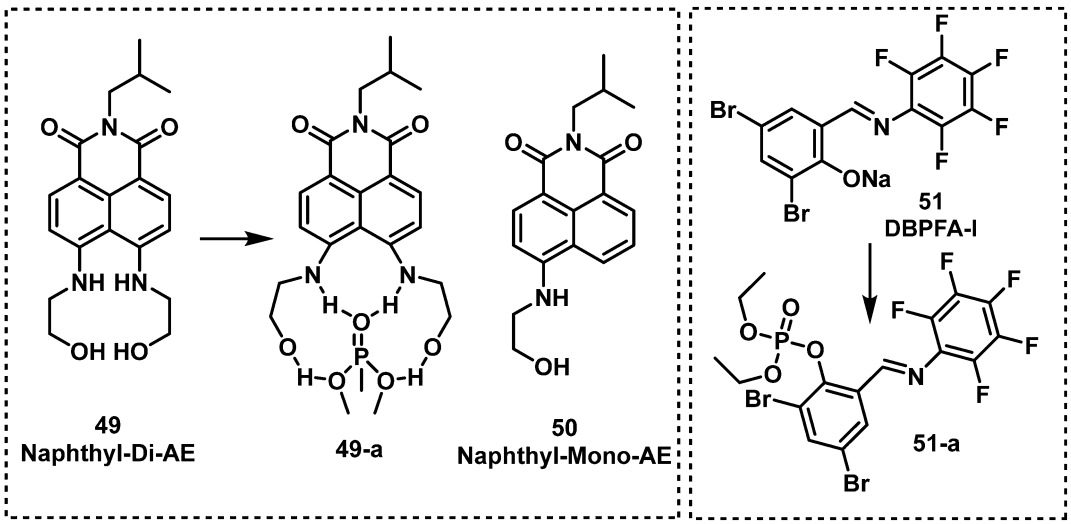

Fig. 11 Chemical structures of fluorescent nerve agent probes **49–51** and their corresponding mechanism of detection for DMMP and DCP.

ortho-OH substituent. This served as the recognition unit for nerve agent detection (DCP).[86] In this design, the phosphorylation of the reactive phenolate on **52** was accompanied by a substantial increase in fluorescence emission at 522 nm. This increase was attributed to the suppression of the internal rotation of **52**. Fluorescence detection was seen in less than 1 min and maximum intensity (a 105-fold enhancement) was reached within 10 min. Probe **52** was found to have a low LOD of 0.71 μg L^{-1} for DCP. Lu and co-workers reported a similar approach for the detection of DCP using **53** (Fig. 12).[87] The introduction of the

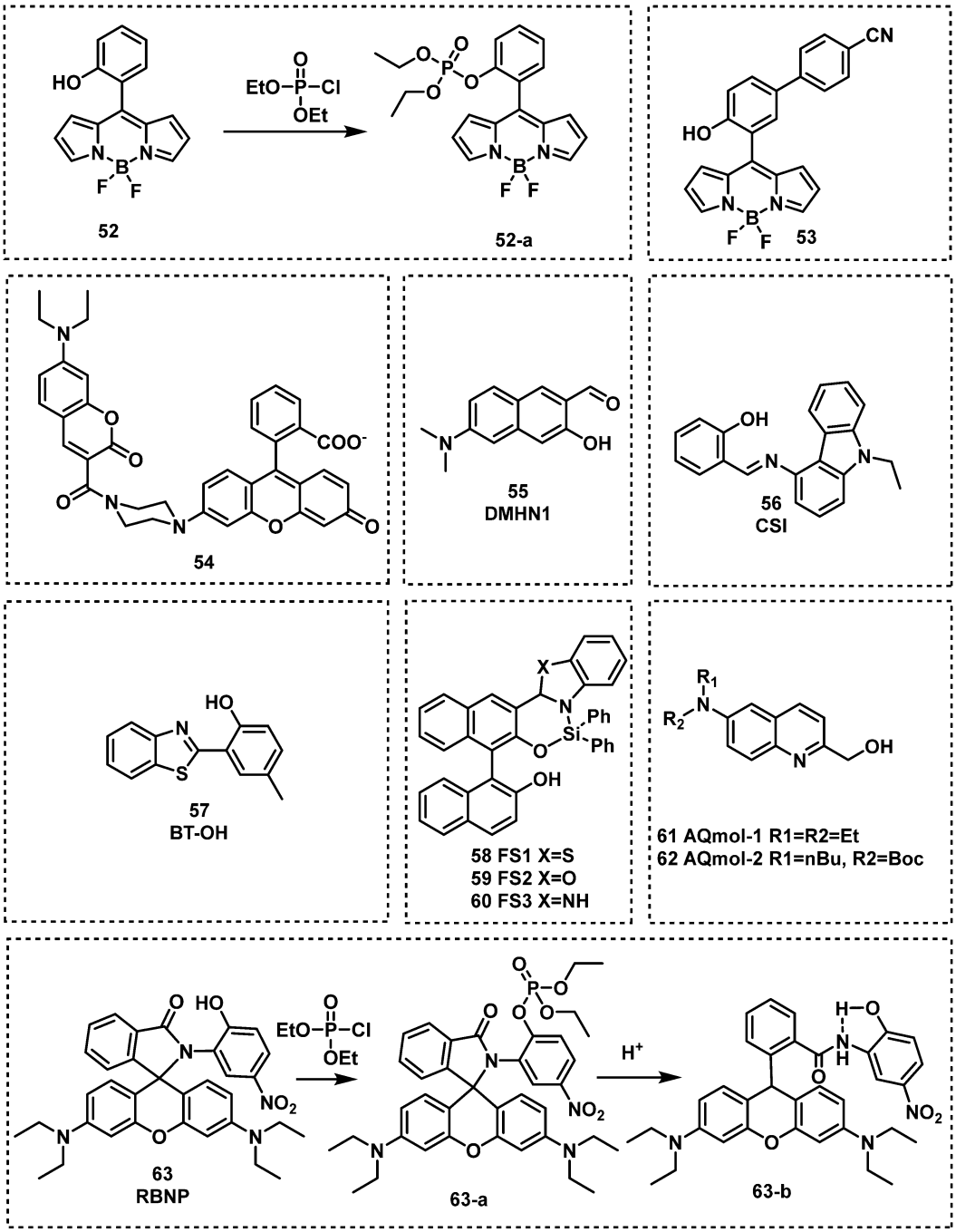

Fig. 12 Chemical structures of fluorescent probes **52–63** for the detection of nerve agent mimics.

electron-withdrawing nitrile functional group was believed to lower background fluorescence, increase the response rate (540 s), and lower the LOD (20.7 ppb), and afforded a considerable fluorescence enhancement (81-fold). Xuan *et al.* reported the first Förster resonance energy transfer (FRET) ratiometric fluorescent probe **54** for the detection of DCP.[88,89] The phenoxide moiety served as the recognition unit for nerve agents, and the coumarin fluorophore served as the fluorescence donor. The coumarin moiety (FRET donor) is coupled through a rigid piperazine linker to the carboxylate position of fluorescein/rhodamine (FRET acceptor). After the reaction with DCP, the free carboxylate is converted to a closed spirolactone form to induce ratiometric response (from 536 to 460 nm). Remarkably, **54** exhibited the ability to detect DCP vapours *via* a handheld UV lamp. In 2019, Jung and Kim developed **DMHN1** (**55**), as a excited-state intramolecular proton transfer (ESIPT) fluorescent turn-on probe.[90] **DMHN1** selectively detected DECP without interference from other similar nerve agent mimics such as DCP and DMMP. **DMHN1** was shown to have an excellent sensitivity (8.16 ppm) and a fast response time (<3 min) and

more importantly, it was developed as a DECP sensing Kit that can be used in real-time on-site situations. In 2019, Kundu and co-workers reported a carbazole-salicylaldehyde-based fluorescent probe **CSI**, (**56**), for the detection of DECP.[91] In the presence of DECP, the fluorescence emission intensity at 434 nm was found to significantly decrease and a simultaneous colour change from colourless to yellow was observed. Based on these observations, Kundu *et al.* developed a paper strip for the rapid naked-eye detection of DECP. Hu and co-workers reported the ESIPT-based benzothiazole fluorescent probe **BT-OH** (**57**) for the detection of DCP. This probe was obtained through the inhibition of the ESIPT process.[92] **BT-OH** displayed rapid response times (within 6 s) with good linearity and specificity for DCP, as well as a low LOD (0.186 mM). Feng *et al.* developed a series of 1,1′-binaphthol–Si complexes, **FS1** (**58**), **FS2** (**59**) and **FS3** (**60**), for use as fluorescent probes for the detection of DCP in DMF.[93] Each complex displayed different emission properties, green (FS2), yellow (FS1), and orange (FS3), respectively. In the presence of DCP, all three probes displayed turn off responses. Each probe was shown to rapidly detect DCP (in less than 4 s) with a low LODs (9.7 nM) and could be observed using the naked eye. Dagnaw *et al.* reported the synthesis of two fluorescent probes, **AQmol-1** (**61**) and **AQmol-2** (**62**), for nerve agent detection.[94] DFP and DCP phosphorylated the hydroxy unit found on these two sensors, and protonated the nitrogen of the quinoline moiety. This effected the donor–acceptor (D–A) fluorescent properties of these molecules, to afford a turn off (**AQmol-1**) or ratiometric (**AQmol-2**) response. **AQmol-2** was found to have an LODs of 0.16 μM for DCP and an LOD of 0.18 μM for DFP. Two rhodamine phenol-based derivatives (**RBNP** and **RBMP**) were developed by Zhang *et al.* for the detection of DCP.[95] Notably, when **RBNP** (**63**) was exposed to DCP, a substantial change in absorption from 438 nm to 563 nm and a increase in fluorescence emission intensity at 588 nm were observed. These changes were accompanined by a fast response (within 10 s), high sensitivity and a low LOD (1.4 nM) for DCP. The detection mechanism of **RBNP** involves the formation of a stable five-membered ring by intramolecular hydrogen bonding upon protonation.

Oxime-functionalized compounds, such as obidoxime and pralidoxime (2-PAM), are well-known treatment methods for nerve agent poisoning. They can reactivate the AChE inhibited by nerve agent and restore cholinergic function. Exploiting this knowledge, fluorescent probes designed for the detection of nerve agents have used the oxime functional group as a recognition unit. As shown in Fig. 13, oximes have been shown to react with nerve agents with a subsequent change in photophysical properties. The Anslyn group were the first to demonstrate this strategy with the design of probes **64** and **65**.[96] Oxime-functionalised **64** was found to have a greater sensitivity than probe **65**, which was functionalised with a hydrazone moiety. The mechanism of action was deduced to be a deprotonation of oxime, which then leads to phosphorylation of the probe with DCP or DFP. This results in a hypsochromic shift of the probe by approximately 50 nm. The same group further developed an oxime-based fluorescent probe **66** employing coumarin as the fluorophore for DFP detection in DMSO with P_4-*t*-Bu as the base to avoid DFP being hydrolyzed in the presence of strong bases like NaOH.[97] While the probe alone in P_4-*t*-Bu exhibited minimal fluorescence, upon phosphorylation by DFP, a strong fluorescence within a millisecond timescale at *ca.* 480 nm was observed. In addition, probe **67** was developed for the chemiluminescence-based detection of DFP by the Anslyn group, which is based on the modulation of the peroxyoxalate chemiluminescence pathway.[98] Dale and Rebek developed four fluorescent probes (**68**, **69**, **70** and **71**) based on the reaction of β-hydroxy oximes with nerve agent mimics.[99] Reaction with DFP was shown to induce cyclization to form the corresponding isoxazoles, which led to changes in their fluorescent properties. In particular, probe **68** exhibited the fastest response time with an increase in fluorescence emission intensity. Using a mixture of **68** and 4-nitroaniline in HEPES buffer, Maurya *et al.* developed a dual-channel optical chemical sensing system for DFP.[100] In 2019, Ali *et al.* reported a fluorescent probe, **TPOD** (**72**), which employed β-hydroxy oximes as a recognition unit for DCP detection.[101] This probe exhibited a low LOD of 0.14 μM by UV-vis absorption and 0.23 μM by fluorescence in CH_3CN–H_2O. **TPOD** was integrated into a test kit that can show dramatic changes in colour and fluorescence within 30 s in the presence of DCP. In 2019, Yang and co-workers designed and synthesized the fluorescent probe, **PTS** (**73**), for the detection of the nerve agent mimic DCP.[102] The mechanism of detection of **PTS** was based on the "covalent assembly" strategy and the Lossen rearrangement, similar to that of **NA570**. Moreover, **PTS** exhibited the ability to detect DCP, with a low LOD (10.4 nM) in a short time frame (within 100 s). Churchill and co-workers incorporated the β-hydroxy oxime functionality on BODIPY and 1,8-naphthalimide fluorophores to develop two fluorescent probes, **B-SAL-OXIME** (**74**) and **Oxinap** (**75**).[103,104] In the presence of DECP, **B-SAL-OXIME** exhibited an approximate 3-fold increase in fluorescence emission intensity (λ_{em} = 508 nm) and an LOD of 997 nM. In comparison, **Oxinap** proved superior for the detection of DECP with an approximate 50-fold increase in fluorescence intensity (λ_{em} = 570 nm), a rapid response time (30 s) and a low LOD (21.9 nM).

Lee and Kim developed a fluoresceinyloxime-based fluorescent probe (**76**), for the detection of DCP.[105] Compound **76** was shown to be selective for DCP with a low LOD (10 nM) in HEPES buffer. Lee *et al.* reported the oxime-based fluorescent probe, probe **77**, for nerve agent detection (GB and GD).[106] Upon treatment of **77** with GB and GD, the reaction was shown to be complete within 5 min, with fluorescence changes observed using a handheld UV lamp. Cai and co-workers designed and synthesized a series of 6-substituted aminoquinolin oxime-based fluorescent probes for the detection of DCP.[107] Out of these three probes, **NA-p3** (**78**) exhibited the lowest LOD for DCP (21 nM) and provided the most substantial change in fluorescence emission intensity (from 400 nm to 500 nm). Qin *et al.* reported an oxime-modified flavonoid probe, **HOFO** (**79**), for the detection of DCP.[108] A 7-fold fluorescence enhancement at 560 nm was observed in the presence of DCP (0.8 mM). When **79** was exposed to DCP, the response was within 90 s, and the LOD was determined to be 0.78 μM. In 2018, the Yoon group

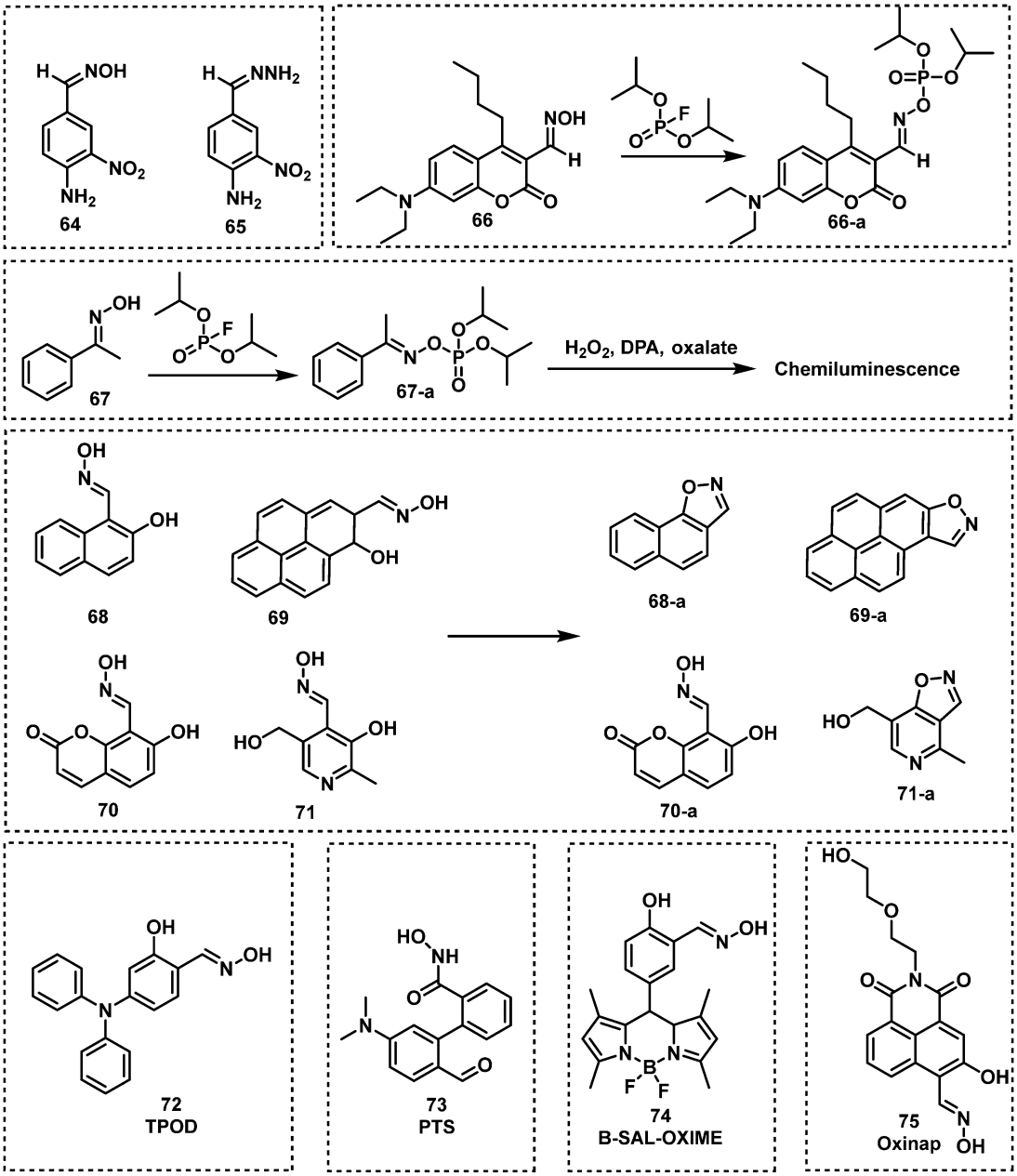

Fig. 13 Chemical structures of oxime-based fluorescent probes **64–75**.

developed an ESIPT-based fluorescent probe **80** for the detection of DECP.[109] Probe **80** was designed using hydroxyphenyl-benzothiazole as the fluorophore and an oxime as the recognition site. A 60-fold fluorescence enhancement, a low LOD (1.3 nM) and high selectivity towards DECP were observed. More recently, Li *et al.* developed the BODIPY probe, **SO-BOD** (**81**), for the detection of DECP, which employed a β-hydroxy oxime as the recognition unit.[110] This probe exhibited a 30-fold fluorescence enhancement at 590 nm, a low LOD (34 nM), and a rapid response ($t_{1/2}$ = 175 s) (Fig. 14).

Exploiting the nucleophilicity of imines, researchers have used imines as recognition units for the detection of nerve agents/mimics. Khan and co-workers reported the two fluorescent probes, **82** and **83**, that consisted of iminocoumarin fluorophores, which were functionalized with a nucleophilic imine moiety for DCP detection.[111] Both **82** and **83** exhibited fluorescence on–off response, fast response time (10 s), and low LODs of 0.065 μM for **82** and 0.21 μM for **83**. In 2020, a similar strategy was reported by Patra *et al.* for the development of fluorescent probe, **BTCP** (**84**), for the detection of DCP.[112] Compound **84** exhibited a ratiometric change in fluorescence emission intensity from 470 to 542 nm with a low LOD (15.8 nM). Which facilitated the visualization of DCP in living A549 cells.

Additional *N*-activation-based strategies for nerve agent detection include the use of piperazine and pyridine (quinoline) functionalities. An example was reported in 2011 by Royo

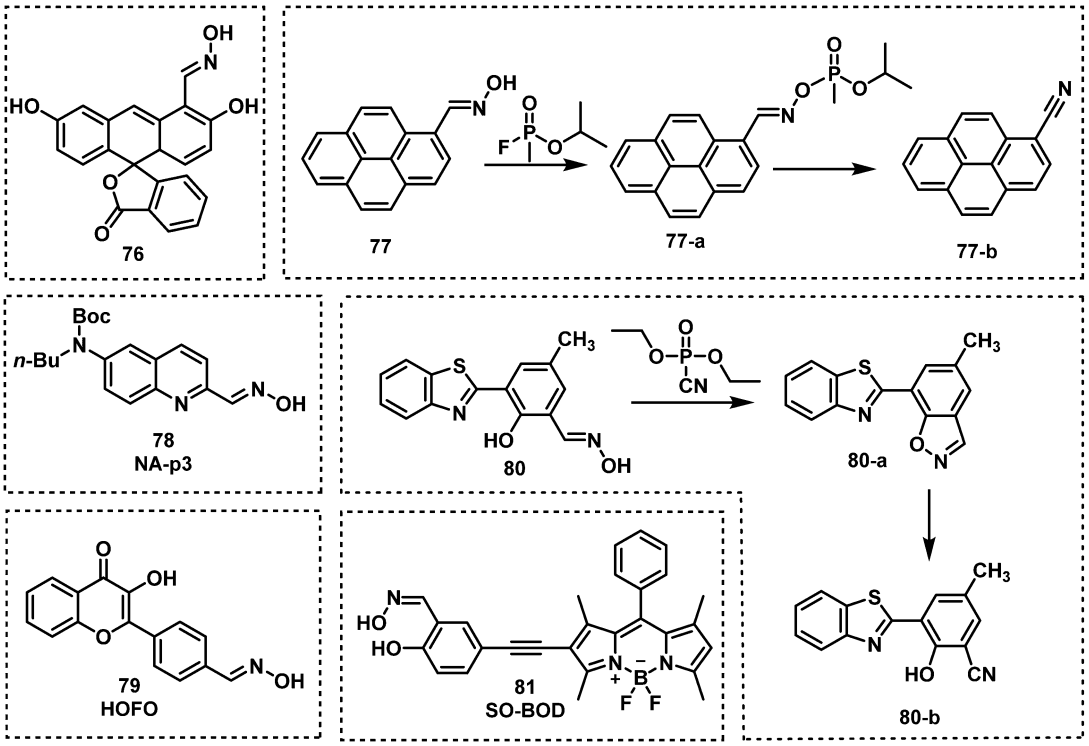

Fig. 14 Chemical structures of fluorescent nerve agent probes utilizing oxime **76–81**.

et al., in which probe **85**, used a pyridine moiety for the recognition of DCNP (Fig. 16).[113] Xu and co-workers exploited the piperazine-moiety on probe **86** to facilitate the detection of DCNP in DMF.[114] This probe displayed strong green emission (λ_{em} = 510 nm) in the presence of DCNP and a low LOD (5.5 nM) was observed. The Wästerby group developed an extensive series of fluorescent probes (**87–93**) for nerve agents using piperazine and pyridine moieties.[115] An array was developed that enabled discrimination between the nerve agents GB, GD, tabun, VX and their mimics by qualitative fluorescence patterns and quantitative multivariate analysis. Notably, in this study, true nerve agents were used instead of their corresponding mimics. Sun and co-workers designed and synthesized fluorescent probe **94**, which contained two pyridine end groups and a tricarbazole backbone. Compound **94** was incorporated into nanofibers and exhibited amplified ratiometric response for the detection of DCP. The nanofibers demonstrated a fast response (3 s) and ultrasensitivity (4 ppb).[116] Gharami *et al.* developed the quinoline-based fluorescent probe **BIMQ** (**95**) for the detection of DCP.[117] This probe underwent nucleophilic substitution with DCP, followed by ring closure to yield the final fluorescent product in $CHCl_3$ These structural modifications resulted in a redshift in fluorescence emission from 405 nm to 471 nm accompanied by a considerable increase in fluorescence. In addition, **95** displayed a rapid response (30 s), with a low LOD for DCP (9.38×10^{-8} M). Yao *et al.* developed a pyridine-based fluorescent probe, **TBPY-TPA** (**96**), for the detection of DCP.[118] Upon reaction with DCP in THF solvent or film, a ratiometric change (410 nm to 522 nm) in emission intensity was observed. The LOD of **TBPY-TPA** for DCP was determined to be approximately 2.6 ppb, and fluorescence quenching was achieved within 25 s. Exploiting the fluorescence phenomenon aggregation-induced emission (AIE),[119,120] Huang and co-workers designed and synthesized a ratiometric fluorescent probe, **DPA-TPE-Py** (**97**), for the rapid, sensitive and selective detection of DCP.[121] The pyridine unit found on **DPA-TPE-Py** reacted with DCP in THF–H_2O to form a pyridinium salt, resulting in a ratiometric change in fluorescence emission intensity from 546 nm to 624 nm. The LOD for DCP was determined to be as low as 1.82 ppb. Churchill and Song reported a series of fluorescent probes, **98–103**, for DCP detection.[122,123] All of these probes selectively detected GD and its mimics with **103** exhibiting the greatest sensitivity (8 nM). Hybridized local and charge–transfer excited state (HLCT) is a mixed state between locally-excited (LE) state and charge-transfer (CT) state.[124] When both LE and CT states lie close to each other mixing results in a hybrid HLCT state that exhibits high exciton utilization and strong fluorescence. Then, in the presence of specific nerve agents the HLCT hybrid decomposes, resulting in fluorescence changes. Inspired by the mechanism of HLCT,[124] Li *et al.* reported two fluorescent probes, **TPA-2AC** (**104**) and **TPA-9AC** (**105**), for the detection of DCP.[125] Upon addition of DCP, **TPA-9AC** showed more obvious sensitivity to DCP than **TPA-2AC**, which might be assigned to its dehybrigization property. **TPA-9AC**-coated test strips rapidly detected DCP in ~1 s with a colour change from green to red (visualized by the naked eye). The LOD of this test strip was 0.15 ppb. The exposure of DCP-treated test strips to ammonia vapour enabled their recycling for additional use (at least six cycles).

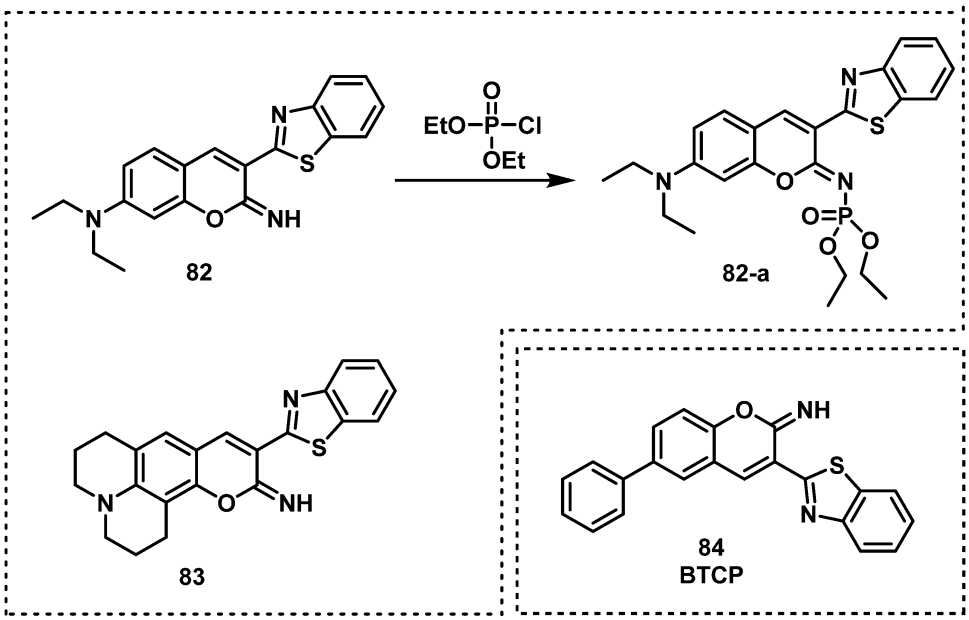

Fig. 15 Chemical structures of fluorescent nerve agent probes based on imine moiety.

Commonly, amino groups are used as the reactive site for nerve agent detection. Upon reaction with nerve agents, most probes exhibit a quenched fluorescence. However, Zhu and co-workers used a simple structural modification to completely overturn the intramolecular rotational driving energy, thus reversing the intramolecular charge transfer (ICT)-based fluorescence quenching mode.[126] Their fluorescent probe, **106**, (Fig. 15), was able to detect DCP and was used in a separate study for the detection of *N*-acetyltransferases (NAT2). The reaction between DCP and **106** in DMSO resulted in a considerable increase in fluorescence emission intensity at 610 nm. Goswami *et al.* reported the rhodamine-based fluorescent probe, **RHM** (**107**), for DCP detection in CH_2Cl_2.[127] The amino functionality on **107** reacted with DCP, which underwent subsequent intramolecular cycloaddition to form a highly fluorescent 7-membered ring λ_{em} = 582 nm (Fig. 17). Gupta and Lee reported the dual functional azoaniline-based fluorescent probe, **Azo** (**108**), for the detection of DCP and copper(II) (Cu^{II}) ions in CH_3CN solution.[128] In the presence of DCP, a colour change from pale yellow to dark red was observed. In separate experiments, Cu^{II} ions were found to induce benzotriazole ring formation, which was accompanied with a fluorescence turn on at 455 nm. Fu *et al.* reported two fluorescent probes, **109** and **110**, for the real-time detection of DCP by incorporating amine groups into Schiff base skeletons.[129] Both probes exhibited good selectivity, a short response time and high sensitivity (0.14 ppb). In 2020, a donor–π–acceptor (D–π–A)-based asymmetrical azine molecule, **DPBN** (**111**), was developed as a fluorescent probe for the detection of DCP. The DCP induced aggregation of **111** resulted in a 1157-fold fluorescence enhancement. Upon the addition of DCP, the the imine nitrogen of the probe is phosphorylated to induce a redshift of the absorption and emission spectra *via* the formation of a new ICT state.[130] Recently, Zheng and co-workers reported two donor–acceptor (D–A) fluorescent probes, **T1** (**112**) and **T2** (**113**), based on a terpyridine scaffold.[131] **T1** and **T2** could form protonated compounds induced by DCP, but due to the different electron – donating units the protonated compounds present different intramolecular properties. Thus, a DCP-dependent ratiometric change in fluorescence emission intensity (from 415 to 500 nm) was observed for **112**, whereas **113** was underwent fluorescence quenching at 550 nm. The LODs of **112** and **113** for DCP were 0.35 μM and 0.30 μM, respectively.

By exploiting metal–ligand coordiation, Weder *et al.* developed a series of fluorescent probes based on the metals Eu^{3+}, La^{3+}, and Zn^{2+}, for the detection of ethyl phosphate in $CHCl_3$–CH_3CN.[132] The Eu^{3+}-based fluorescent probe (**114**) exhibited a considerable blueshift and increase in fluorescence emission intensity in the presence of ethyl phosphate. Based on a similar strategy, Sarkar reported a Eu^{3+}-based probe, **115**, which exhibited good selectivity for DFP.[133] Inspired by the designs of **114** and **115**, Martínez-Máñez *et al.* developed two BODIPY-based fluorescent probes, **116** and **117**, for the detection of V-type nerve agent mimic demeton-S in acetonitrile.[134] These two probes displayed strong emission intensities at 572 nm and 573 nm, respectively. In the presence of demeton-S, these probes exhibited a colour change and fluorescence quenching. The Simanoto group reported Fe^{2+}–bipyridine metal complex **118**, for the detection of DCP.[135] Incubation with DCP results in destabilization of the ligand framework, which leads to the loss of Fe^{2+} and the subsequent transition from red to colourless in CH_3CN. Gupta and Patra reported the Europium(III) fluorescent probe (**119**) for the detection of DCP.[136] The addition of DCP to a CH_3CN solution of **119** resulted in a substantial luminescence enhancement at 619 nm. Larsen *et al.* reported a Zn^{2+}-based fluorescent probe **120** for the detection of DIMP.[137] Upon treatment with DIMP, the phosphoryl oxygen

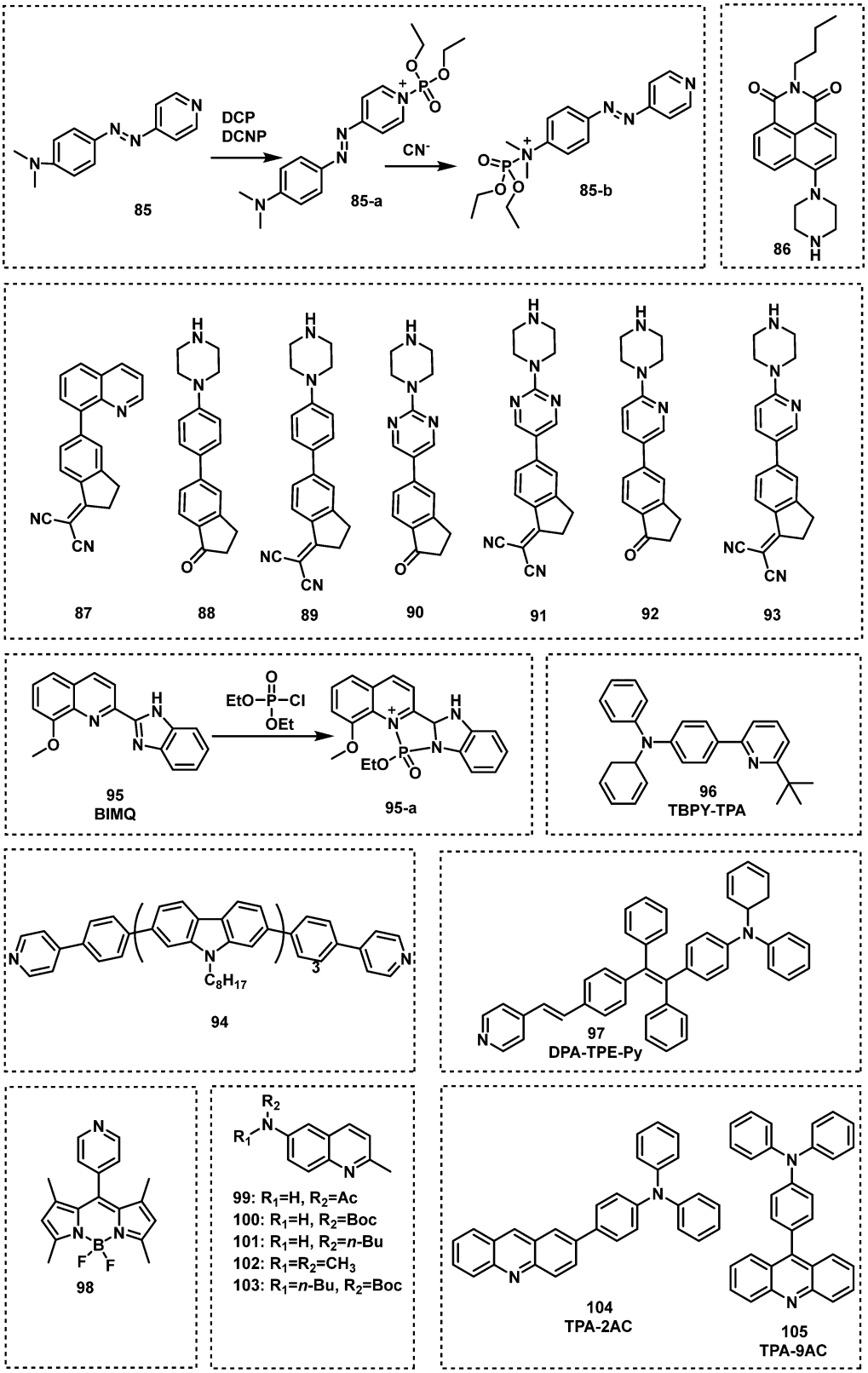

Fig. 16 Chemical structures of fluorescent probes **85–105** utilizing a piperazine/pyridine moiety.

reacted with the metal centre of porphyrin zinc(II), which led to the red shifts in the absorption and emission spectra (Fig. 18 and 19).

Sheet *et al.* developed an organoiridium(III)-based ON–OFF–ON fluorescent probe, **121**, for DCP detection, which used a transition metal complex for the detection of nerve agent

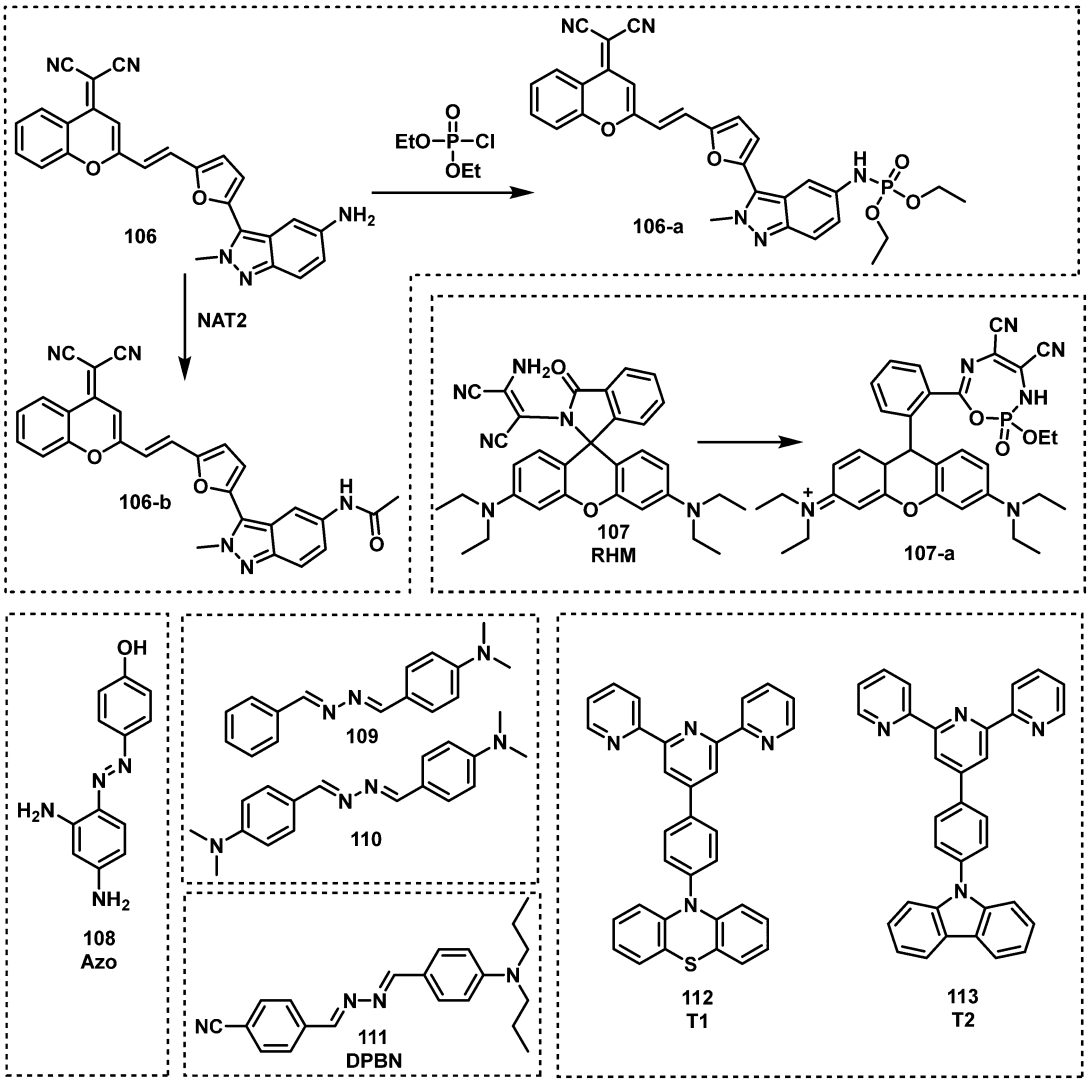

Fig. 17 Chemical structures of amino-functionalized fluorescent probes **106–113**.

mimics through ligand-based direct phosphorylation reactions and luminescence colour switching.[138] The two phenolic hydroxyl groups of this probe acted as the recognition units. Upon reaction with DCP, the fluorescence emission redshifted from 518 nm to 565 nm, with a full reaction time determined to be approx. 20 min. For this ''ON–OFF–ON'' probe, the ON–OFF process occurred in less than 6 min, and the OFF–ON process occurs from 6 min to 20 min. Raj *et al.* designed and synthesized two Co^{2+}-naphthalimide-based fluorescent probes, **K1**·Co^{2+} (**122**) and **K2**·Co^{2+} (**123**).[139] Both **K1**·Co^{2+} and **K2**·Co^{2+} exhibited a 2-fold fluorescence enhancement upon contact with DECP, and **K1**·Co^{2+} had an LOD for DECP of 21 nM. More recently, this group reported a series of dimethyltin(IV) compounds (**124–127**) for DCP detection.[140] Compounds **124–127** were emissive at approximately 470 nm, however, when exposed to DCP, the fluorescence of these probes was quenched. Fluorescent strips and silica tablets developed using these probes were used for on-the spot detection of DCP.

As mentioned earlier, many nerve agents possess either a fluoride, cyanide or thiol-based leaving group. This feature has led many researchers to focus on developing fluorescent probes that can indirectly detect nerve agents by monitoring the release of these leaving groups. The distinct advantage of this approach is the ability to discriminate between types of nerve agents since each type releases a different leaving group, *e.g.*, VX/VM releases thiol, sarin, soman and cyclosarin release fluoride ion, and tabun releases cyanide anion. In addition, the design of autoinductive systems allows the ultrasensitive detection of nerve agents.[141] Kumar and Rana exploited electron deficient squaraine dye (**SQ**) to detect and discriminate between the nerve agents VM and tabun.[142] The addition of fluoride to a solution of either VM or tabun results in the subsequent release of cyanide and thiolate anions, respectively. Nucleophilic cyanide and thiolate anions subsequently react with **SQ** in a reversible manner, which results in the dye changing from blue to colourless in $CHCl_3$ (Fig. 20). Thiophilic mercury was then added to the solution to release VM-associated thiol from **SQ**

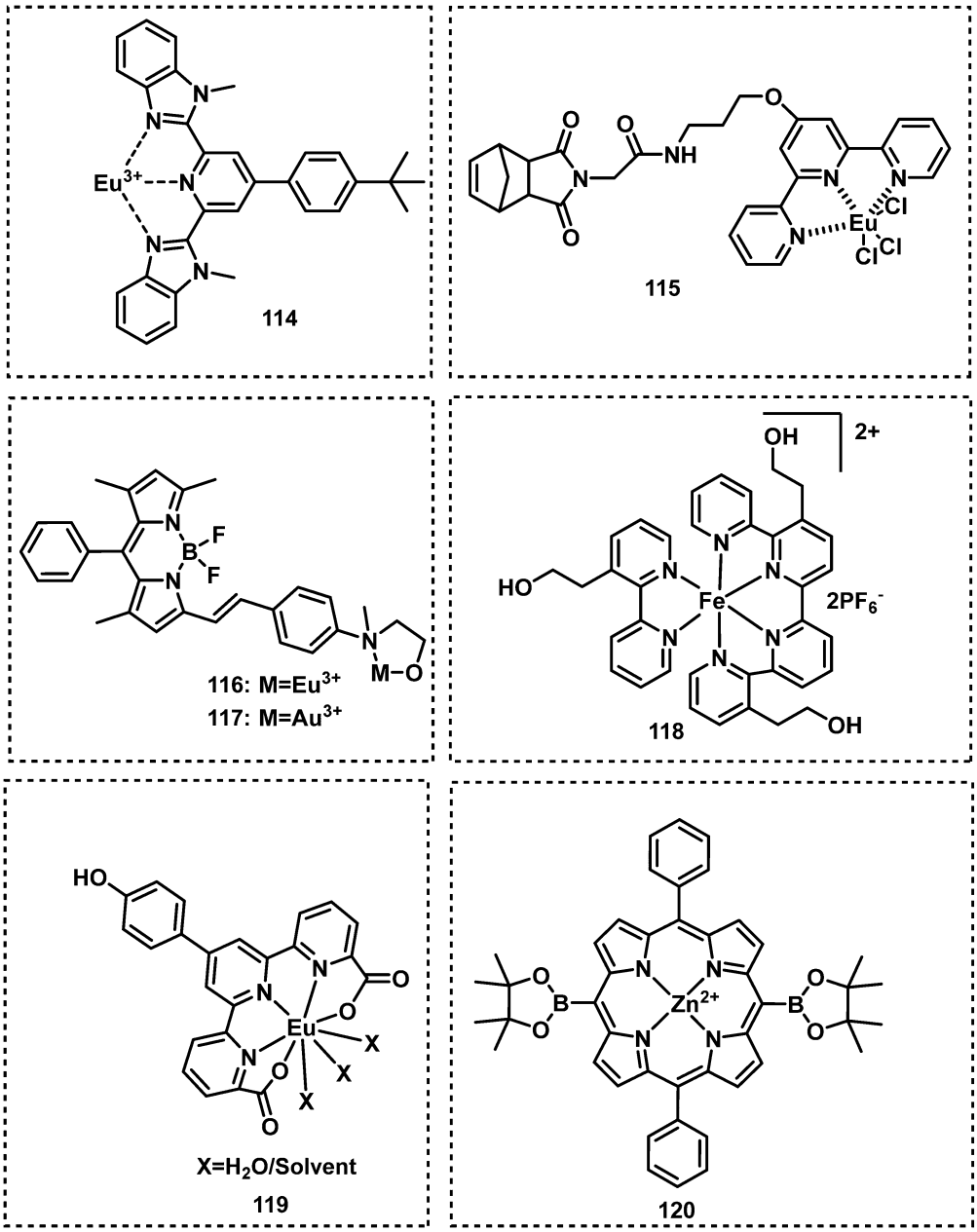

Fig. 18 Chemical structures of metal-based fluorescent probes **114–120**.

and restore the photophysical properties of the dye. For tabun, no colour change occurred since only cyanide ions are released. In recent years, the Anslyn group has focused on the development of autoinductive cascade systems for the ultrasensitive detection of DFP.[143] Fluoride ions were released as the result of the reaction between DFP and benzaldoxime. As shown in Fig. 21, the released fluoride concentration was amplifiled by the autoinductive fluoride amplification (**129**). A fluoride-specific ratiometric fluorescent reporter **130** reacted with the amplified fluoride to release the fluorophore (Fig. 21). The colorimetric and fluorometric readouts enable quantitative assays with low micromolar limits of detection for fluoride from DFP. The same authors attempted to develop an improved system for the detection of fluoride-releasing nerve agents.[144] Benzoyl fluoride was employed as a latent source of fluoride for signal amplification and optical fluoride detection. The system displayed a 4-fold signal enhancement for each fluoride unit generated and exhibited a more rapid autoinductive cascade than that previously reported. In 2017, the Anslyn group developed a new autoinductive system for VX detection.[145] This system used a conjugate acceptor based on Meldrum's acid (**131**) as a latent source of thiol for signal amplification and the optical detection of thiols. Fluorescent probe **132** was also employed for the fluorescence detection of thiols in this system. In recent years, researchers have turned their attention to discriminating between V- and G-nerve agents. The Anslyn group employed **130** and **133** as fluorescence based

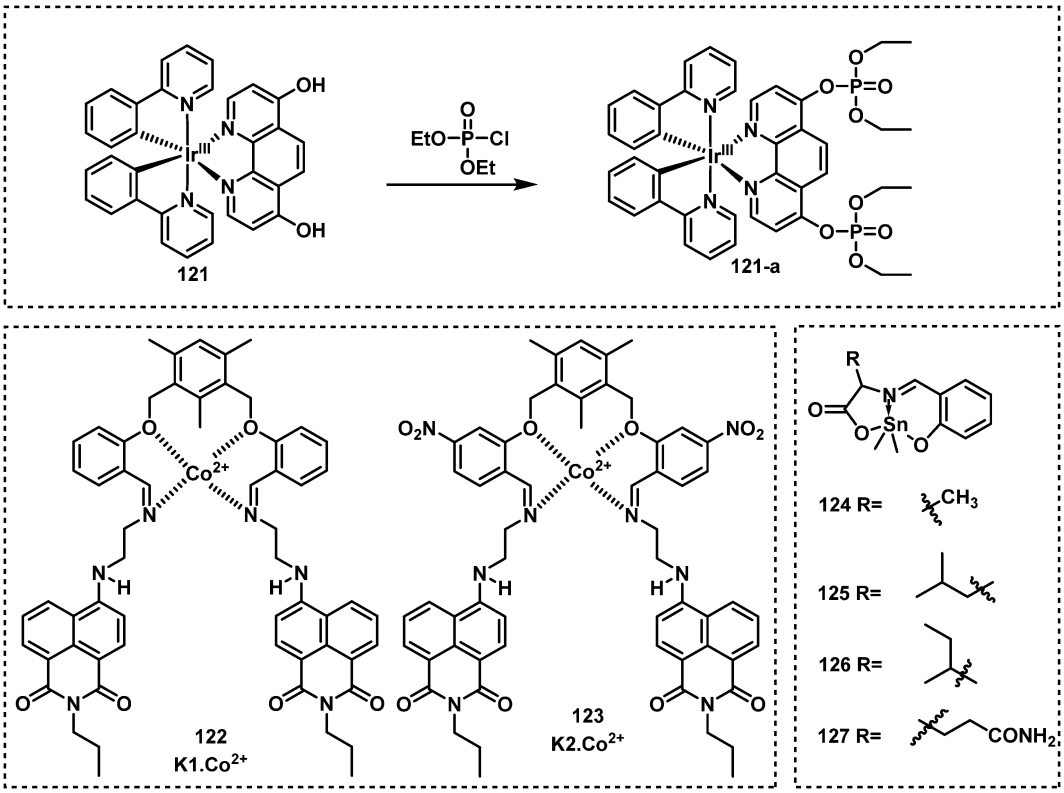

Fig. 19 Metal complexes **121–127** used for the detection of nerve agent mimics.

probes for the quantification and differentiation of G- and V-nerve agent mimics. The analytic system was developed using a self-made device that included a homemade LEGO dark-box, a cell phone, and 96-well plate. Using this system, the authors collected photographs of the fluorescence responses and an algorithm enabled differentiation between G- and V-nerve agent mimics.[146] In 2021, the same group developed an autoinductive system for DCNP detection through a self-propagating cascade.[147] This system is based on the hydrogel material of compounds **134** and **135**. A Meldrums acid-derived linker is incorporated that modulate the absorbance changes, dye release, and physical changes of the hydrogel system upon interaction with DCNP. Wu and co-workers reported **FP1**, **136**, a fluorescent probe functionalized with two different recognition units for the detection and discrimination of fluoride-containing G-series and thiol-containing V-series nerve agents.[148] The silyl protecting group on **136** was designed to be removed in the presence of fluoride ions and the maleimide group on **136** is designed to react with thiols. Compound **136** exhibited considerable fluorescence enhancements at 404 nm for VX and 460 nm for GB and low LODs for VX (0.2 μM) and GB (10 μM). Xu *et al.* reported an OFF–ON fluorescent probe, **HCY** (**137**), for the detection of DECP in DMF–H_2O.[149] When in contact with DECP, the fluorescence emission of **137** (λ_{em} = 435 nm) increased 178-fold. This result was ascribed to the nucleophilic addition of CN^- to **HCY**. The probe exhibited a fast response (less than 3 min) and good sensitivity with a low LOD (4.5 nM). Das *et al.* reported the fluorescent probe **BSNA** (**138**) for DECP detection.[150] The mechanism of this probe is based on relay recognition of F^- and DECP. **BSNA** reacted with F^- to produce BBCI, which further reacted with DECP to form a six-membered fluorescent cyclic product.

Fluorescent probes (**57–60**) that use hydroxyl units to facilitate nerve agent detection are readily affected by structurally similar species (*e.g.*, phosgene) or changes in pH of the test solution. Fluorescent probes (**22–36**, **38–42**) that are designed to undergo a phosphorylation-intramolecular cyclization reaction display high selectivity for nerve agents; the major limitation to this strategy is the long reaction times. The use of oximes as a recognition unit proved superior to hydroxyl units (**64–81**), leading to shortened reaction times. Probes PTS (**73**), **80**, and SO-BOD (**81**) developed based on this strategy exhibited good sensing performances. Although pyridine-based fluorescent probes (**85–105**) react rapidly with soman and its simulants, these probes are generally not selective over strong acids such as H_2SO_4, HCl, and HNO_3. Therefore, current fluorescent probes are mainly designed for a specific nerve agent, which means more universal sensing systems are required for the detection of a broad range of nerve agents. Another issue related to the fluorescence probes developed is that their real-world applicability has yet to be evaluated.

5. Fluorescent probes designed for the detection of choking agents

Choking agents cause acute toxic pulmonary oedema by directly attacking the respiratory system through inhalation,

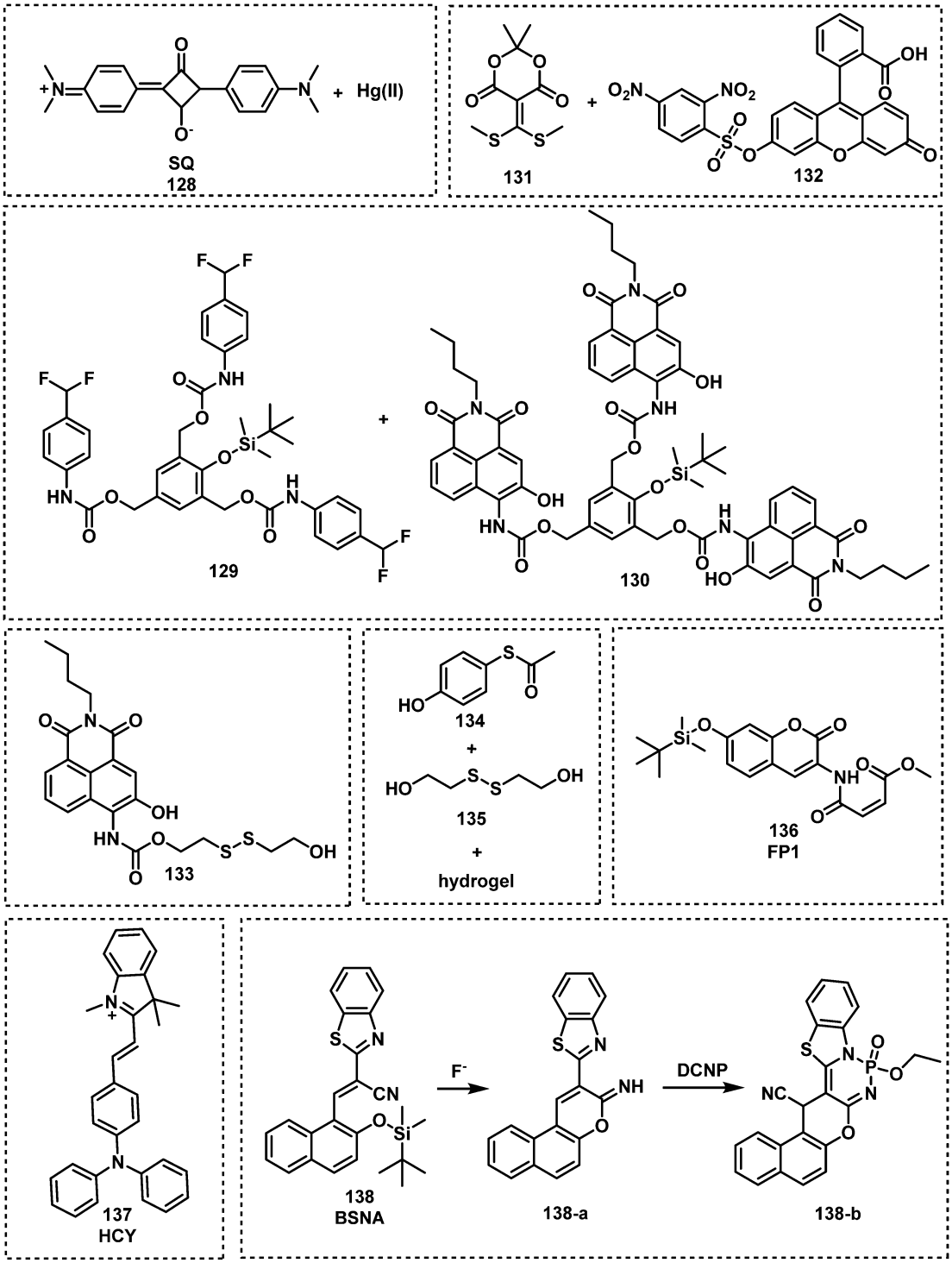

Fig. 20 Chemical structures of fluorescent probes **128–138** for the indirect detection of CWA by monitoring the respective release of fluoride anion, cyanide ion and thiols.

acute hypoxia and asphyxia and death. For these reasons, CWAs are also called pulmonary agents or lung-damaging agents.[151] Notable examples of choking agents include chlorine, phosgene, and diphosgene. Chlorine gas was one of the first CWAs used in 1915 by the German army.[6] This CWA was gradually replaced by phosgene and diphosgene during WWI.[152] Phosgene was one of the most stocked CWAs during WWII. However, the emergence of nerve agents has led to choking agents being seen as a lesser threat. In today's chemical world, phosgene, diphosgene and triphosgene (Fig. 22) are now widely used as reagents for the synthesis of pharmacologically important compounds. Therefore, they are now listed as dual-use chemicals by the United Nations

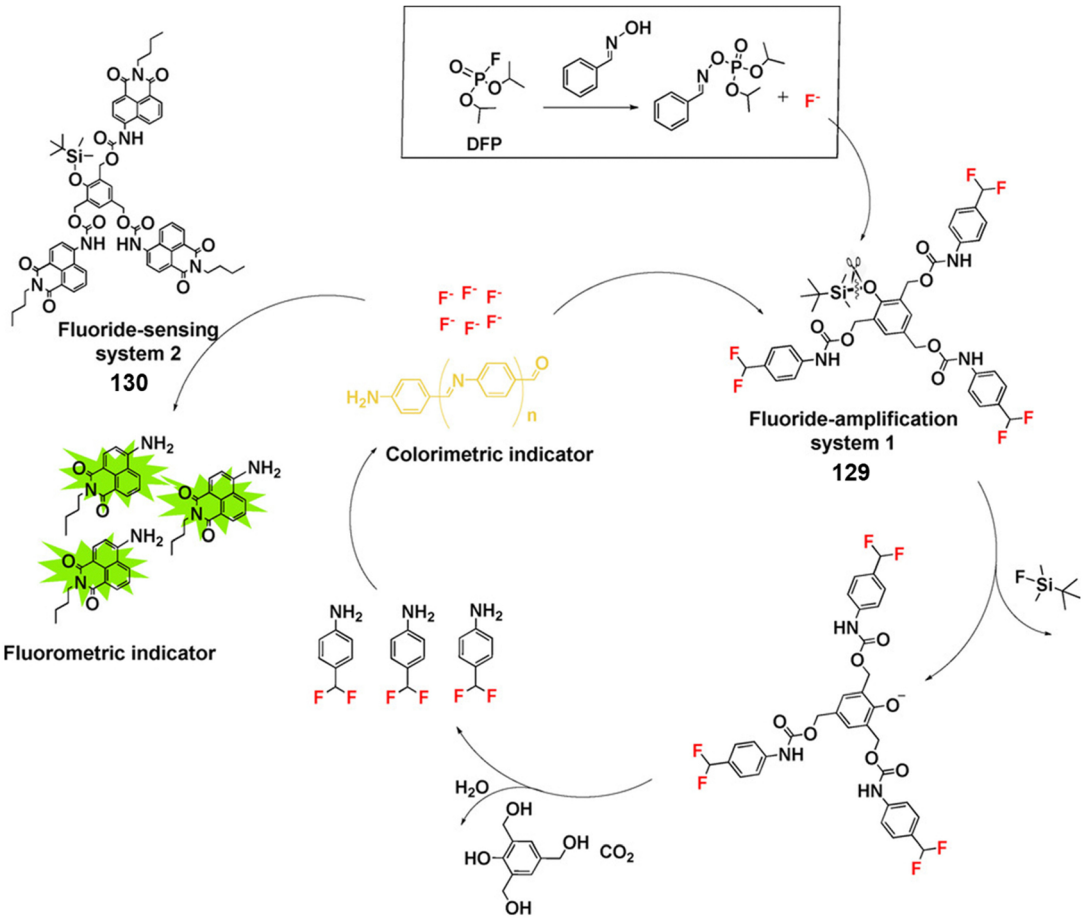

Fig. 21 Fluoride generating, self-propagating and sensing systems (**129** and **130**) for the detection of DFP through signal amplification. Reproduced with permission from ref. 143. Copyright (2017) Wiley-VCH Verlag GmbH & Co. KGaA, Weinheim.

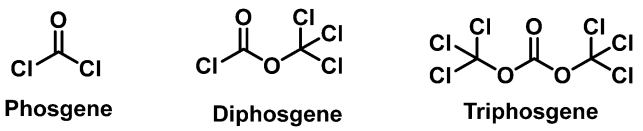

Fig. 22 Chemical structures of well-known choking agents: phosgene, diphosgene and triphosgene.

Table 4 Acute exposure guideline levels of choking agents

		10 min	30 min	60 min	4 h	8 h
ppm						
Chlorine	AEGL 1	0.50	0.50	0.50	0.50	0.50
	AEGL 2	2.8	2.8	2.0	1.0	0.71
	AEGL 3	50	28	20	10	7.1
ppm						
Phosgene	AEGL 1	NR	NR	NR	NR	NR
	AEGL 2	0.60	0.60	0.30	0.080	0.040
	AEGL 3	3.6	1.5	0.75	0.20	0.090

NR = not recommended due to insufficient data.

Office for Disarmament Affairs. The AEGLs of Chlorine and Phosgene were listed in Table 4. The current probe strategies used for the detection of choking agents employ recognition units that contain two adjacent nucleophilic units that then undergo ring formation in the presence of a choking agent (Fig. 23). These ring forming reactions result in significant changes to the photophysical properties of the probes.

The *o*-phenylenediamine moiety is one of the most used recognition units for phosgene detection. This is because of its ability to undergo a cyclization reaction with phosgene to form benzimidazolone. Exploiting this chemical reactivity, the Yoon group developed fluorescent probe, **PY-OPD** (**139**), for the fluorescence-based discrimination of phosgene and nerve agent mimic DCP in $CHCl_3$. (Fig. 24).[153] Compound **139** consisted of a pyronin Y fluorophore that was functionalized with the *o*-phenylenediamine recognition unit. DCP-mediated phosphorylation of the free amino unit resulted in an increase in fluorescence at 538 nm. In contrast, phosgene reacted with **139** to form the benzimidazolone product and afforded a fluorescence enhancement at 593 nm.

Expanding on this strategy, the fluorescent probe, **PDAC** (**140**), was developed to detect and discriminate between DCP and phosgene in $CHCl_3$ (Fig. 25).[154] Compound **140** consisted of the *o*-phenylenediamine recognition unit and anthracene–carboxyimide as the fluorophore. Exposure of **140** to DCP

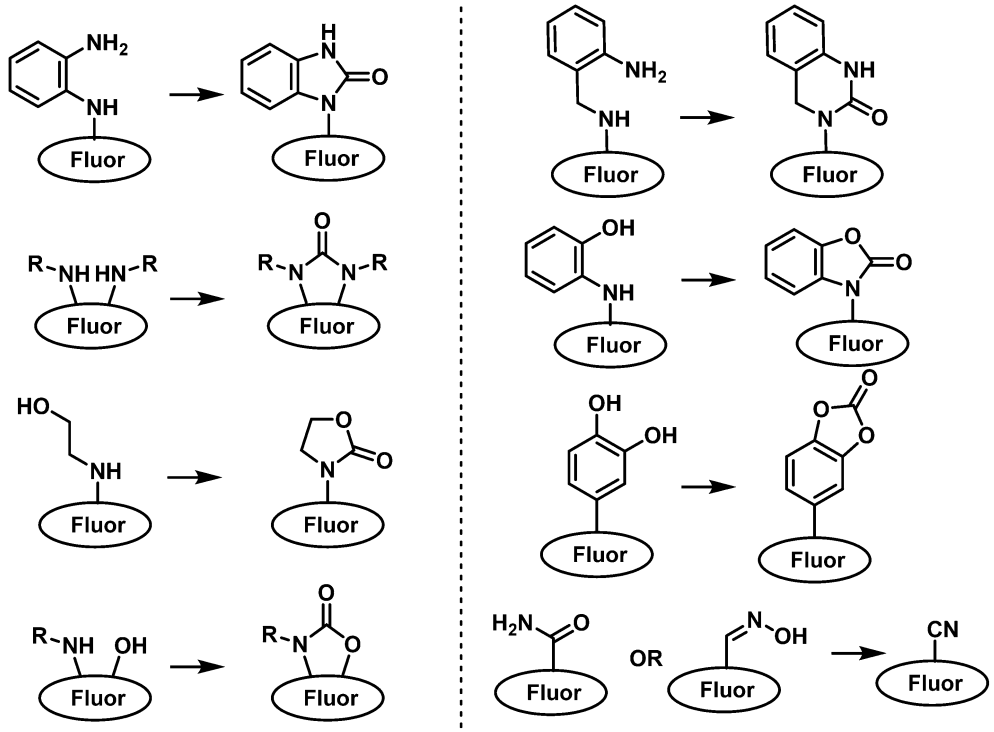

Fig. 23 General chemical reaction-based fluorescence design strategies for detection of choking agents.

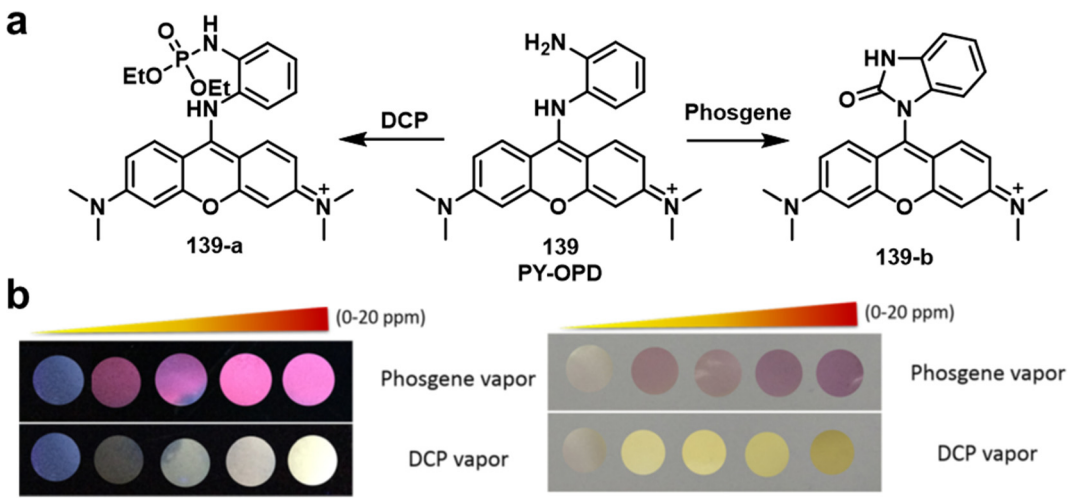

Fig. 24 (a) Different mechanisms of detection for **139** to allow the discrimination between DCP and phosgene. (b) Fluorescence (left) and colorimetric responses (right) of **139**-coated polyethylene oxide membranes exposed to different concentrations of phosgene and DCP vapour (0–20 ppm). Reproduced with permission from ref. 153. Copyright (2016) Wiley-VCH Verlag GmbH & Co. KGaA, Weinheim.

resulted a clear increase in fluorescence emission at 588 nm with a low LOD (88 nM). The probe also exhibited an enhanced fluorescence response at 500 nm, with a fast response time (less than 2 min) and a low LOD (72 nM) for the detection of phosgene. Three fluorescent probes, **NBD-OPD** (**141**), **RB-OPD** (**142**) and **NAP-OPD** (**143**) were developed, using 4-chloro-7-nitrobenzo[*c*][1,2,5]oxadiazole, rhodamine, and 1,8-naphthalimide as the fluorophores, respectively, all were functionalized with the *o*-phenylenediamine recognition unit.[155] Interestingly, all of these probes were selective for the detection of phosgene. The addition of phosgene to **141** in $CHCl_3$, resulted in the change in colour from dark orange to yellow and a considerable fluorescence enhancement at 575 nm. Exposure of **142** to phosgene induced spirolactam ring opening, which was accompanied by benzimidazolone formation and the pink fluorescence of rhodamine (λ_{em} = 310 nm). Compound **143** also displayed considerable fluorescence enhancement after the addition of phosgene, with a low LOD (2.8 ppb). The sensing experiments of **RB-OPD** and **NAP-OPD** were performed in CH_3CN and *p*-xylene, respectively.

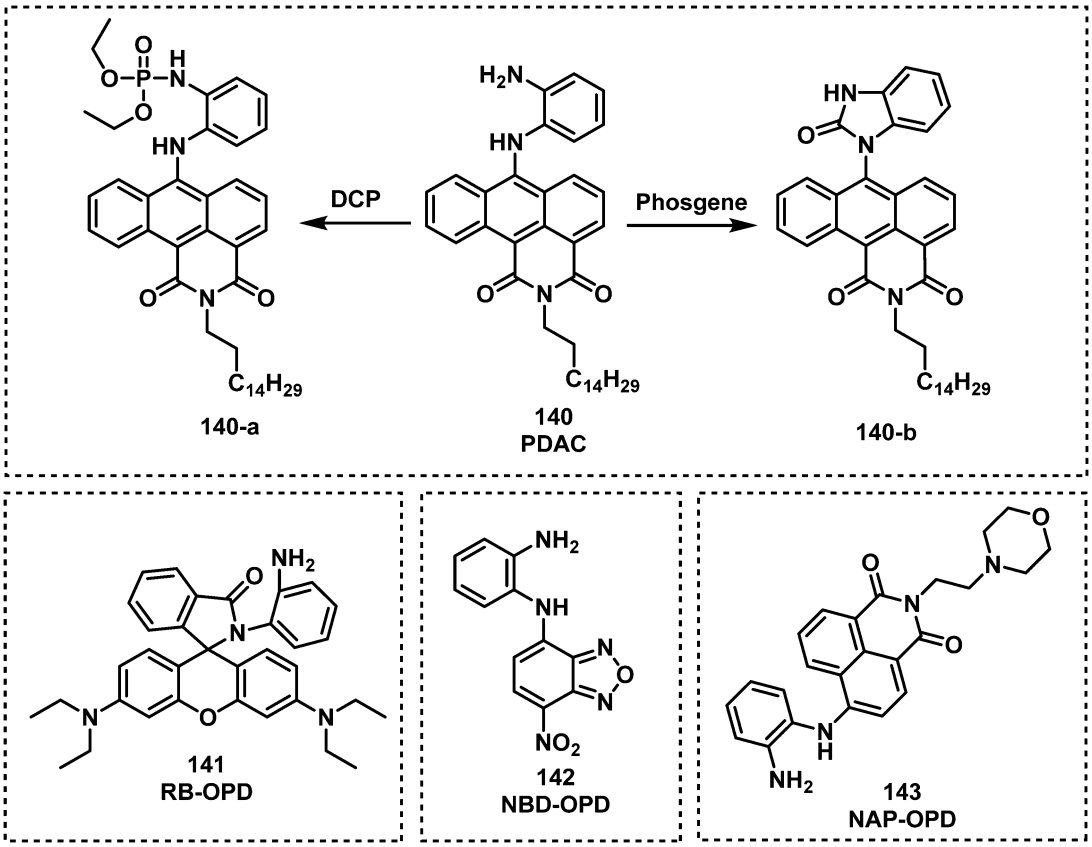

Fig. 25 Chemical structures of fluorescent choking agent probes utilizing an *o*-phenylenediamine moiety to form benzimidazolone **140–143**.

Several other researchers have used the *o*-phenylenediamine-based approach (Fig. 26). The fluorescent probe ***o*-Pac** (**144**) developed by Xia and co-workers exhibited the ability to detect phosgene in $CHCl_3$.[156] The structure of **144** consisted of an *o*-phenylenediamine unit and a coumarin fluorophore, exhibiting a fast response time (less than 0.5 min), a 533-fold fluorescence enhancement at 446 nm, and a low LOD (3 nM) in the presence of phosgene. The Song group reported on a BODIPY-based fluorescent probe ***o*-Pab** (**145**), which was functionalized with an *o*-phenylenediamine for phosgene detection.[157] When in contact with phosgene, **145** exhibited a rapid response (approximately 15 s) and a 9800-fold increase in fluorescence intensity at 530 nm. The same group also developed the fluorescent probe **Phos-1** (**146**) for phosgene detection, intergrating a *o*-phenylenediamine unit into the naphthalimide fluorophore.[158] Reaction of **146** with phosgene was shown to be sensitive with an LOD of 1.3 nM and complete within 20 min. Xie and co-workers reported the AIE-based fluorescent probe **OPD-TPE-Py-2CN** (**147**) for phosgene detection in THF–H_2O.[159] An LOD of 1.87 ppm was determined, and its fluorescence emission changed from blue (475 nm) to green (495 nm). While Zhang and Rudkevich developed the fluorescent probes **148** and **149**, for phosgene detection. Upon contact with phosgene, probes **148** and **149** exhibited a fluorescence change from 424 nm to 464 nm and a low LOD (5×10^{-5} M).[160]

Exploiting two types of nucleophilic nitrogen on ESIPT fluorophore **150**, the Yoon group demonstrated the probes ability to detect phosgene in $CHCl_3$.[161] As shown in Fig. 27, the addition of phosgene resulted in the formation of cyclic product **150-a**. This reaction resulted in a change in the colour of the solution from colourless to yellow and a ratiometric change in fluorescence emission (445 to 495 nm). Compound **150** exhibited a low LOD (0.14 ppm) and responded rapidly when treated with phosgene (6 μM, 2 min). Recently, the Yoon group reported the rhodamine-based fluorescent probe **151** for the detection of phosgene in $CHCl_3$.[162] The spirolactam of **151** opened in the presence of phosgene, which was accompanied by a colour change from colourless to pink and a strong increase in fluorescence emission at 578 nm. This response is within 2 min. Han and co-workers reported the ethylene diamine-functionalized rhodamine-derived fluorescent probe, **dRB-EDA** (**152**), for the detection of phosgene in DMF.[163] This probe was found to be initially colourless and nonfluorescent because the spirolactam was closed. Phosgene was shown to react with the ethylene-diamine unit and the acylated intermediate underwent intramolecular cyclization to afford a ring-opened rhodamine fluorophore. This mechanism of detection affords an LOD of 50 nM for phosgene in DMF. Zhang and co-workers developed a similar ethylenediamine-based strategy with **8-EDAB** (**153**).[164] Compound **153** was initially weakly emissive at 445 nm, but after coming into contact with phosgene, a new fluorescence emission appeared at 512 nm. A ratiometric response was observed in less than 1.5 s, with a 23 300-fold

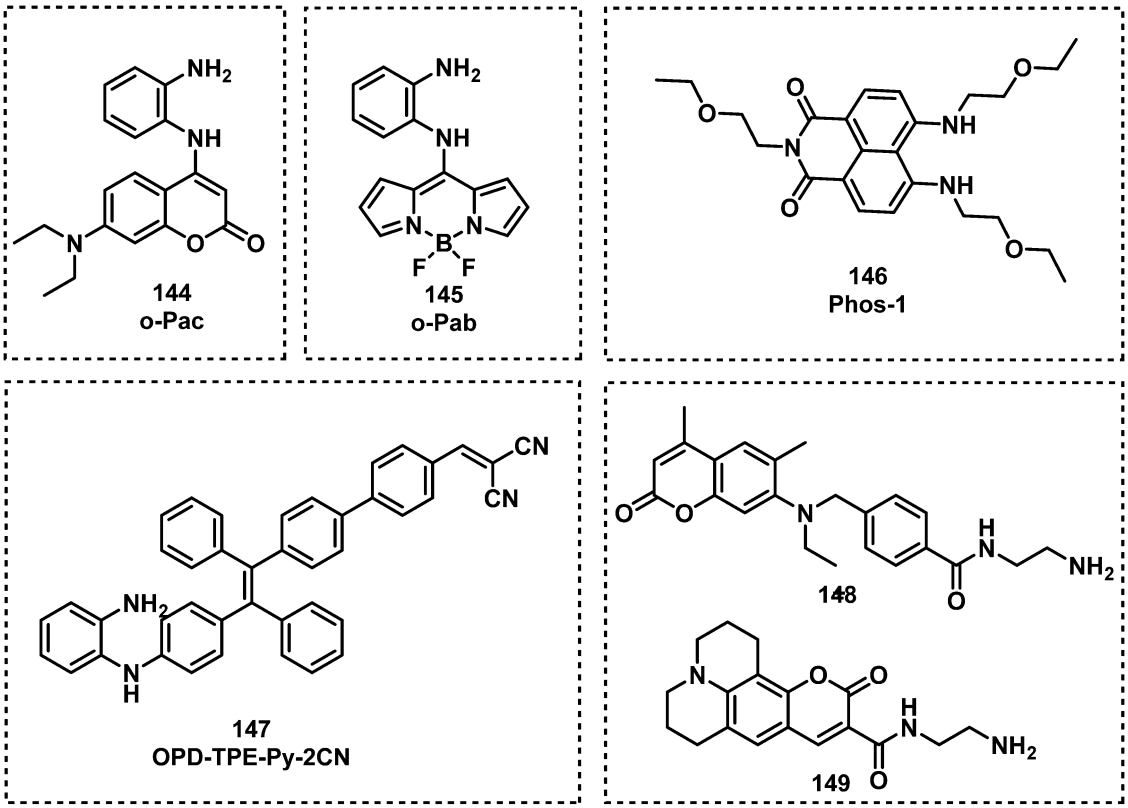

Fig. 26 Chemical structures of fluorescent probes **144–149** for the detection of phosgene.

increase in fluorescence emission. Liu *et al.* reported an anthracene carboximide-based fluorescent probe, **AC-6ED** (**154**), with the ethylenediamine group as the recognition unit for phosgene detection.[165] Probe **154** exhibited a fast response time (less than 20 s) and a low LOD (0.09 nM). Zhang *et al.* reported an *o*-phenylenediamine-functionalized benzothiadiazole fluorescent probe, **BTA** (**155**), for the detection of oxalyl chloride and phosgene.[166] Incubation with either oxalyl chloride or phosgene and **155** resulted in a piperazine-2,3-dione ring or a 2-imidazolidinone ring respectively. This modification resulted in a 28-fold increase in fluorescence emission at 516 nm for oxalyl chloride, and an 8-fold increase at 508 nm for phosgene. The LODs of oxalyl chloride and phosgene were 3 nM and 20 nM, respectively. Wang and co-workers reported fluorescent probe **Phos-2** (**156**) for phosgene, diphosgene, and triphosgene detection.[167] The *o*-phenylenediamine-functionalized naphthalimide afforded a 10-fold increase in fluorescence emission intensity in the presence of phosgene and its analogues (LODs of 0.2 nM for triphosgene and 0.7 nM for diphosgene). Compound **156**-coated test strips facilitated the sensitive (5 ppm) naked-eye detection of phosgene in the gas phase. All chemical structures of these fluorescent probes are given in Fig. 27.

Exploiting the nucleophilicity of imino functional groups, researchers have developed imino-functionalized fluorescent probes for the detection of phosgene. Feng *et al.* developed an iminocoumarin-based fluorescent probe, **IC-phos** (**157**), for the detection of phosgene.[168] Compound **157** reacts with phosgene in less that 2 min. to form a cyclic carbamate product and a ratiometric fluorescence response (482 to 550 nm) with high sensitivity in CH_3CN and vapour (LODs of 27 nM in CH_3CN and 0.1 mg L^{-1} in air). Zhou *et al.* reported the diamine-functionalized naphthalimide fluorescent probe **158** for phosgene detection.[169] Compound **158** exhibited rapid phosgene-mediated carbonylation (20 min) of each amine to form a cyclic tetrahydropyrimidin-2(1*H*)-one ring. This ring formation resulted in a change in fluorescence emission from 511 to 442 nm with an LOD of 2.25 μM. Cheng *et al.* developed the AIE-based fluorescent probe, **DATPE** (**159**), for phosgene detection in THF–H_2O.[170] *o*-Phenylenediamine was chosen as the recognition moiety, while two peripheral triphenylethylene units were employed as the AIEgens. In the presence of phosgene, **159** formed the expected product with an increase in fluorescence emission at 496 nm. Hu *et al.* reported a similar design with the fluorescent probe, **TPE-CI** (**160**), for phosgene detection in THF–H_2O. Probe **160** combined the fluorophores TICT-based 3-benzo[*d*]imidazole-chromen-2-imine and AIE-based tetraphenylethene (TPE),[171] and responded in less than 6 s in THF–H_2O and 2 min in air (LODs of 0.36 μM in THF–H_2O and 0.27 ppm in air). Yang *et al.* developed the fluorescent probe, bis-(1*H*-benzimidazol-2-yl)-methanone (**161**), which was designed to react with phosgene and generate a six-membered fluorescent cyclic carbamylated product (λ_{em} = 428 nm).[172] This fluorescent product formed within 30 s upon exposure to phosgene (LOD of 3.3 nM). Zeng and co-workers developed a 2-(2-aminophenyl)quinazolin-4(3*H*)-one-based

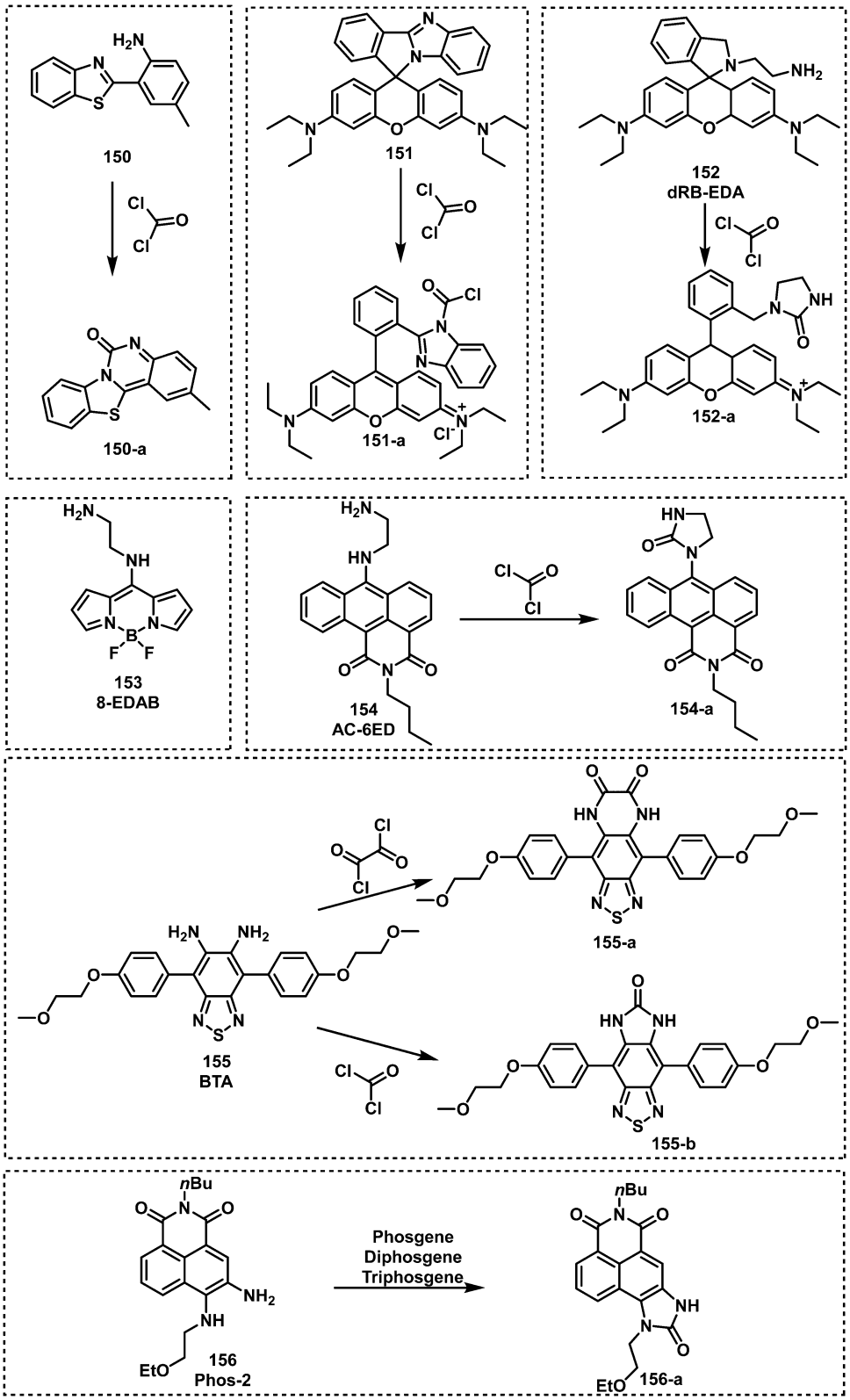

Fig. 27 Chemical structures of fluorescent probes **150–156** developed for the detection of phosgene.

fluorescent probe, **APQ** (**162**), which detects phosgene *via* the formation of the cyclic fluorescent product.[173] The formation of this product was rapid (<20 s) and afforded a clear fluorescence emission at 461 nm. In a study reported in 2021, Yang and co-workers synthesized the fluorescent probe 2-(1*H*-benzimidazol-2-yl)aniline (**163**), which could either detect phosgene or nitrite

(NO_2^-).[174] Compound **163** exhibited a ratiometric change in fluorescence emission (416 nm to 480 nm), a fast response (1 min), and high sensitivity (1.27 nM) for phosgene. However, the addition of $NaNO_2$ to **163** in HCl solution resulted in a decrease in fluorescence emission at 485 nm. In addition, **163**-coated TLC plates and test strips facilitated the naked-eye detection of phosgene in the gas phase and solution. The authors further used **163** to detect NO_2^- in food samples. In 2021, the fluorescent probe **COUBM** (**164**) was developed by Patra and co-workers for the detection of phosgene in $CHCl_3$ and in the gas phase.[175] Probe **164** reacts with phosgene to form a fluorescent cyclic carbamylated product as determined by NMR. An increase in fluorescence emission intensity at 450 nm was ascribed to the inhibition of PeT. AIE-based fluorophores give rise to strong fluorescence emission when aggregated or in their solid-state, but show minimal emission in dilute solutions.[176] In 2021, Hu *et al.* developed **DPA-CI** (**165**), which can detect phosgene in solution and in gaseous conditions *via* a change in TICT and AIE fluorescent mechanisms.[177] **DAP-CI** was developed by incorporating 2-imine-3-benzo[*d*]imidazole and diphenylamine as the enhanced push-pull electronic structure into a coumarin fluorophore. **DPA-CI** exhibited a fast response (less than 8 s in THF and 2 min in air) and a low LOD (0.27 μM in THF and 0.11 ppm in air) (Fig. 28).

Sayar *et al.* exploited the reactivity of 2-aminobenzylamine with phosgene to develop the BODIPY-based fluorescent probe, **BOD-SYR** (**166**).[178] The reaction between phosgene and **166** in CH_3CN resulted in the formation of a six-membered ring that was accompanied by a 300-fold fluorescence enhancement at 511 nm (Fig. 29). An LOD of 179 nM for phosgene was calculated and cyclization occurred rapidly (<2 min). The authors used **166** to develop a handheld phosgene detector, which includes a paper-based indicator cartridge and a black-box apparatus, to issue early warnings during emergencies. The authors placed the cartridge in sealed tubes and exposed it to varying concentrations of phosgene. A smartphone with ultraviolet light-emitting diodes was used to take images of cartridge. Then these authors analysed the images by simple colour code detection to detect phosgene. Based on this strategy, two BODIPY-based fluorescent probes, **167** and **168**, were developed by Cao and co-workers.[179] They evaluated the difference in reactivity and fluorescence response between the asymmetric mono-substituted **167** and symmetric disubstituted **168** (Fig. 29). The addition of phosgene to **167** in CH_3CN showed a considerable fluorescence enhancement at 534 nm, which occurred in <30 s. In contrast, **168** demonstrated a ratiometric fluorescence response (565 to 465 nm) in 2 min when exposed to phosgene in CH_3CN. Moreover, **168** exhibited a linear response to phosgene with an LOD of 2.36 nM. Wang *et al.* expanded this reaction-based strategy with the napthalimide fluorophore to develop the fluorescent probe, **Phos-3** (**169**).[180] Compound **169** underwent

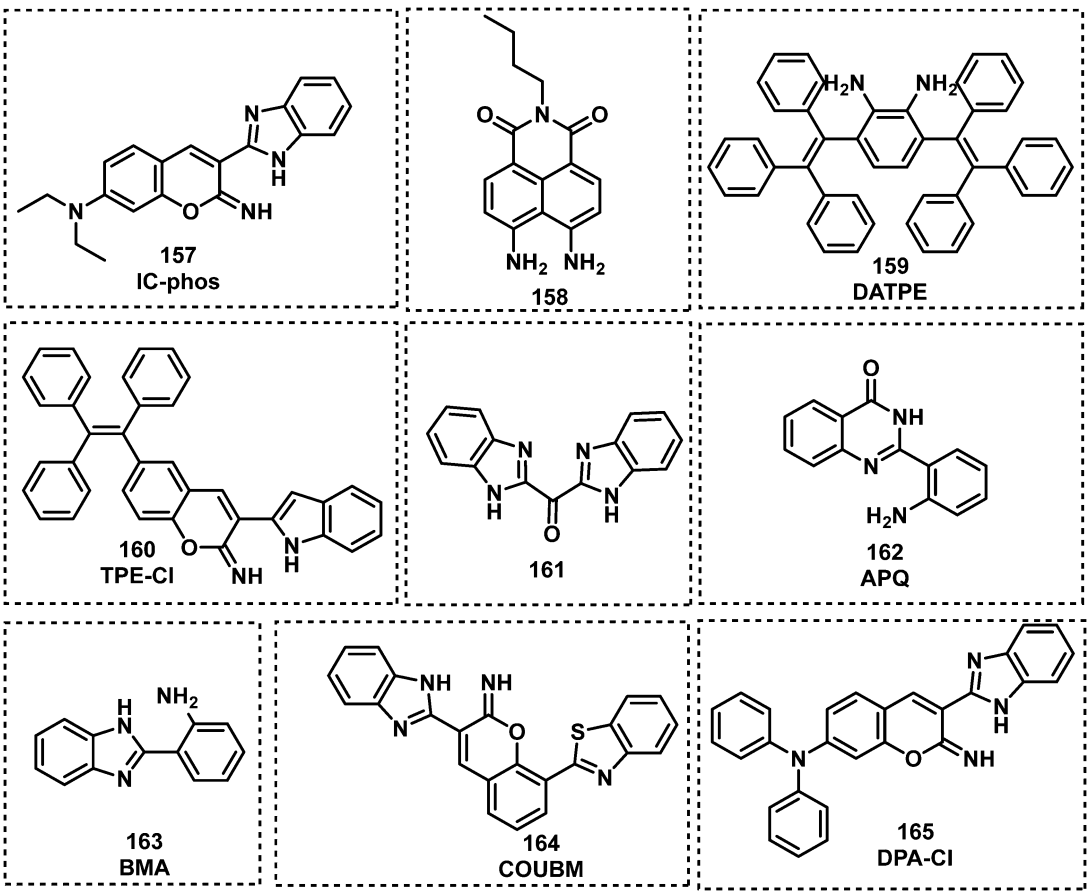

Fig. 28 Chemical structures of fluorescent probes **157–165** developed for the detection of choking agents.

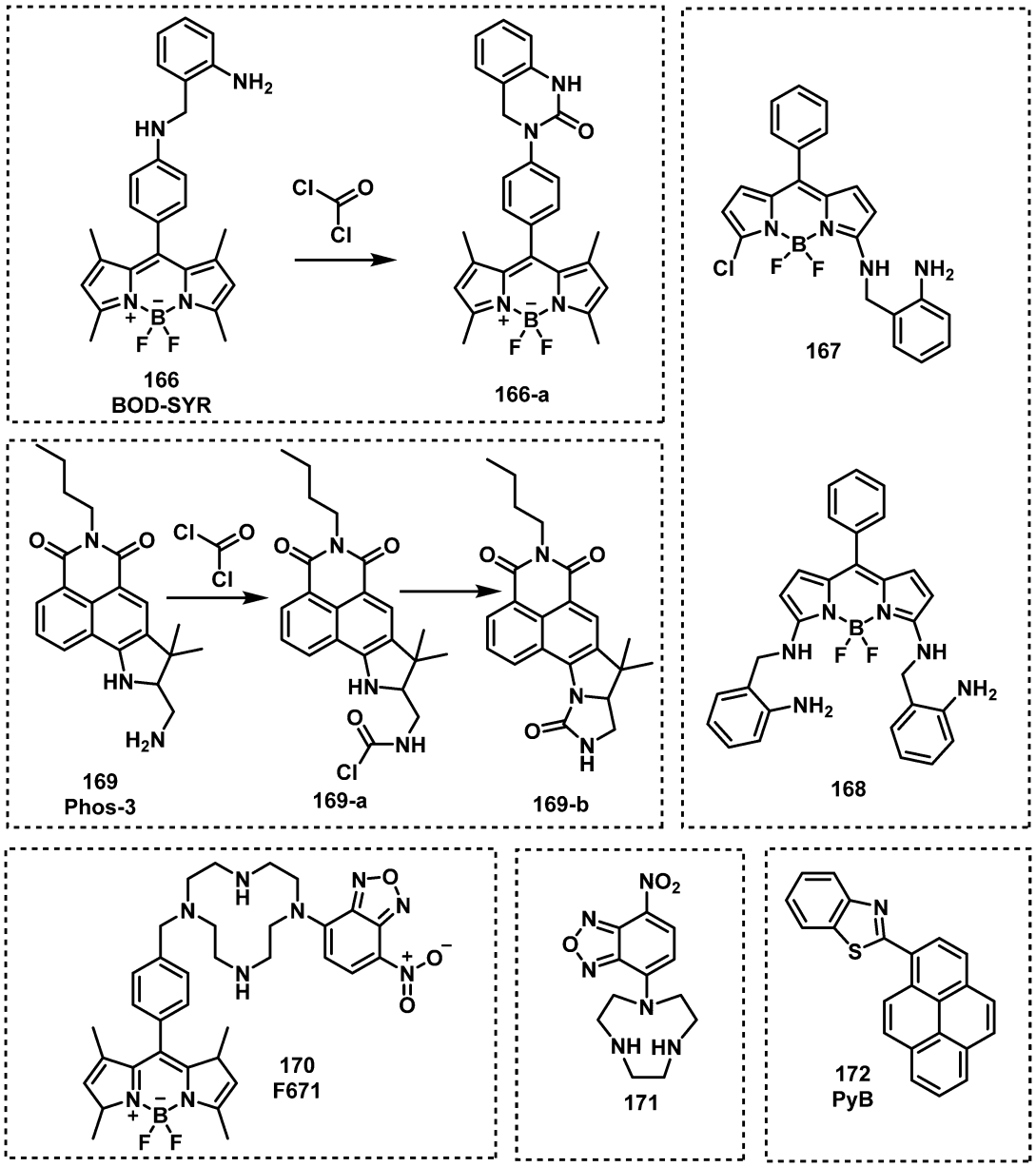

Fig. 29 Chemical structures of fluorescent probes **166–172** developed for the detection of choking agents.

two successive carbamylation reactions upon contact with phosgene (Fig. 29), and was embedded in polymer nanofibres *via* electrospinning, responding rapidly with a high sensitivity towards phosgene (25 ppb). Tan and co-workers designed and synthesized the FRET-based fluorescent probe, **F671** (**170**), for the detection of phosgene.[181] The overlap between the fluorescence emission of the donor (BODIPY) and the absorption of the acceptor (NBD) contributed to the formation of FRET process, resulting in the fluorescence quenching of BODIPY. Incubation with phosgene resulted in a 9.7-fold fluorescence enhancement at 535 nm. Probe **170** exhibited an excellent sensitivity for the detection of phosgene in $CHCl_3$ (0.36 nM) and phosgene vapour (0.14 ppm). It was embedded in degreasing cotton to serve as a specific gaseous phosgene detector. Based on a similar strategy, the You group employed a 1,4,7-triazacyclononane group as the recognition unit for phosgene and 7-nitro-2,1,3-benzoxadiazole (NBD) as the fluorophore for the development of probe **171**.[182] Exposure of **171** to phosgene resulted in the formation of a highly fluorescent bis-carbamylated product with a fluorescence emission intensity at 525 nm. The response of **171** to phosgene occurred within 20 s with excellent sensitivity (1.2 nM). In 2019, the fluorescent probe, **PyB** (**172**), was developed by Gangopadhyay and Mahapatra for the detection of phosgene in $CHCl_3$.[183] The fluorescence response was ascribed to PeT and ICT mechanisms, which were altered by the carbonylation of the nitrogen on the benzothiazole unit. Remarkably, **172** was shown to rapidly detect (<50 s) phosgene at nanomolar concentrations.

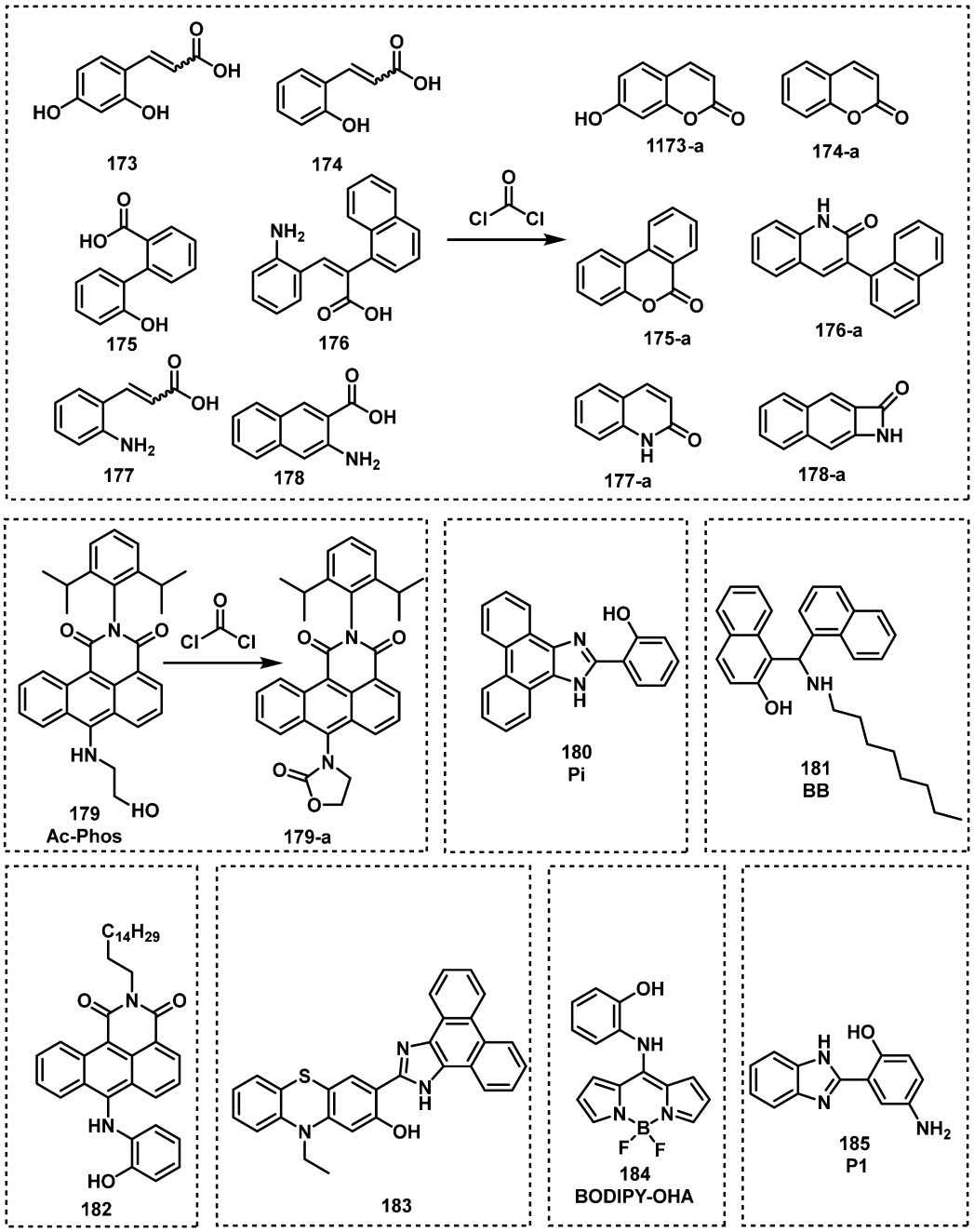

Fig. 30 Chemical structures of fluorescent probes **173–185** based on sequential nucleophilic substitution and followed by cyclization reactions used for the detection of choking agents.

Through using a fundamental understanding in organic chemistry, researchers were able identify various other recognition units for phosgene detection. Hydroxyl-based functionalities are well-known to undergo carbonylation reactions with acid chlorides such as phosgene. A notable report was provided by Kundu and Hwang, in which they identified and exploited the ability of several different molecules (**173–178**) to undergo phosgene-mediated intramolecular cyclization reactions and afford cyclic-based fluorescent products (Fig. 30).[184] Compounds **173–178** were shown to be highly selective for phosgene with low LODs (1–18 nM). In 2018, Hu and co-workers reported the anthracene carboxyimide-based fluorescent probe, **AC-Phos** (**179**), functionalized with an ethanolamine arm.[185] The addition of phosgene to **179** resulted in the formation of **179-a** which gave rise to a 25-fold fluorescence enhancement at 615 nm and a change in colour from red to orange. The authors attributed these observations to the inhibition of ICT. This reaction mechanism provided excellent sensitivity (2.3 nM) with a rapid response (<5 min). Zeng *et al.* reported the ESIPT-fluorescent probe **Pi** (**180**) for phosgene detection in $CHCl_3$.[186] ESIPT was inhibited by phosgene *via* the formation of a cyclic product and this reaction gave rise to a ratiometric fluorescence response.

For example, **180** exhibited a rapid response (within 2 min) and a low LOD (0.14 μM). Gangopadhyay and Mahapatra developed a simple, targeted Betti base, **BB** (**181**) for the fluorescence detection of phosgene.[187] The amino and hydroxyl groups of BB reacted with phosgene to form a six-membered ring and produced a large fluorescence increase at 430 nm. This reaction with phosgene occurred in <1 min while displaying good sensitivity (0.4 μM). The Yoon group developed fluorescent probe, **182**, which consisted of an *o*-hydroxyaniline functionalized anthracene carboxyimide.[188] In the presence of phosgene, **182** formed a cyclic carbamate moiety and exhibited a 920-fold enhancement in fluorescence at 484 nm. The reaction was rapid (<15 s) and had high sensitivity (4.6 nM). Wang *et al.* reported the phenothiazine-based fluorescent probe **183**, containing hydroxyl and imidazolyl groups as the recognition units for phosgene.[189] Compound **183** was found to be weakly emissive by itself in $CHCl_3$, but upon addition of phosgene, the fluorescence intensity at 492 nm substantially increased. With the sensing properties identified, a **183**-loaded polymeric film was shown to detect phosgene vapour confirming potential practical utility. Chen *et al.* reported the *o*-hydroxyaniline-functionalized fluorescent probe **BODIPY-OHA** (**184**) for phosgene detection.[190] The adjacent hydroxyl and amino groups of the probe coupled with phosgene to form a benzoxazolinone product, thereby exhibiting a marked colour change from green to yellow and a significant turn-on response at 530 nm. Compound **184** was incorporated onto portable strips to serve as a test kit for the detection of phosgene. Li *et al.* reported the ESIPT-based fluorescent probe, **P1** (**185**), for phosgene detection.[191] The hydroxyl and imidazole groups of **185** reacted with phosgene to form a six-membered ring product. Due to the inhibition of ESIPT, a ratiometric fluorescence response was observed in CH_2Cl_2 with a decrease in fluorescence emission at 540 nm and increase at 358 nm, displaying a LOD of 5.3 nM.

Kim *et al.* reported the catechol-based fluorescent probe, **1-CN** (**186**) for the detection of phosgene in CH_3CN (Fig. 31).[192] Compound **186** rapidly reacted (<3 s) with phosgene to form a cyclic carbonate ester and afforded an 850-fold increase in fluorescence emission intensity at 516 nm. The Song group exploited the propensity of hydrazides to form oxadiazolones with phosgene (Fig. 31) and synthesized a series of hydrazide-based fluorescent probes **187–191**.[193] As an example, **188** exhibited the greatest response towards phosgene (1.5 s) with a low LOD (0.15 nM). Du and co-workers synthesized the Si-rhodamine-based fluorescent probe **SiR-amide** (**192**) for the detection of phosgene in CH_3CN.[194] This strategy exploited the dehydration of amides to the corresponding nitrile functionalities. In this study, the synthetic transformation was performed in CH_3CN, which led to a 20-fold increase in fluorescence emission intensity at 679 nm (Fig. 31). Similarly, Gangopadhyay *et al.* functionalized anthracene with a primary amide to afford the fluorescent probe **9-AM** (**193**).[195] The phosgene-mediated conversion of the primary amide to nitrile was rapid (<1.5 min) and afforded a substantial increase in fluorescence emission intensity at 440 nm.

Oximes are also known to undergo dehydration reactions with phosgene to form the corresponding nitrile functionality. Kim *et al.* reported the BODIPY-based fluorescent probe **1-oxime** (**194**) for the detection of phosgene in 2017.[196] The interaction between **194** and phosgene in CH_3CN, transformed the *meso*-oxime to a *meso*-nitrile, resulting in a large fluorescence increase at 570 nm. Compound **194** exhibited a fast response (10 s) and a low LOD (0.09 ppb). In 2019, Bai and co-workers developed the ESIPT-based fluorescent probe, **HBT-Phos** (**195**), for the detection of phosgene.[197] Probe **195** consisted of the traditional ESIPT fluorophore 2-(2′-hydroxyphenyl)benzothiazole (**HBT**) that was functionalized with an oxime moiety (Fig. 32),[198] and was found to react with phosgene in CH_3CN and undergo dehydrative synthetic transformation to afford the corresponding nitrile moiety. This transformation resulted in a 1750-fold increase in fluorescence emission intensity at 474 nm. In 2019, Maiti and co-workers reported an oxime-functionalized napthalimide fluorescent probe, **R1** (**196**), for phosgene detection.[199] In contrast to oximes alone, the presence of an adjacent hydroxyl unit resulted in the formation of a fused naphtha-isoxazole fluorescent product when **196** was exposed to phosgene in CH_3CN. This phosgene-mediated transformation of **196** resulted in a ratiometric change in fluorescence emisson intensity (577 to 495 nm). In 2020, Ma *et al.* reported the iridium(III)-based metal complex **Ir-OXIME** (**197**) for the phosphorescent detection of phosgene in $CHCl_3$.[200] This metal complex was initially found to have weak phosphorescence, which was believed to be due to the quenching from the oxime moiety. The transformation of oxime **197** to the corresponding nitrile by phosgene was shown to occur in $CHCl_3$ and resulted in a substantial increase in phosphorescence emission at 688 nm. In 2020, the coumarin based fluorescent probe, **DCCO** (**198**), was developed for the detection of phosgene in CH_3CN–H_2O and the gas phase by Paul and co-workers.[201] As expected, phosgene resulted in the conversion of **198** into the corresponding nitrile derivative, which led to a 13-fold fluorescence enhancement at 488 nm. In 2020, Huang and co-workers incorporated oxime functionality onto the naphthalimide fluorophore to afford fluorescent probe **199** for the detection of phosgene in CH_3CN.[202] Probe **199** was shown to be initially nonfluorescent, but upon contact with phosgene, a subsequent Beckmann rearrangement resulted in the formation of 4-acetamido-1,8-naphthalimide, which exhibited bright blue fluorescence emission (λ_{em} = 450 nm). More recently, Zhu and co-workers developed the fluorescent probe **200**, which consisted of oxime-functionalized 5-chlorosalicylaldehyde.[203] Compound **200** exhibited a significant increase in fluorescence emission at 410 nm after incubation with phosgene in CH_2Cl_2. Reusable **200**-coated test strips were prepared and used as a point-of-use phosgene testing.

Although a number of fluorescent probes for the detection of choking agent have been developed, the selectivity of these probes remains limited, and they can react with formaldehyde and nitric oxide. Only a handful of chocking agents were validated in the gas phase. Most of the fluorescent probes developed for choking agents have rapid response rate (less than 2 min). However, the fluorescent probes (**195**, **199**, **200**) using oxime as recognition unit are less reactive (over 10 minutes). Among all probes for choking agents, ethylenediamine-based probes, such

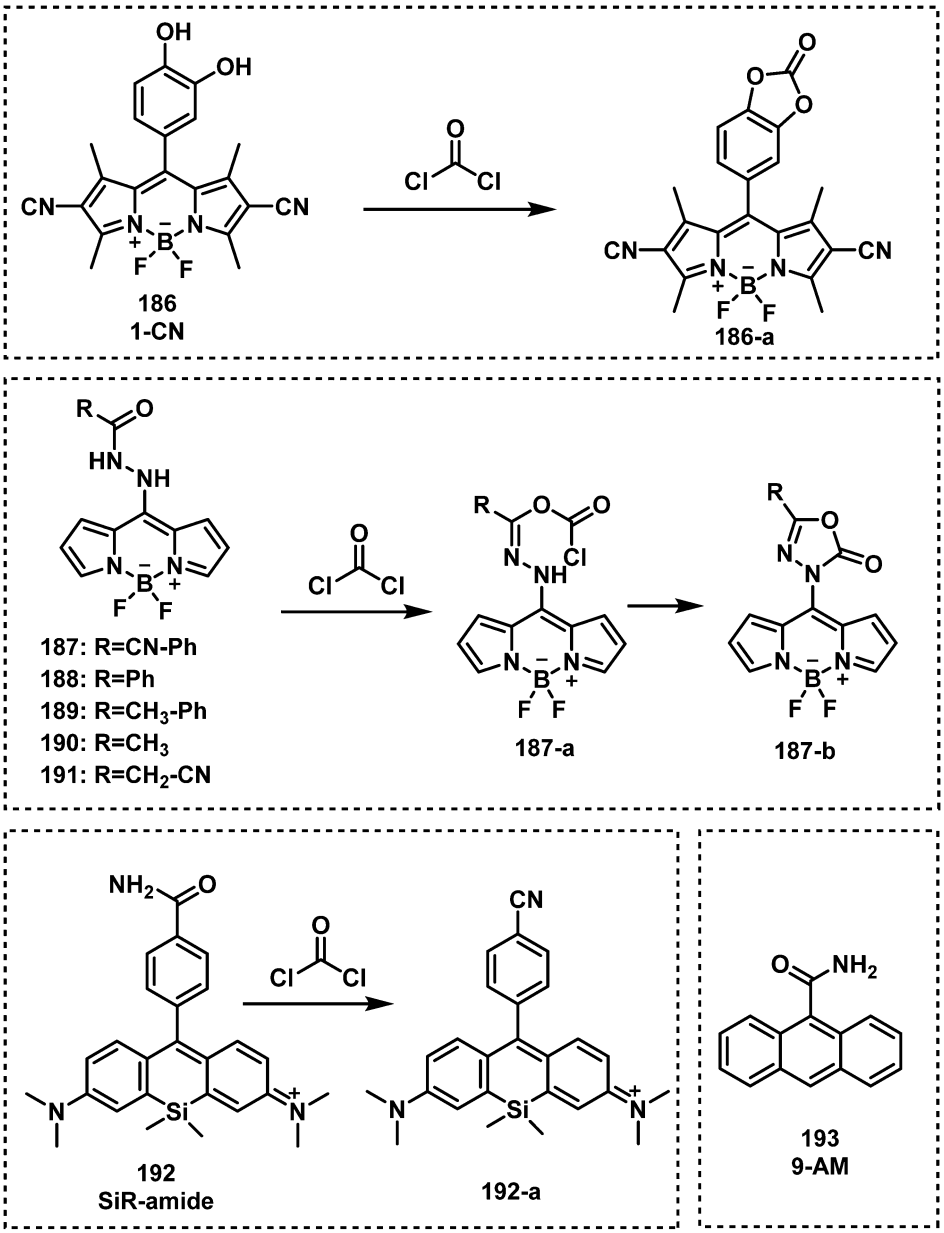

Fig. 31 Chemical structures of fluorescent probes **186–193** for choking agent detection.

as **8-EDAB** (**153**) and **AC-6ED** (**154**), exhibited a better sensitivity (LOD less than 0.12 nM) and faster response rate (less than 20 s).

6. Fluorescent probes for blood agents

Cyanide is the least toxic of the ''lethal'' chemical agents. The most representative examples of blood agents are hydrogen cyanide (HCN), cyanogen chloride (ClCN), and sodium cyanide (NaCN). Interestingly, these chemicals were first believed to only exert toxicity on blood cells. This misconception led to their classification as blood agents. In fact, the main target of toxicity for blood agents is the inhibition of cytochrome *c* oxidase in mitochondria. This behaviour prevents oxidative phosphorylation and causes cellular ATP-deficiency.[204,205] Like nerve agents, blood agents are fast-acting (several minutes) and cause death at low doses (2.8 mg kg^{-1} for humans by oral administration). Large quantities of HCN were used during WWI; however, during combat it was surprisingly found to be suboptimal. During WWII, Nazi Germany used Zyklon B, which consisted of HCN, a warming eye irritant and diatomaceous earth, to kill at least a million people in its Nazi concentration camps. Today, CN^- is widely used in industry for gold mining, steel manufacture, and metal electroplating purposes. Therefore, similar to phosgene, CN^- is now classed as a dual-use chemical by the United Nations Office for Disarmament Affairs. Surprisingly, recent studies indicate that CN^- ions are generated within cells, playing crucial physiological roles to support

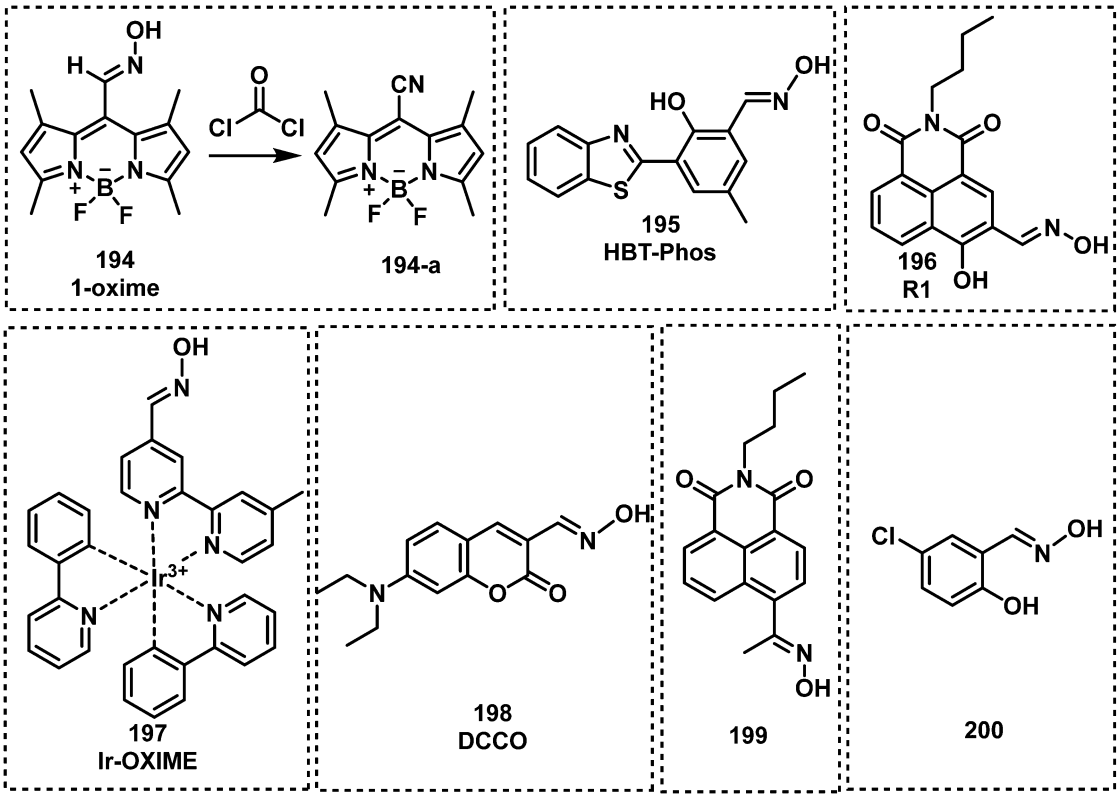

Fig. 32 Chemical structures of fluorescent probes **194–200** utilizing the oxime moiety for the detection of choking agents.

Table 5 Acute exposure guideline levels of blood agents

		10 min	30 min	60 min	4 h	8 h
ppm						
Hydrogen cyanide	AEGL 1	2.5	2.5	2.0	1.3	1.0
	AEGL 2	17	10	7.1	3.5	2.5
	AEGL 3	27	21	15	8.6	6.6
mg m^{-3}						
Sodium cyanide	AEGL 1	5.0	5.0	4.0	2.6	2.0
	AEGL 2	34	20	14	7.0	5.0
	AEGL 3	54	42	30	17	13
mg m^{-3}						
Potassium cyanide	AEGL 1	6.6	6.6	5.3	3.5	2.7
	AEGL 2	45	27	19	9.3	6.6
	AEGL 3	72	56	40	23	18

cellular function.[206,207] Cyanide is unique among CWAs, whose long-term lethal dose is much greater than short-term lethal dose since it can be detoxified at a relative stable rate by rhodanese and 3-mercaptopyruvate sulfurtransferase in the human body. The AEGLs of blood agents were listed in Table 5. As a result of its toxicity and role in several different applications, extensive work has been devoted to the development of fluorescent probes for the detection of CN^- ions.[29–34] A survey of recent literature suggests a scarcity in fluorescent probes for ClCN. Therefore, we anticipate the exploitation of smart sensing strategies for this toxic blood agent. In this section, we summarize select examples of recently developed fluorescent probes for the detection of cyanide. At this moment in time, there are only a limited number of reported fluorescent probes for the detection blood agents (Fig. 33). Most of these strategies rely on the nucleophilic reactivity of CN^-. Other strategies for cyanide detection are based on the interaction with metal ions, boronic acid derivatives, and H^+. Probes suitable for the detection of blood agents are probes **201–285** (Fig. 34–47).

It is well known that the electrophilicity of the carbon-nitrogen imine (C=N) is greatly enhanced as a cationic species. Thus, researchers have exploited several cationic iminum containing compounds such as indoliums (*i.e.*, cyanine dye) for the detection of cyanide (Fig. 34).[208] In general, CN^- can undergo nucleophilic addition with the cationic C=N unit on the indolium of cyanines and hemicyanine dyes, which blocks π-conjugation and results in a change to their photophysical properties. Raymo *et al.* exploited the ability of spiropyrane to detect CN^-. In the presence of CN^-, the [1,3]oxazine ring of spiropyranes opens to form a 4-nitrophenylazophenolate chromophore with the concomitant appearance of an intense band in the visible region of the absorption spectrum.[209,210] As such, these probes are not fluorescent probes but colorimetric probes. The Sirisaksoontorn group reported a similar spiropyran-based colorimetric probe, **SP** (**201**), for CN^- detection.[211] This group demonstrated the ability of **201** to detect CN^- ion concentrations in cassava leaves. Maurya *et al.* reported spiropyran fluorescent probe **L4** (**202**) for cyanide detection.[212] Compound **202** reacted with CN^- ions in CH_3CN–H_2O which resulted in a fluorescence emission increase at 520 nm. Dong *et al.* synthesized the naphthopyran derivative **L** (**203**) for the ratiometric fluorescence detection of CN^- ions in aqueous media and using

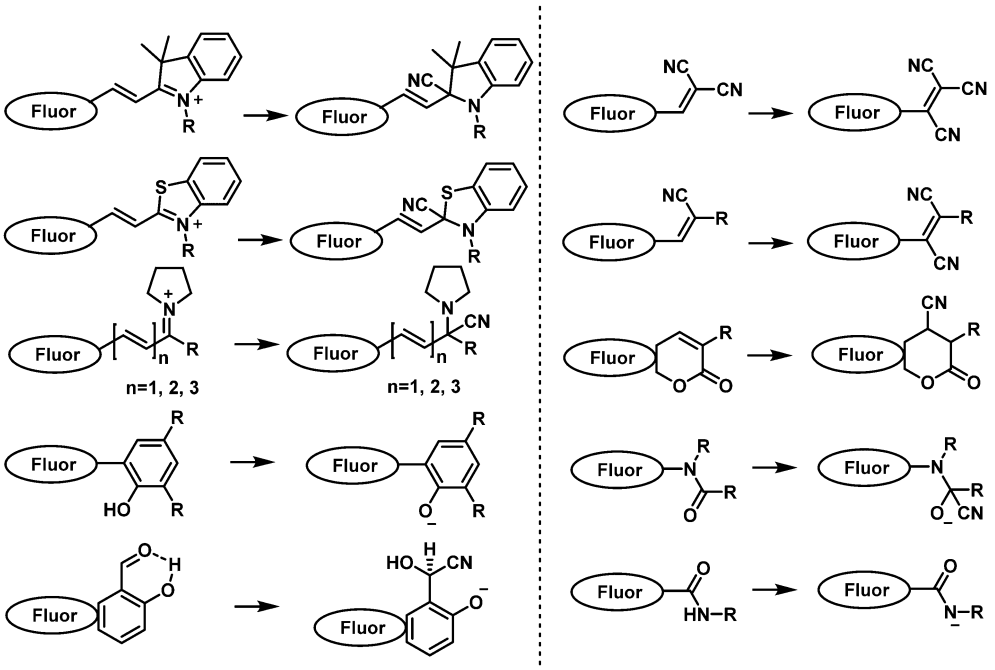

Fig. 33 Schematic representation of the common strategies used to generate fluorescent probes for the detection of blood agents.

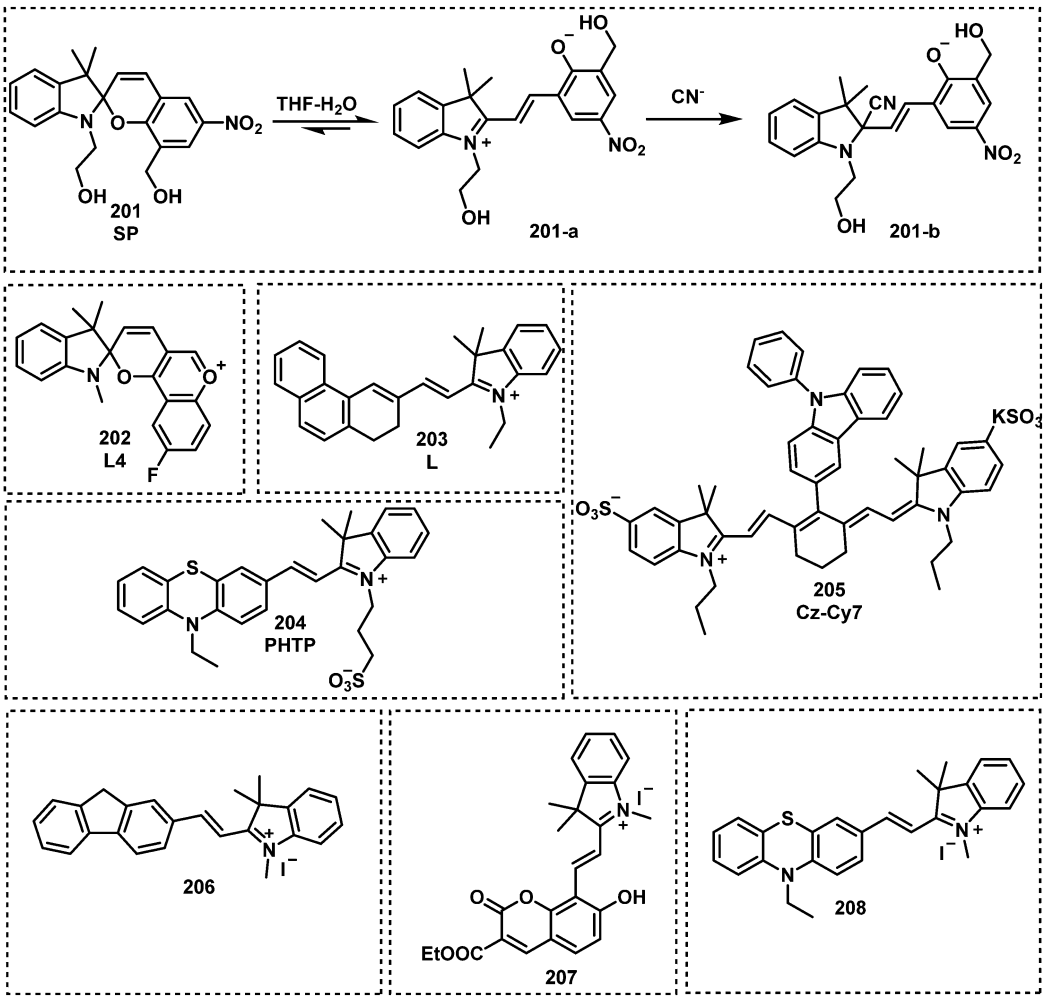

Fig. 34 Chemical structures of fluorescent probes **201–208** based on an indolium scaffold.

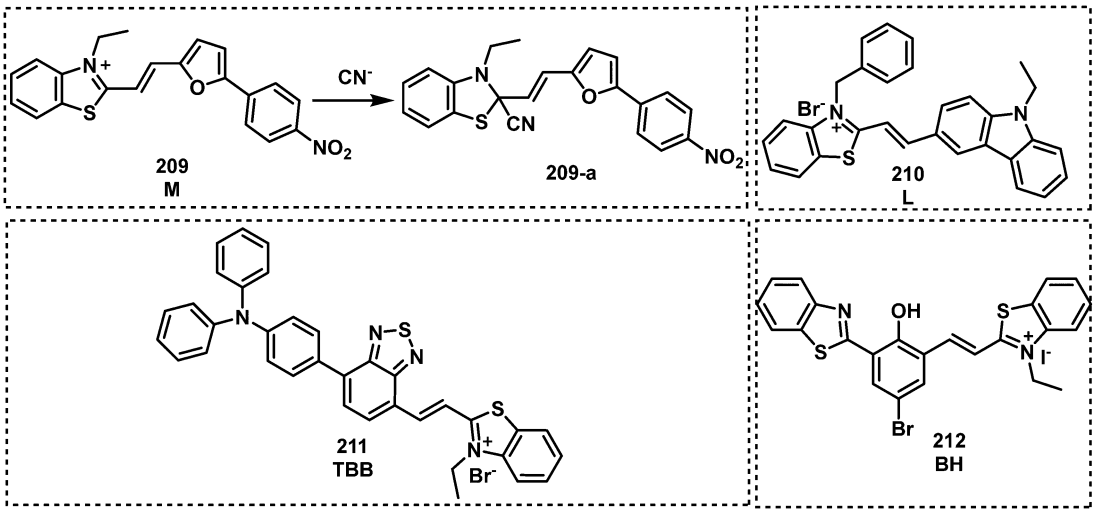

Fig. 35 Chemical structures of fluorescent probes **209–212** utilizing a benzothiazole moiety for the detection of cyanide ions.

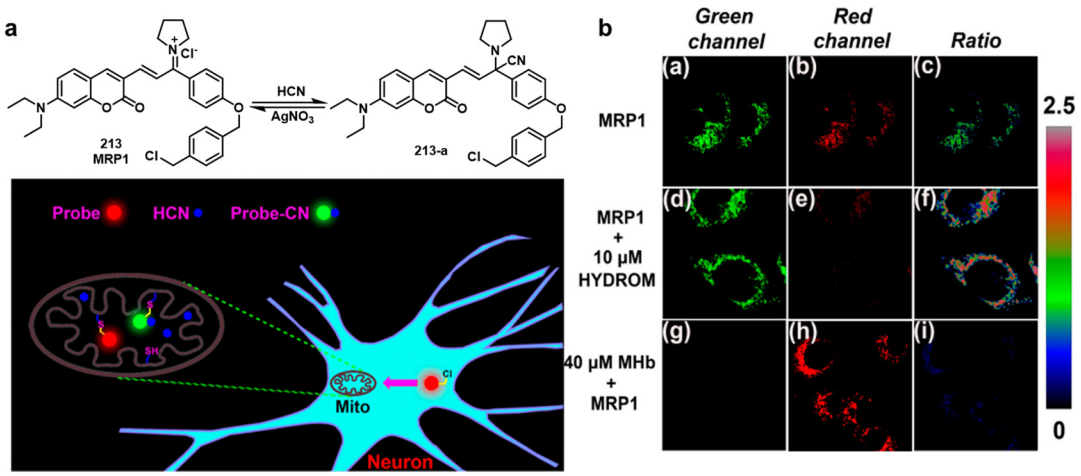

Fig. 36 (a) Proposed detection mechanism of **213** for mitochondrial HCN. (c) Visualization of endogenous mitochondrial HCN in PC12 cells *via* laser confocal microscopy. Reproduced with permission from ref. 207. Copyright (2018) American Chemical Society.

test strips.[213] Probe **203** was shown to rapidly respond to CN^- (90 s) with an LOD of 0.756 μM. Zhu and co-workers reported the dual-channel fluorescent probe **PHTP** (**204**), to detect either CN^- or bisulfite (SO_3^{2-}) ions in DMF–H_2O.[214] **204** was initially weakly emissive, however, the addition of CN^- or SO_3^{2-} to **204** – in DMF–H_2O resulted in a substantial increase fluorescence emission at 507 nm or 450 nm, respectively. Compound **204** displayed an LOD of 98 nM for CN^- and an LOD of 3.0 nM for SO_3^{2-}. The Li group developed the carbazole-cyanine-based fluorescent probe **Cz-Cy7** (**205**), which could detect either CN^- or HClO.[215] For example, **205** exhibited a fluorescence emission at 795 nm, which decreased upon nucleophilic addition of CN^- ions to the indolenium moiety. HClO underwent an oxycracking reaction with the double bond of **Cz-Cy7** to decrease the fluorescence intensity at 740 nm. The LODs for cyanide and HClO were measured to be 0.09 μM and 14 nM, respectively. On the basis of a similar strategy, Dong,[216] An[217] and Li[218] used fluorene coumarin phenothiazide as the fluorescent unit and indolium as the recognition unit to develop a series of fluorescent probes, **206–208**, for cyanide detection.

Similar to cationic indolium, benzothiazole units have been used to develop cyanine-based species for the detection of CN^- ions (Fig. 35). Wang *et al.* developed the turn-off fluorescent probe **M** (**209**) for the detection of CN^- ions. The nucleophilic addition of CN^- to the cationic iminium of the benzothiazole unit resulted in a fluorescence decrease at 550 nm in DMSO–H_2O.[219] Structure **209** was successfully used for the detection of CN^- ions in HeLa cells. Hou *et al.* synthesized benzothiazolium-ethylcarbazole derivate **L** (**210**) for the detection of CN^- ions in a neutral aqueous solution.[220] Compound **210** exhibited a rapid response, a large Stokes shift (260 nm) and an LOD of 0.339 μM. Fluorescence colocalization studies revealed the localization of **210** at the mitochondria, which enabled the study of CN^- at the mitochondria. Zhai and co-workers reported the benzothiazolium-based turn-on fluorescent probe, **TBB** (**211**), for the detection of CN^- in THF–H_2O.[221] Similar to the other design strategies,

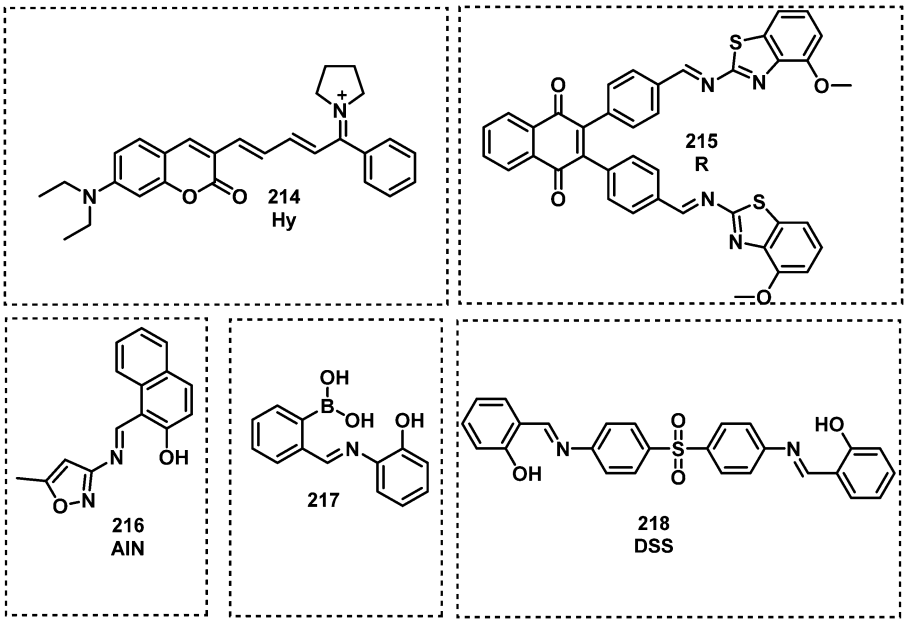

Fig. 37 Chemical structures of **214–218,** fluorescent probes for cyanide detection.

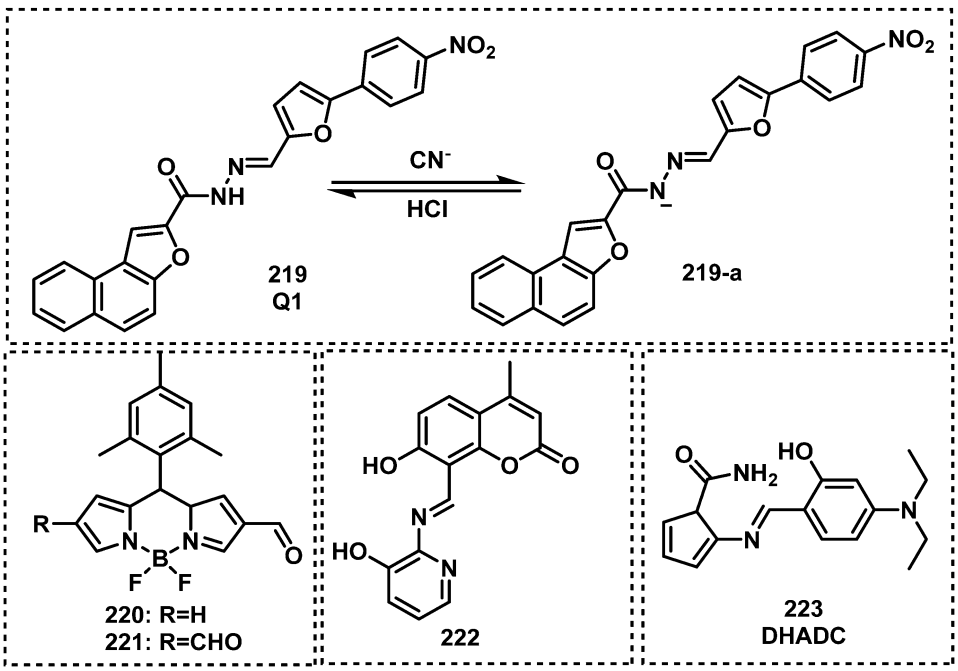

Fig. 38 Chemical structures of fluorescent probes **219–223** designed for the detection of cyanide.

CN^- reacted with the C═N bond of benzothiazolium to block π-conjugation and resulted in a substantial increase in fluorescence emission at 589 nm. For example, **211** reacted with CN^- within 3 min and afforded an LOD of 134 nM. In 2021, Erdemir and Malkondu developed the ICT/ESIPT-based probe **BH** (**212**) for the detection of CN^- ions in DMSO–H_2O.[222] The addition of CN^- resulted in both fluorogenic (nonfluorescent to fluorescent) and chromogenic colour (from blue to yellow) changes. Further, **212** was used to detect CN^- ion concentrations in lake water samples and apricot seeds.

The Sessler group reported the mitochondria-specific fluorescent probe **MRP1** (**213**) for cyanide detection in neurons, HepG2, and PC12 cells.[207] Probe **213** consisted of coumarin (reporter), pyrrolidinium as the recognition unit and a benzyl chloride substituent for mitochondrial retention. It was successfully used to image different concentrations of exogenous HCN

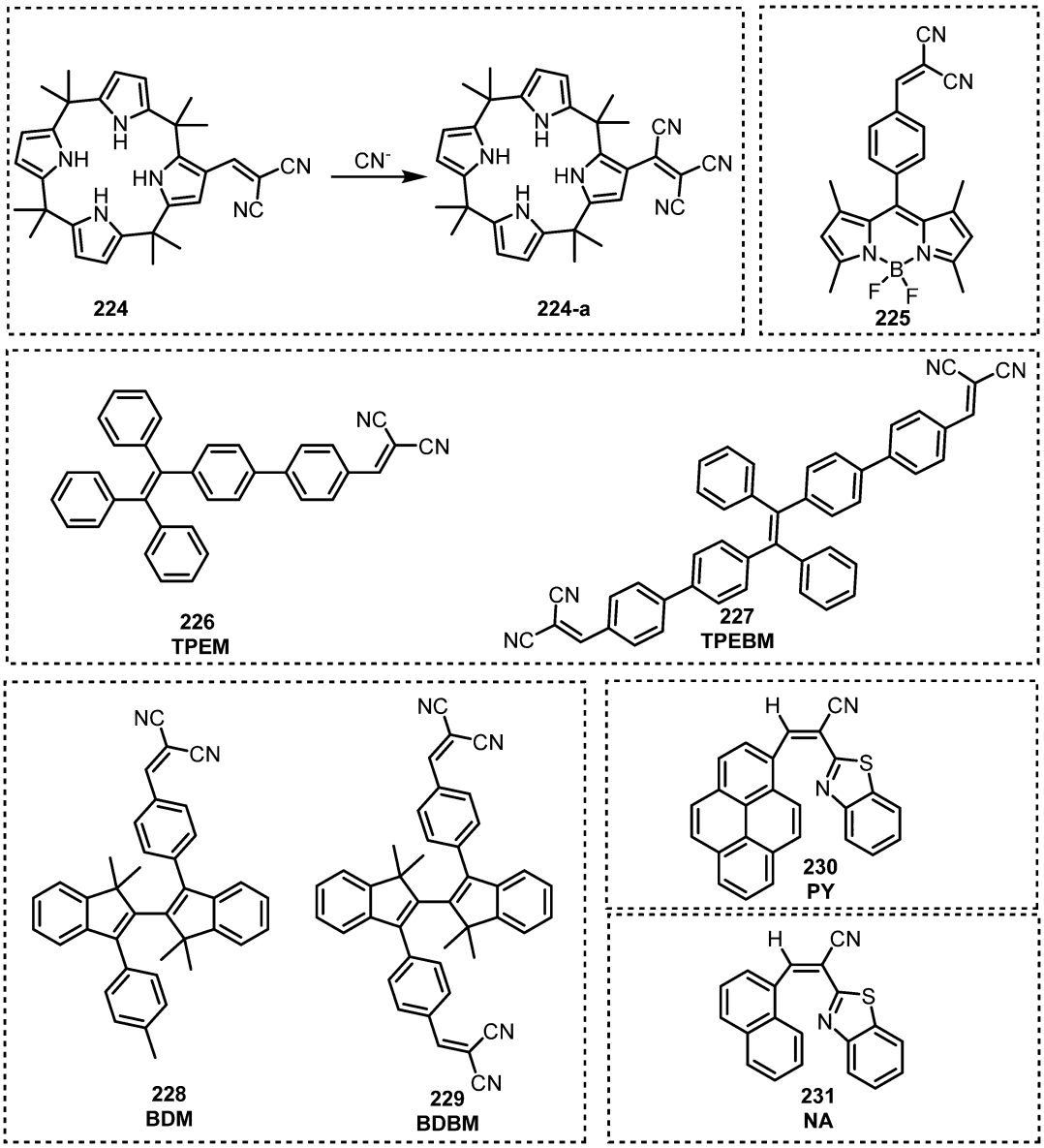

Fig. 39 Chemical structures of fluorescent probes **224–231** utilizing mono/di-cyanovinyl groups.

in the mitochondria of HepG2 cells. Endogenous HCN, which was stimulated by hydromorphine (HYDROM), was successfully identified in the mitochondria of PC12 cells and neurons. Long and co-workers extended the carbon chain of **213** to develop the near-infrared (NIR) fluorescent probe **Hy** (**214**).[223] Compound **214** displayed an initial fluorescence emission at 688 nm and the addition of CN^- ions resulted in a ratiometric change in fluorescence emission (from 688 to 519 nm). Kumar *et al.* reported the naphthoquinone-based fluorescent probe **R** (**215**),[224] which exploits the nucleophilic addition of CN^- ions of imines. This reaction resulted in an increase in fluorescence emission at 429 nm. This probe was used as a practical tool for CN^- detection in tap water and in food. Jung *et al.* reported the imine-based naphthol fluorescent probe **AIN** (**216**) for cyanide detection in DMF.[225] It was nonfluorescent, but with the addition of CN^- ions a new fluorescence emission at 498 nm was observed. Wang *et al.* reported the boronic acid-based fluorescent probe **217** for the detection of CN^- ions in CH_3CN–H_2O.[226] Probe **217** selectively detected cyanide *via* the nucleophilic addition of CN^- to the imine moiety of the boronic acid-based receptor. Based on a similar strategy, Wan *et al.* reported **DSS** (**218**), a fluorescent probe derived from a Schiff base, for the detection of cyanide and F^-.[227] Upon the addition of cyanide or F^-, new fluorescence emission signals were observed at 475 nm or 536 nm, respectively. The sucessful detection was demonstrated in DMSO–H_2O.

Qu *et al.* reported the fluorescent probe **Q1** (**219**) for the detection of cyanide based on a simple deprotonation mechanism.[228] In the prescence of CN^- leads to the formation of **219-a** *via* deportonation with a fluorescence decrease at 564 nm and colour change from yellow to orange. While **219-a** showed an immediate colour and fluorescent recovery within a short time of 10 s after the addition of HCl. Remarkably,

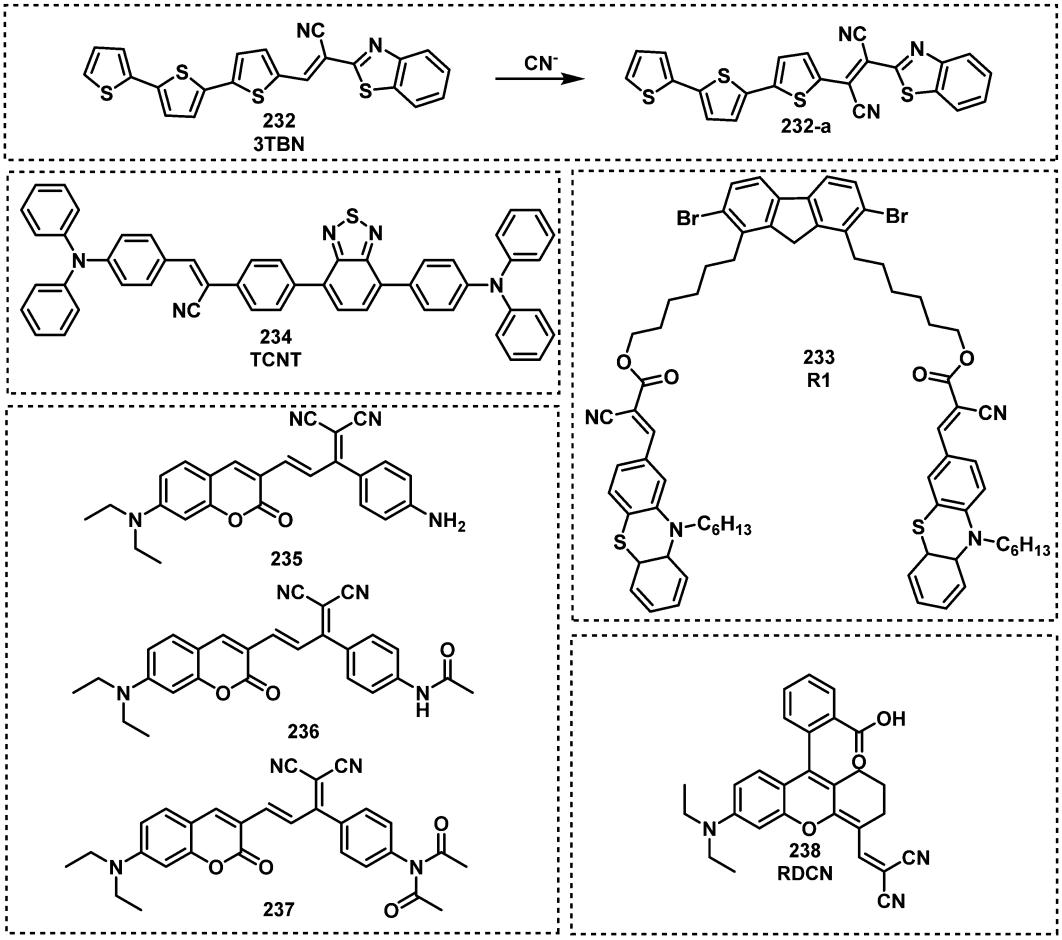

Fig. 40 Chemical structures of fluorescent probes **232–238** developed for the detection of cyanide ions.

219 exhibited the ability to be recycled at least 10 times with fast response times (within 3 s). Wu and co-workers reported the β-formyl-BODIPY-based fluorescent probes **220** and **221** for the detection of CN^- ions in CH_3CN–H_2O.[229] This strategy exploited the reactivity of aldehydes to undergo nucleophilic addition with CN^-. A ratiometric change in fluorescence emission intensity was observed for **221** (from 523 to 670 nm) when treated with CN^-. More recently, Wu *et al.* developed the imine-functionalized coumarin fluorescent probe, **222**, for the detection of CN^- ions in DMSO–H_2O.[230] Kim *et al.* developed the turn-on fluorescent probe **DHADC** (**223**) to detect Zn^{2+} and cyanide.[231] This probe displayed a fluorescence enhancement at 508 nm after treatment with Zn^{2+}. With cyanide, **223** exhibited an increase in fluorescence at 528 nm. The LODs of **223** were 2.55 and 44.6 μM for Zn^{2+} and cyanide, respectively.

Cyanovinyl functionalities are commonly used to increase the π-conjugation of chromophores. In 2009, the Lee group demonstrated for the first time the use of dicyanovinyl to detect CN^- ions, which employed calix[4]pyrrole as the receptor.[232] CN^- ions could attack the α-position of the dicyanovinyl unit to generate stabilized anionic species **224-a**. Lee and co-workers extended this strategy to the development of the BODIPY-based fluorescent probe **225** for cyanide detection.[233] A 43-fold increase in fluorescence emission (λ_{em} = 510 nm) was observed after the addition of CN^- to a **225**-containing THF–H_2O solution. In 2014, the Yu group developed a class of TPE-based fluorescent probes, **TPEM** (**226**) and **TPEBM** (**227**) for the detection of CN^- ions in DMSO–H_2O.[234] These two probes possessed AIE photophysical properties with solvatochromism. These two probes, **226** and **227**, were used to detect CN^- ions in aqueous solutions with the aid of the surfactant cetyltrimethylammonium bromide (CTAB). Both displayed low LODs (0.2 μM) and a rapid response (100 s) that enabled their use for the test paper-based detection of cyanide. Based on a similar strategy, two 2,2'-biindenyl-based fluorescent probes, **BDM** (**228**) and **BDBM** (**229**), were developed by Chen and co-workers in 2015 for cyanide detection in THF/dioxane–H_2O.[235] Both **228** and **229** were functionalized with a dicyanovinyl unit for CN^- ion detection. Notably, **229** exhibited an LOD of 0.29 μM and a short response time of 100 s. In 2017, Hua and co-workers reported the FRET-based fluorescent probes **PY** (**230**) and **NA** (**231**) for cyanide detection.[236] The FRET acceptor and donor were aryl moiety and benzothiazole group, respectively. Both probes exhibited ratiometric responses in the presence of cyanide. Among them, probe **231** exhibited a fast response rate (within 3 s) and a low LOD (63 nM). These probes were absorbed onto silica gel plates for the naked-eye detection of CN^- ions.

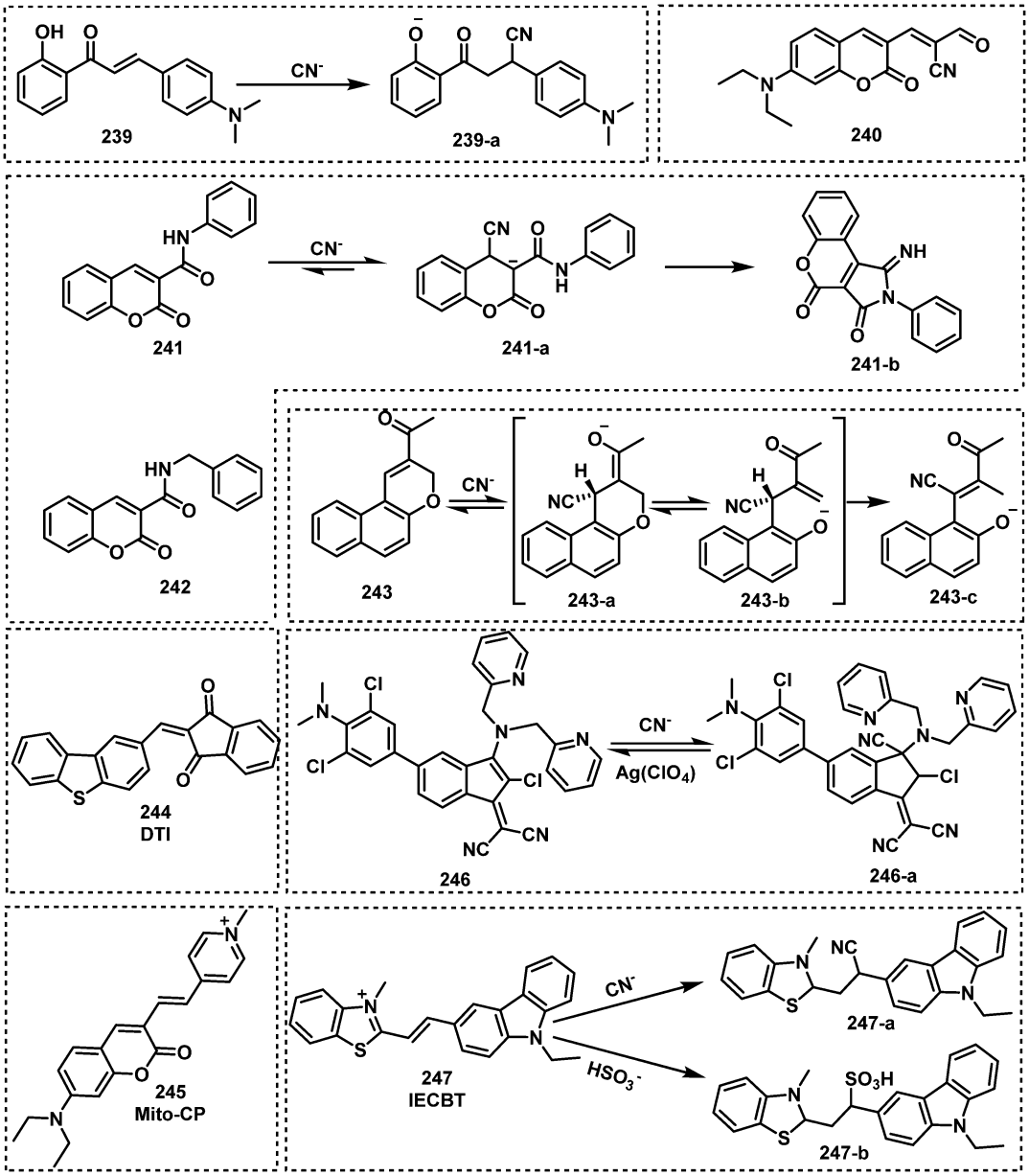

Fig. 41 Chemical structures of fluorescent probes **239–247**.

Niu *et al.* reported the oligothiophene-conjugated benzothiazole **3TBN** (**232**) for the detection of CN^- ions in DMSO–H_2O (Fig. 40).[237] This scaffold possessed the CN^- reactive unit cyanovinyl electrophilic C=C group. In the presence of CN^-, a notable turn-on fluorescent response was observed at 525 nm due to the attack of CN^- on the β-cyanovinyl carbon of **232**. The probe was used to evaluate CN^- ion concentrations in food samples and live HeLa cells. Sivalingam and co-workers designed and synthesized the D–π–A fluorescent probe **R1** (**233**) for the detection of CN^- in solid- and solution-states.[238] In the presence of CN^-, ICT from the phenothiazine (D) to the cyanovinyl unit (A) was completely blocked, and resulted in fluorescence quenching at 618 nm in THF. Due to the AIE effect of **233**, the probe also exhibited strong orange fluorescence in the solid state. Upon contact with CN^-, the orange fluorescence of **234** coated silica gel plates was quenched accompanied with a colour change from yellow to colourless. Deng *et al.* reported the red-emitting AIE fluorescent probe **TCNT** (**234**) for the detection of CN^- ions in DMF-PBS.[239] The reaction between CN^- ions and **234** resulted in an increase in the fluorescence emission intensity at 596 nm. Due to its excellent cell permeability and biocompatibility, **234** was used to study the distribution of CN^- ions in live HepG-2 cells and *ex vivo* organs. Aydıner developed three coumarin-based fluorescent probes, **235–237** functionalized with the dicyanovinyl moiety.[240] This additional functionalisation afforded desirable NIR emission and enhanced the ability of CN^- to undergo Michael addition with the scaffold of these probes. This reaction resulted in the

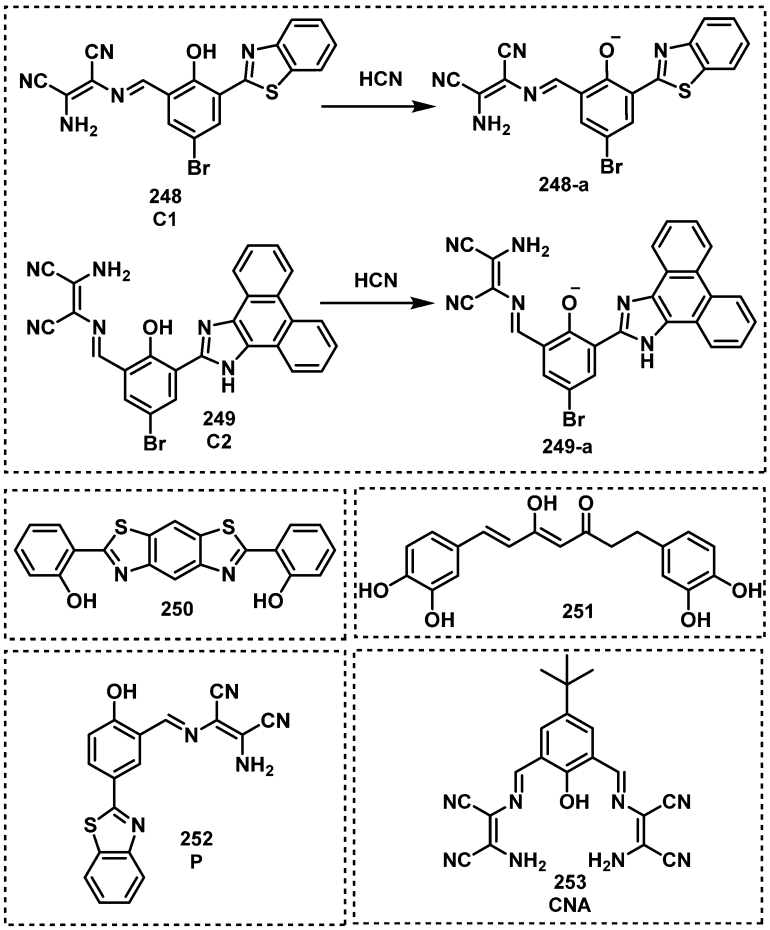

Fig. 42 Structures of fluorescent probes utilizing phenolic hydroxyl **248–253**.

fluorescence quenching of each probe. More recently, Mu *et al.* developed **RDCN** (**238**), a dual-response fluorescent probe for the detection of cyanide and hydrazine. **RDCN** showed strong fluorescence emission at 645 nm.[241] After treatment with cyanide, a fluorescence enhancement at 470 nm was observed. The LOD of **RDCN** for cyanide was 0.33 μM. After adding cyanide, the initial emission at 645 nm decreased and a new emission signal appeared at 565 nm. Many other researchers including Chen,[242] Chow,[243] Zhao,[244] Hua,[245] He[246] and Zade[247] have developed fluorescent probes for cyanide detection.

CN^- ions are well known to undergo nucleophilic addition with Michael acceptors, as briefly shown in Fig. 41. Park and Kim developed the chalcone (α,β-unsaturated ketone)-based fluorescent probe **239** for CN^- ion detection.[248] As expected, CN^- ions underwent nucleophilic addition with **239** and afforded a 1300-fold fluorescence increase at 469 nm (Fig. 41). Yuan and co-workers designed and synthesized **240**, based upon a similar strategy to that of Park and Kim.[249] The CN^- ion was shown to react with the 2-formylacrylonitrile moiety, which gives raise to a ratiometric change in fluorescence emission intensity (573 to 480 nm). This probe exhibited a low LOD (328 nM) and rapid response (1 min). Sun *et al.* synthesized two 3-amidocoumarin derivatives, **241** and **242**, as fluorescent probes for the detection of CN^- ions in CH_3CN solution.[250] This mechanism of detection was confirmed *via* single-X-ray crystal analysis. Cyanide was added to the coumarin group followed by an intramolecular cyclization reaction between the cyano and amido groups. In 2012, a benzochromene-based probe, **243**, was developed by Lee and Kim.[251] The addition of CN^- to **243** resulted in the ring opening to form a phenol derivative **243-c**. An initial green fluorescence emission was observed at 518 nm, but upon CN^- mediated ring opening, a ratiometric change was observed with a new emission at 350 nm. Zou *et al.* developed the AIE-based a naked-eye colorimetric and fluorescent probe **DTI** (**244**) to detect cyanide in DMSO–H_2O.[252] The fluorescence of **244** at 581 nm was gradually quenched after cyanide addition. The mitochondria-targeted ratiometric fluorescent probe **Mito-CP** (**245**) was developed for the detection of CN^- ions by Zhu and co-workers in THF-PBS solution and cassava cells.[253] In the presence of CN^- ions, an obvious change from red to colourless was observed, and the fluorescence emission changed from 646 to 482 nm. Probe **245** was successfully used to image endogenous CN^- ions in plant tissues and PC12 cells. Interestingly, Gomez *et al.* developed an indene-based fluorescent probe, **246**, which could reversibly detect CN^- ions in DMSO–H_2O solution.[254] Probe **246** exhibited a 1000-fold increase in fluorescence emission intensity and the probe could be recycled by $AgNO_3$. In 2016, Chao *et al.* designed and synthesized a carbazole-benzothiazole-based fluorescent

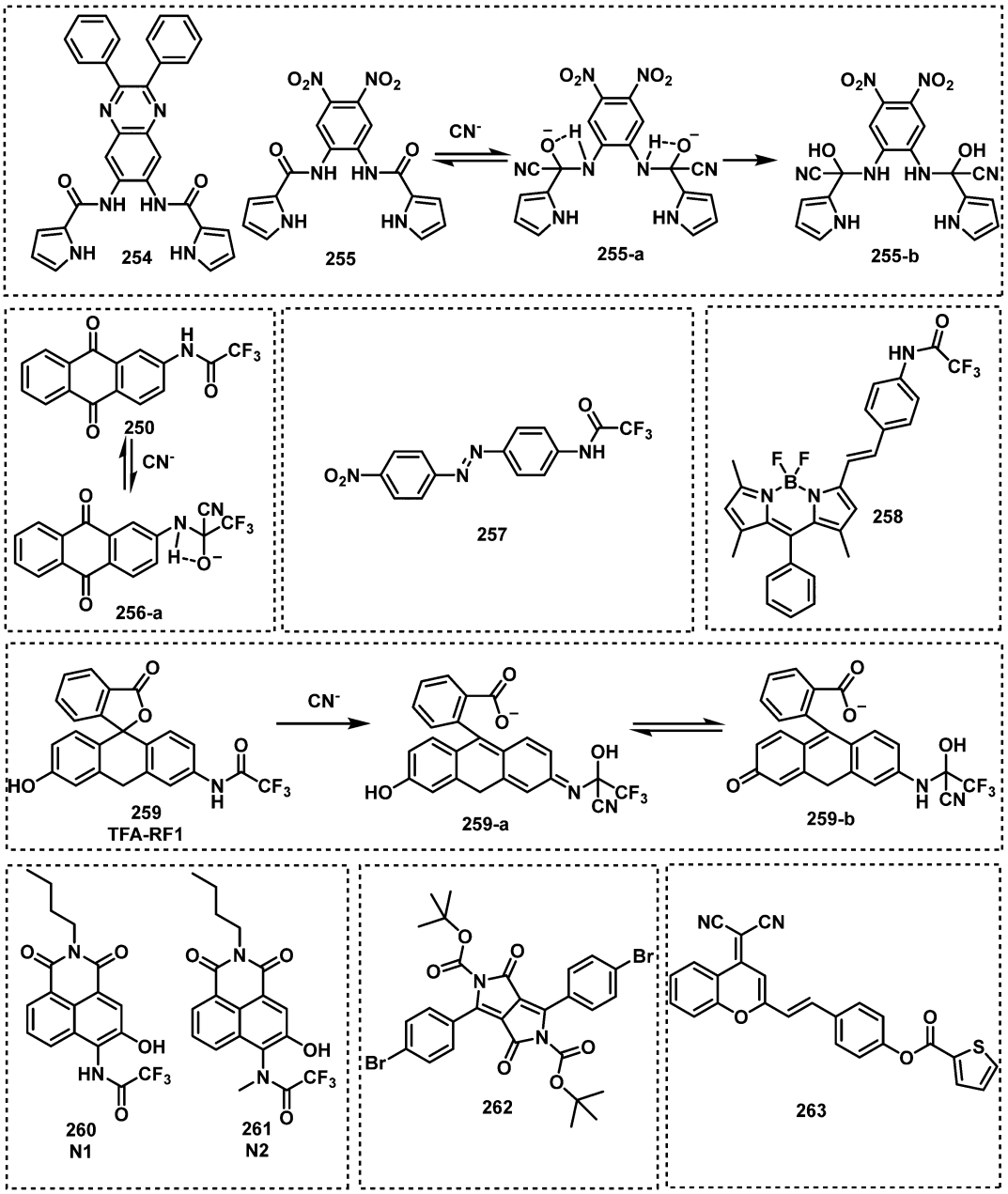

Fig. 43 Structures of fluorescent probes based on carbonyl moiety **254–263**.

probe, **IECBT** (**247**).[255] The probe detected cyanide and HSO_3^- under different conditions. Cyanide decreased the fluorescence emission of **247** at 575 nm, while a new peak at 376 nm was observed. After encountering HSO_3^-, the fluorescence emission at 568 nm was quenched. **247** also exhibited remarkable pH-dependent behaviour and could be employed as a pH indicator. The probe exhibited low LODs (0.94 μM for cyanide and 0.53 μM for HSO_3^-), and was applied to image cyanide and HSO_3^- in live U251 cells. Finally, **247** was used to noninvasively measure the extremely alkaline pH of *Escherichia coli* cells.

Due to the relatively low pK_a of phenols, they can undergo deprotonation *via* CN^- ions. Erdemira and Malkondu developed benzothiazole- and phenanthroimidazole-based probes, **C1** (**248**) and **C2** (**249**), for cyanide detection in CH_3CN–H_2O.[256] The fluorescence of **248** increased at 597 nm upon interaction with cyanide. Whereas, the fluorescence of **249** was quenched by cyanide due to ICT. Assadollahnejad and co-workers developed the phenol–bisthiazolopyridine hybrid-based fluorescent probe **250** for the detection of cyanide.[257] The deprotonation of the phenol results in a fluorescence enhancement at 505 nm. Curcumin (**251**) is a natural product with known antioxidant and anticancer properties.[258] In addition, its emissive properties were used for the detection of cyanide.[259] After treatment with cyanide, the fluorescence emission of curcumin at 520 nm was quenched *via* deprotonation but other anions did not cause this change. Curcumin exhibited a low LOD of 2.3 μM and was

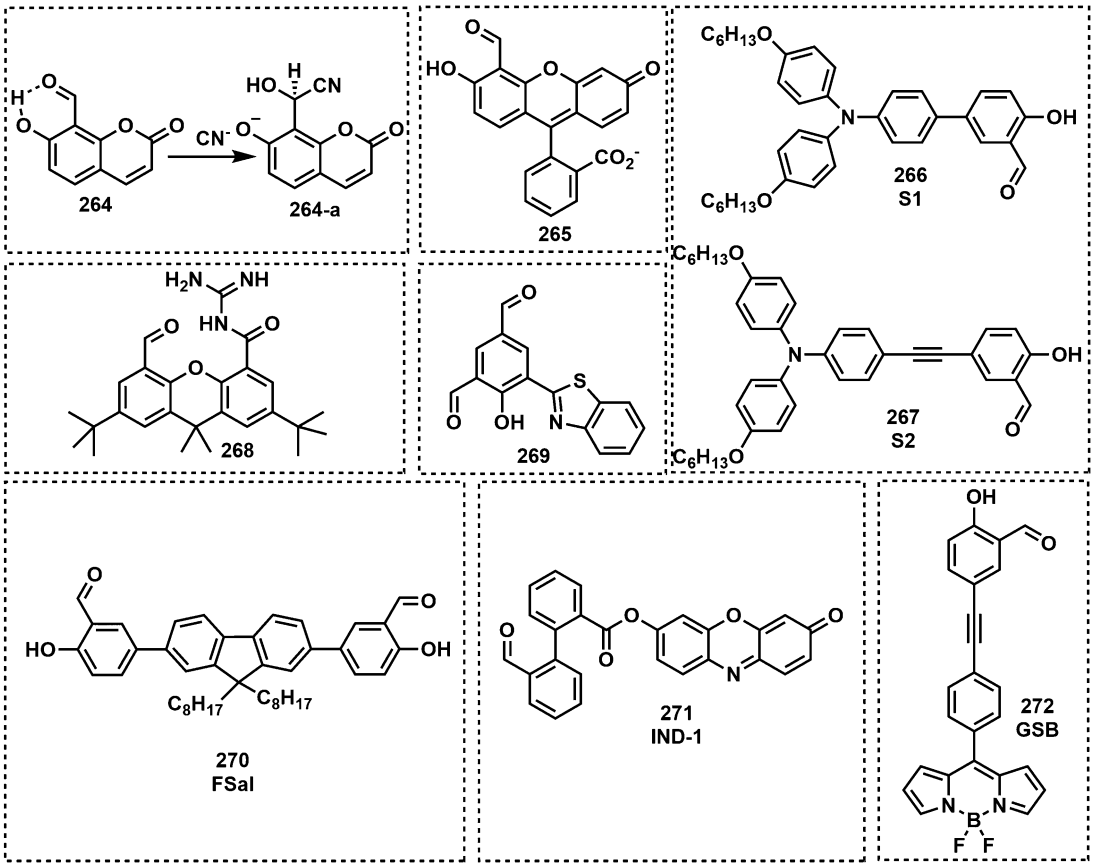

Fig. 44 Chemical structures of fluorescent probes **264–272** based on the salicylaldehyde moiety used for the detection of CN^-.

applied to image cyanide in HEK293T cells. Malkondu *et al.* developed the red- and blue-emitting fluorescent probe **P** (**252**) to detect cyanide and hypochlorite ions.[260] Compound **252** consists of benzothiazole functionalized with a diaminomaleonitrile unit. Cyanide treatment led to remarkable red emission, while hypochlorite caused distinct blue emission. Probe **P** displayed a 112-fold increase in emission at 480 nm within 1 min after interacting with cyanide. Moreover, a 112-fold enhancement in fluorescence emission was observed upon the addition of hypochlorite. This probe provided LODs of 1.32 μM for cyanide and 0.136 μM for hypochlorite. In 2021, Nandhini and co-workers designed and synthesized an imine-based probe, **CNA** (**253**), for cyanide detection in the solid and solution phases.[261] After coming into contact with cyanide, **253** exhibited red-emission in both media. The LOD of **253** for cyanide was 0.5 μM.

Compounds containing carbonyl units are well-known to react with CN^- ions to form cyanohydrins. This transformation can be promoted by intermolecular hydrogen bonding interactions. Dipyrrole carboxamide, trifluoroacetyls and thiophenecarbonyls have all been used for CN^- ion detection since their strong electron withdrawing groups promote nucleophilic addition. Chen *et al.* synthesized two pyrrole carboxamide compounds **254** and **255** for use as fluorescent probes for cyanide detection (Fig. 43).[262] Both compounds react with CN^- ions to form the corresponding cyanohydrin derivatives. The fluorescence maximum of **254** at 425 nm exhibited a bathochromic shift to 554 nm. Niu *et al.* employed anthraquinone as the fluorophore and trifluoromethylamide as the recognition unit to develop the colorimetric probe **256**.[263] The same group synthesized an azo-based colorimetric probe (**257**) to detect cyanide.[264] Akkaya and co-workers reported the BODIPY-based fluorescent probe for cyanide, probe **258**.[265] This structurally simple probe exhibited a large decrease in fluorescence at 571 nm and a colour change from red to blue after the addition of cyanide. Lv and co-workers synthesized **TFA-RF1** (**259**), a rhodol-based fluorescent probe for the detection of cyanide.[266] Probe **259** was initially colourless and nonfluorescent, but cyanide induced ring opening of the corresponding spirolactone, which was accompanied by strong fluorescence emission at 520 nm and an obvious colour change to yellow. Hao and co-workers reported naphthalimide as a fluorophore to develop a highly selective fluorescent probe for cyanide detection, **N2** (**261**) in DMSO–H_2O.[267] It is found that trifluoroacetamide-based fluorescent probes including **N1** (**260**) are easily attacked by various anions (cyanide, F^-, AcO^-) and even solvents. Thus, they developed a methylated trifluoroacetamide group as a recognition unit for the detection of cyanide because the susceptible H-atom of trifluoroacetamide was substituted by methyl group. The resulting compound, **261**, exhibited blue fluorescence (λ_{em} = 425 nm), whereas the fluorescence changed to green (λ_{em} = 535 nm) upon the addition of cyanide. In 2012, Jeong, Lee and Jang developed a diketopyrrolopyrrole-based fluorescent probe, **262**, for the detection of cyanide.[268]

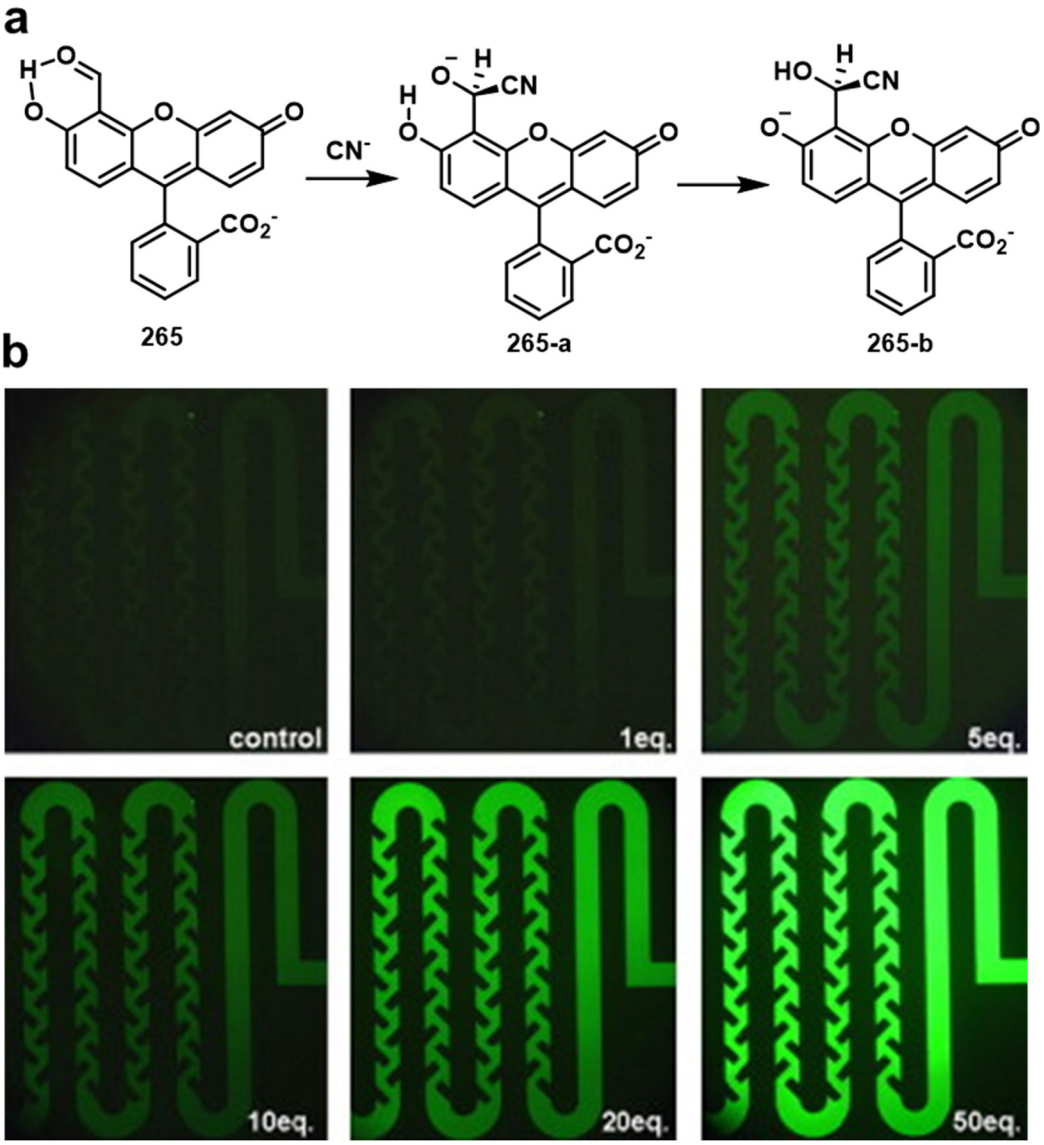

Fig. 45 (a) Proposed sensing mechanism of **265** towards cyanide. (b) Fluorescence image of **265** mixtures with different concentrations of cyanide in a microfluidic system at a flow rate of 10 μL min^{-1}. Reproduced with permission from ref. 271. Copyright (2008) Elsevier B.V.

Cyanide addition to the carbonyl carbon atom in the lactam ring changed the colour of the probe from green to red and quenched the fluorescence at 512 nm. Wang *et al.* developed the 2-thiophenecarbonyl-based fluorescent probe, **263**, for cyanide detection.[269] The probe itself is nonfluorescent and yellow in colour. Upon reaction with cyanide, the colour changed from yellow to green, and strong NIR fluorescence emission was observed at 717 nm. The probe exhibited a low LOD (1.44 μM).

Salicylaldehyde-based compounds readily undergo nucleophilic addition due to the activation of the aldehyde by intramolecular hydrogen bonding from the phenol (Fig. 44). Lee and co-workers exploited this known reactivity in the development of coumarin-based fluorescent probe, **264**, containing a salicylaldehyde unit (Fig. 44).[270] Initially, **264** was found to be nonfluorescent, however, the addition of CN^- resulted in a 190-fold fluorescence emission increase at 450 nm. The Yoon group incorporated the salicylaldehyde recognition unit onto fluorescein to develop fluorescent probe **265** (Fig. 45).[271] The addition of CN^- to a CH_3CN–H_2O solution containing **265** resulted in a 200-fold increase in fluorescence emission intensity at 520 nm, and was successfully used for imaging CN^- ion concentrations in HaCaT cells. Furthermore, **265** was used to develop a microfluidic platform for cyanide detection. Pati and Zade developed two fluorescent probes, **S1** (**266**) and **S2** (**267**), for cyanide detection in THF–H_2O.[272] Both probes consisted of salicylaldehyde and triphenylamine with different π-conjugation linker. **266** and **267** had LODs of 1.55 and 0.72 μM, respectively, and produced 350-fold and 25-fold fluorescence enhancements at 534 and 516 nm. Jo and co-workers reported the xanthene-based fluorescent probe, **268**, for the detection of CN^- ions in H_2O–CH_3CN.[273] This probe was functionalized with an aromatic aldehyde and acylguanidine group, which interacted *via*

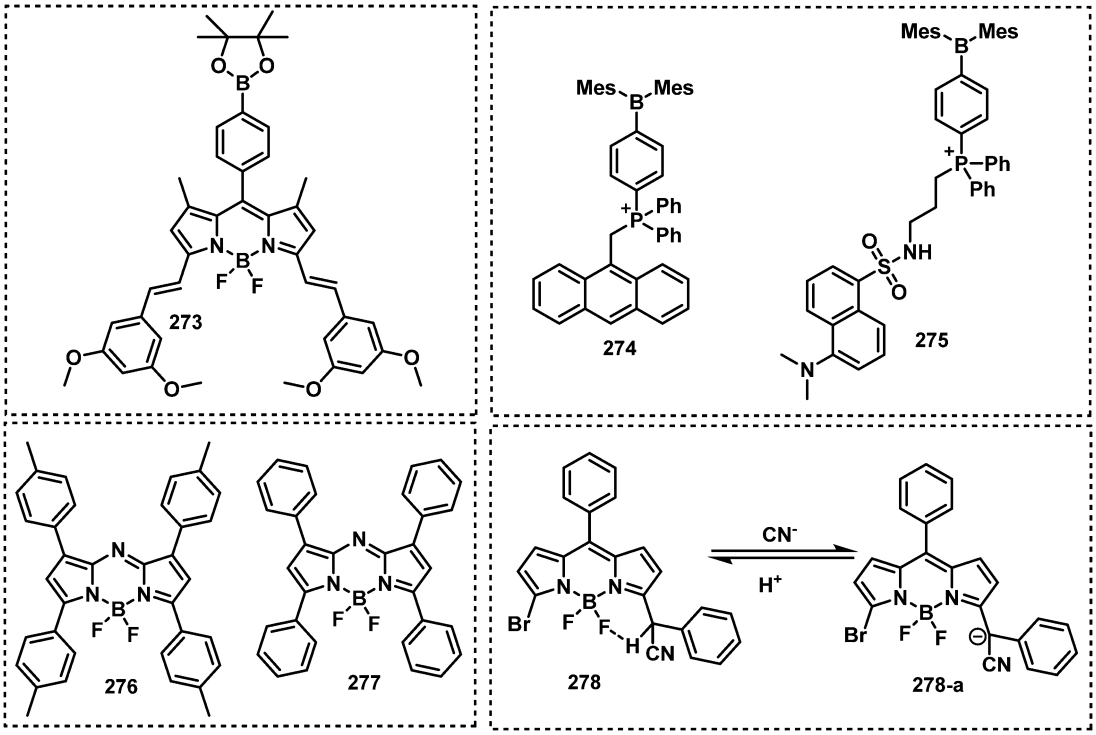

Fig. 46 Chemical structures of fluorescent probes **273–278** for the detection of cyanide.

multiple-intramolecular hydrogen bonds. A 7-fold fluorescence enhancement at 440 nm was observed upon interaction with cyanide. This enhancement was ascribed to an efficient chemical transformation of the aldehyde group, functioning as the fluorescence quencher group as well as the cyanide receptor site, and subsequent restoration of the xanthene fluorescence. In 2013, Goswami *et al.* reported the ESIPT-based fluorescent probe **269** for cyanide detection in CH_3CN–H_2O.[274] CN^- ions were found to rapidly react with the *ortho* aldehyde unit and inhibit ESIPT in CH_3CN–H_2O. This behaviour resulted in a ratiometric change in fluorescence emission intensity from the decrease in keto fluorescence emission at 521 nm and the increase in the enol fluorescence emission peak at 436 nm. Bera *et al.* reported the salicylaldehyde appended fluorene-based fluorescent probe **FSal** (**270**) for the detection of CN^- ions in H_2O.[275] This probe displayed fluorescence emission at 520 nm *via* inhibition of ESIPT after reaction with CN^-. Probe **270** exhibited high selectivity and a low LOD (0.06 ppm), and was able to detect CN^- ions in living SH-SY5Y cells. Lee and co-workers developed the fluorescent probe, **IND-1** (**271**),[276] which was designed to undergo the benzoin reaction with CN^- and subsequent intramolecular cyclization to release the fluorophore resorufin. Compound **271** was successfully used for the detection of CN^- ions in PBS–DMSO. Sukato *et al.* developed the salicylaldehyde-functonalised BODIPY fluorescent probe, **GSB** (**272**), for cyanide detection.[277] Upon the addition of CN^- ions, a 220-fold fluorescence emission increase at 529 nm was observed, which was employed for the successful imaging of CN^- ions in living HepG-2 cells.

Wang, Li and Cao reported the synthesis of **273**, a boryl-functionalized BODIPY fluorescent probe that could detect either fluoride or cyanide ions in THF–H_2O.[278] In the presence of cyanide ions, the decomposition of the BODIPY cores might arise from a nucleophilic displacement that breaks a B–N bond resulting in a B–C≡N bond, which exhibited a blue shift from 599 nm to 575 nm and the appearance of a new fluorescence emission at 478 nm. Due to the different reactivities, **273** could selectively detect and differentiate between fluoride and cyanide in THF–H_2O. Kim and co-workers reported the fluorescent probes **274** and **275** for cyanide detection in H_2O–CH_3OH.[279] CN^- ions reacted with the sp^2 boron unit to form sp^3 anions which resulted in an increase in fluorescence emission corresponding to anthryl and dansyl fluorophores, respectively. Dvivedi, Kumar and Ravikanth developed the 1,3,5,7-tetraaryl aza-BODIPY fluorescent probe (**276**) for cyanide detection in CH_3CN.[280] CN^- ions react with the C=N core of aza-BODIPY to shift the fluorescence emission from the NIR region (691 nm) to the visible region (602 nm) with a concomitant increase in fluorescence emission intensity. Wu *et al.* subsequently investigated the reactivity between aza-BODIPY and CN^-,[281] in which they discovered that the rate of nucleophilic addition of the CN^- dipyrromethene moiety was influenced by the presence of electron-rich groups. Fu *et al.* used BODIPY with activated C–H groups (probe **278**) as a fluorescent cyanide probe.[282] After the addition of cyanide, the fluorescence intensity at 533 nm decreased significantly, and the colour changed from orange to pink because the phenylacetonitrile group became electron-rich *via* deprotonation of the CH group, and thus activated the PeT process. Furthermore, the reaction product returned to the original state of the probe by the addition of trifluoroacetic acid. This probe had a low LOD of 148 nM and was employed to develop a test strip.

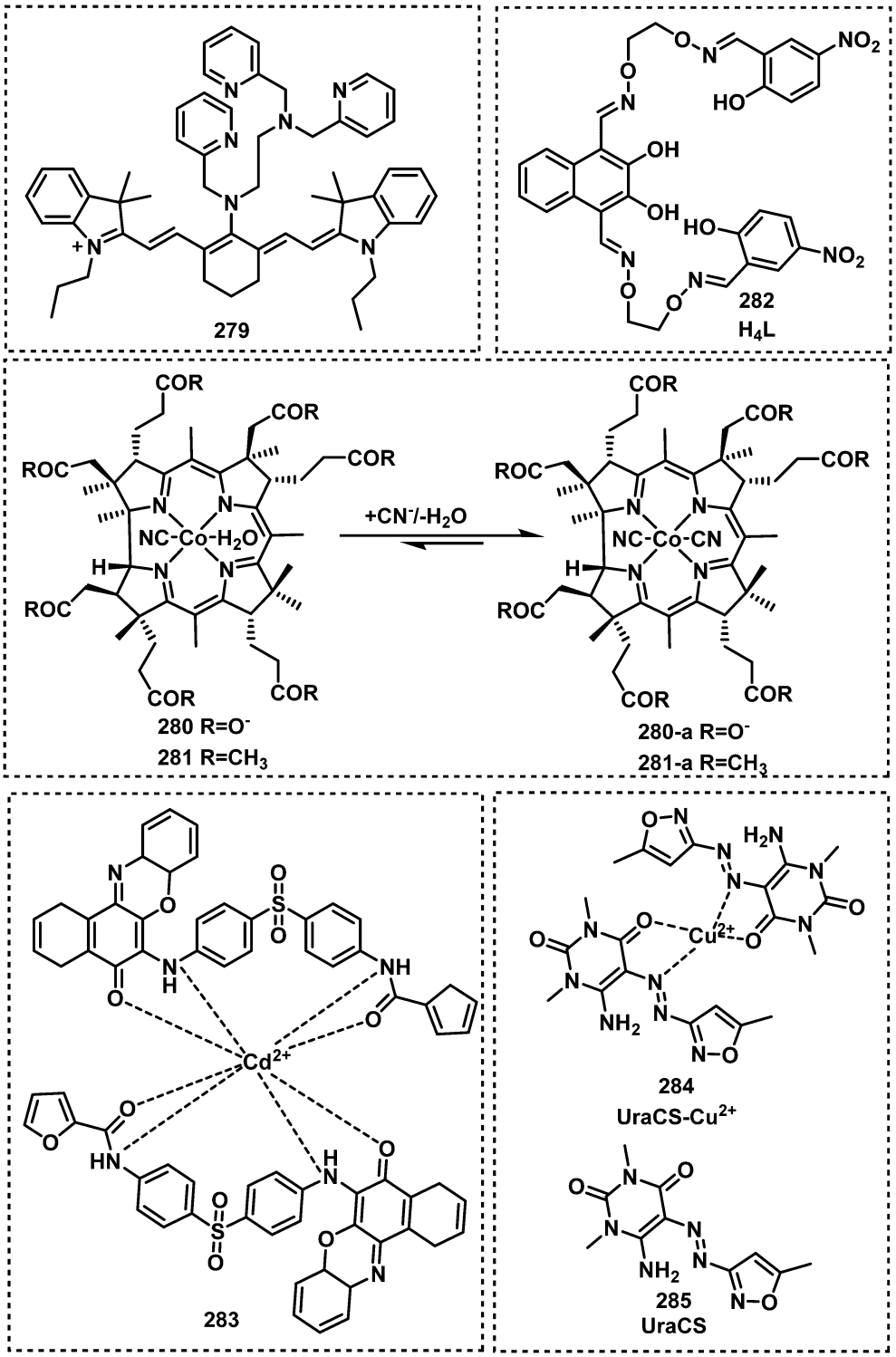

Fig. 47 Chemical structures of fluorescent probes **279–285** utilizing metal complexes for the detection of cyanide.

As seen in several literature reports, CN^- ions are known to have a strong affinity for metal ions such as cobalt, cadmium and copper. Various research groups have therefore exploited these properties for the detection of CN^- ions. In 2010, the Yoon group developed a water-soluble and NIR fluorescent probe for cyanide detection, which was prepared by mixing probe **279** with $Cu(ClO_4)_2$ in aqueous solution.[283] Upon treatment with cyanide, a significant fluorescence enhancement at 748 nm was observed. The probe was used to image cyanide produced by *P. aeruginosa* in *C. elegans*. In 2015, Zelder and Tivana reported the corrin-based probe, **280** and **281**, for cyanide detection (Fig. 47).[284] Liu *et al.* reported the naphthalenediol based

bis(salamo) fluorescent probe H_4L (**282**) for the detection of CN^- ions. **282** formed the fluorescent Zn^{2+}-complex in DMF–H_2O solution.[285] The fluorescence of **Zn-282** was then shown to decrease substantially upon coordination from CN^- ions. Similarly, Ravichandiran and co-workers developed phenoxazine-based fluorescent probe **283** for the detection of CN^- ions in DMF–H_2O.[286] Probe **283** initially formed a fluorescent Cd^{2+}-based metal complex with a fluorescence emission intensity at 530 nm. The coordination of CN^- ions resulted in fluorescence quenching of the metal complex. Khoshsoroor and co-workers reported the use of the uracil derivative **UraCS-Cu2**$^+$ (**284**) as a fluorescent probe for the detection of CN^- ions.[287] **UraCS** (**285**) acted as a suitable ligand for complexation with Cu^{2+} ions, which gave rise to an emissive metal probe **284** (λ_{em} = 378 nm). The fluorescence emission of this metal complex was quenched upon coordination from CN^- ions.

Although these reported fluorescent probes exhibited good selectivity and sensitivity, those that use imine and trifluoroacetamide-based functionalities interact with F^- and AcO^- ions and show unwanted solvatochromism. To date, a limited number of probes including **270**, **279**, and **Hcy-DCV** (**305**) have been reported to detect CN^- in 100% aqueous solution. Ratiometric fluorescent probes including **203**, **MRP1** (**213**), and **Hy** (**214**) have improved the sensing capability in cellular imaging applications. Mitochondria are considered to be the most sensitive organelle to cyanide toxicity. Despite this knowledge, only three mitochondria-targeting fluorescent probes are reported, including **L** (**210**), **MRP1** (**213**), and **Mito-CP** (**245**). The development of recyclable fluorescent probes including those incorporating carbon-nitrogen imine, acidic protons, and trifluoroacetyls as recogntion units are an effective way to expand the application and further reduce the cost. The reaction product can be converted to the original probe by the addition of silver salt, HCl, or trifluoroacetic acid. Probes shown to have such properties include **MRP1** (**213**), **Q1** (**219**), **246**, **250**, **255**, and **278**.

7. Fluorescent probes for the target enzymes and metabolites of CWAs

Monitoring AChE activity is key to achieving a greater understanding of its role in several physiological processes, and it also offers the opportunity to study the role of nerve agents in living systems.[288] On the basis of the excimer-monomer transition mode,[289] Chen *et al.* designed and synthesized a choline-labelled pyrene probe, **Py-Ch** (**286**), for monitoring AChE activity (Fig. 48).[290] They employed poly(vinylsulfonate) (PVS) to induce aggregation of **286** and shift the fluorescence from 375 nm to 486 nm. AChE-mediated hydrolysis forms the corresponding carboxylic acid, which is expelled from PVS and leads to fluorescence enhancements at 375 nm. Wu and co-workers developed an inkjet printed paper-based test strip for AChE with an indoxyl acetate substrate (**288**).[291] After reaction with AChE, a colourless product **288-a** was produced. Which needs to undergo oxidative coupling to generate a blue product, which is more sensitive for human eyes to discriminate. Wang and co-workers developed the fluorescent probe, **MCYN** (**289**) for monitoring AChE activity in PBS.[292] Inspired by the AChE inhibitor neostigmine, they selected dimethyl carbamate as the recognition unit and merocyanine was employed as the fluorophore due to its extraordinary optical properties. A fast response rate (20 min) and a low LOD (0.36 U mL^{-1}) were observed for AChE using **289**. These properties enabled it to be successfully used to monitor AChE activity in depressive mouse brains. In 2020 Ma *et al.* reported an NIR fluorescent probe, **CyN** (**290**), for the detection of AChE activity.[293] Probe **290** was initially nonfluorescent at 700 nm, however, the presence of AChE resulted increase in fluorescence emission intensity. It was used to visualize AChE activity in PC12 cells and zebrafish. The observations indicated that the major sites of endogenic AChE activity were the yolk sacs and neuromasts of zebrafish. In 2021, He and co-workers also developed a BODIPY-based fluorescent probe **BD-AChE** (**291**) for the detection of AChE activity.[294] The LOD of **291** was 0.21 U mL^{-1}, and the response time was approximately 15 min. With the assistance of **291**, they found that the AChE activity decreased in the brains of mice aging models. Long-term dietary restriction can also significantly decrease the AChE levels in the brains of aging mice. In 2020, the Yoon group reported a new approach to detect AChE activity by combining dimethylcarbamate choline with a self-immolative scaffold.[295] Based on this strategy, a series of probes for AChE was synthesized. Among these probes, **P10** (**301**) exhibited excellent detection performance, which can eliminate the interference from butyrylcholinesterase and carboxylesterase. The probe displayed a low LOD of 0.017 U mL^{-1} for AChE. Further, **301** was used to detect the AChE activity in U87MG cells. The probe can image the distribution of AChE activity in the brains of mice, which might be of significance in clinical studies. Inspired by **289**, a series of fluorescent sensors for the detection of nerve agents and AChE (the target enzyme of nerve agents) activity were developed.[296] Quinolines were chosen as fluorophores, while pyridine and dimethyl carbamate were chosen as the recognition groups for nerve agents and AChE, respectively. Among these sensors, **HBQ-AE** (**302**) exhibited a fast response rate (within 10 s for nerve agents and 8 min for AChE), good sensitivity (the LOD was 6 nM and 0.2 U mL^{-1}, respectively) and a high off/on contrast ratio. The probe was further applied to detect AChE activity in mouse blood and living PC12 cells. Although the use of dimethyl carbamate as a recognition unit for AChE (**289–300**) exhibited high selectivity over common hydrolases, most of these probes required several hours for the reaction to complete. This is not applicable for the rapid diagnosis of nerve agent poisoning (Fig. 49–55).

The riot control agent CS is a strong lachrymator that leads to a burning sensation and tearing of the eyes; and is used by law enforcement agencies as a nonlethal option for crowd control.[297] CS is generally produced by the reaction of 2-chlorobenzaldehyde with malononitrile through the Knoevenagel condensation, and CS is spontaneously hydrolysed to malononitrile. Therefore, malononitrile is a key component of CS, and it is also a precursor of HCN. Thus, Jung *et al.* developed a turn-on fluorescent probe, **Mal-P1** (**303**), for malononitrile detection.[298] The LOD of **Mal-P1** was 6.6 ppb, and the response time was

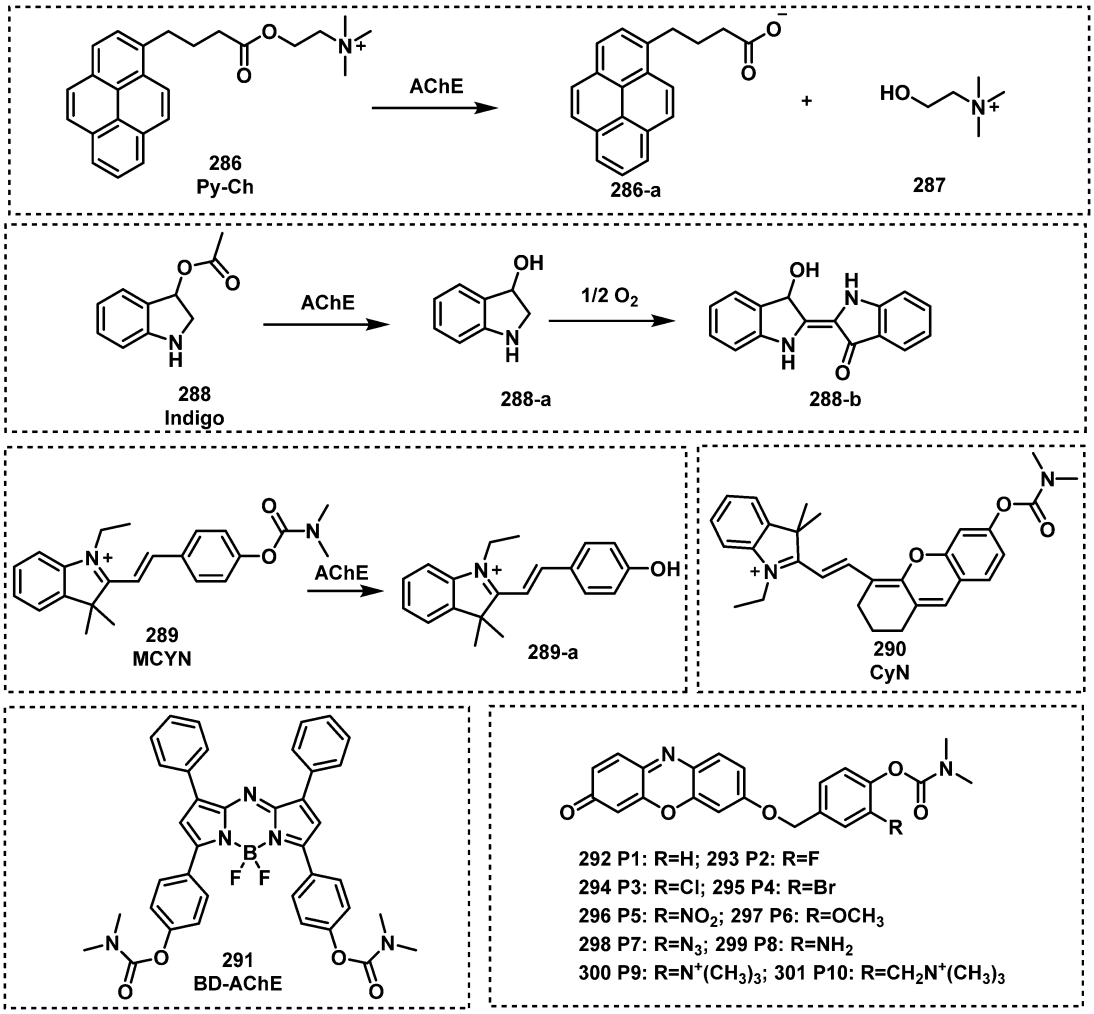

Fig. 48 Structures of fluorescent probes for the detection of AChE **286–301**.

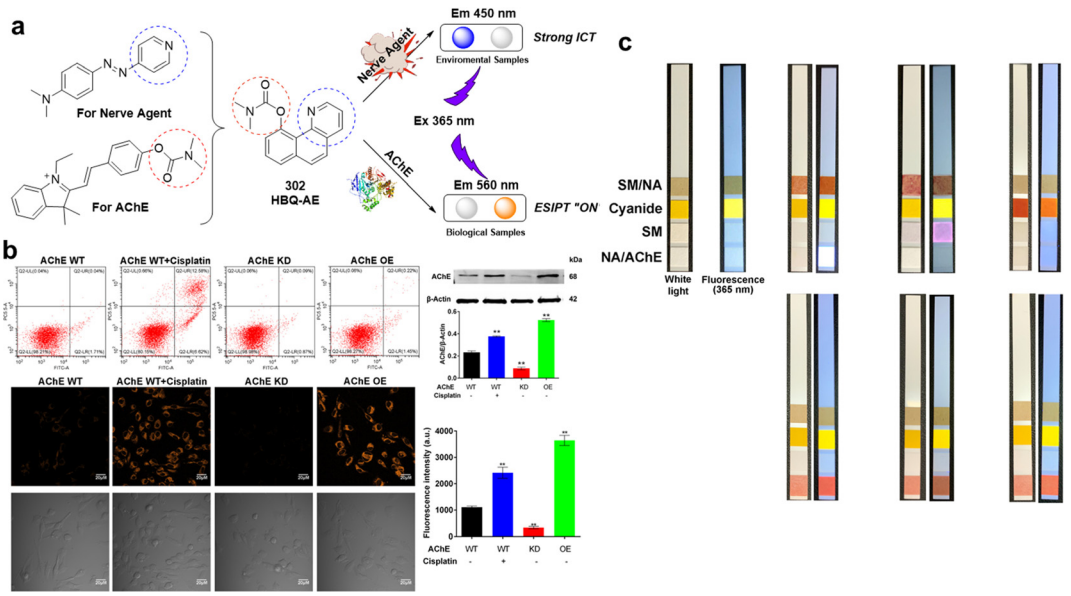

Fig. 49 (a) Design strategy of HBQ-AE and fluorescence signal changes upon the addition of nerve agent and AChE. (b) Fluorescence images of PC12 cells for AChE activity using HBQ-AE. (c) Diagram of test paper for chemical warfare agents. Reproduced with permission from ref. 296. Copyright (2020) Elsevier B.V.

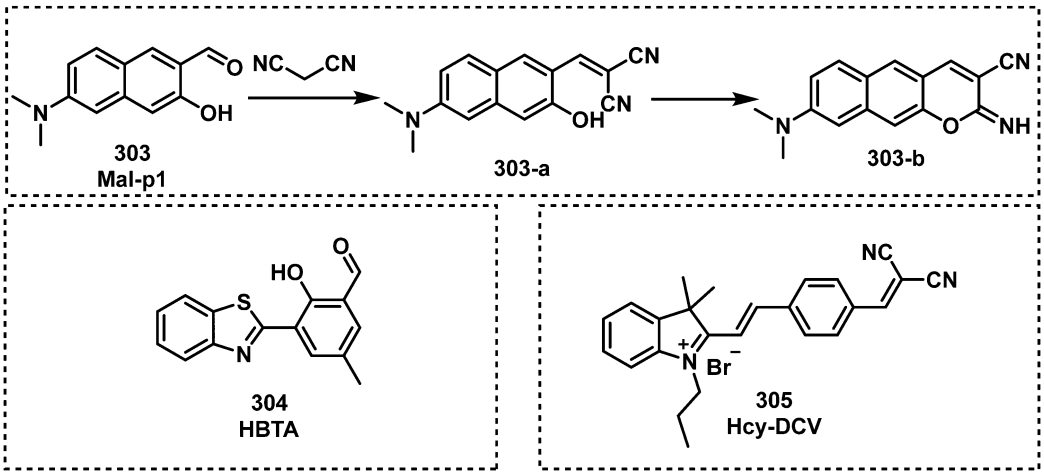

Fig. 50 Structures of fluorescent probes for malononitrile detection **303–305**.

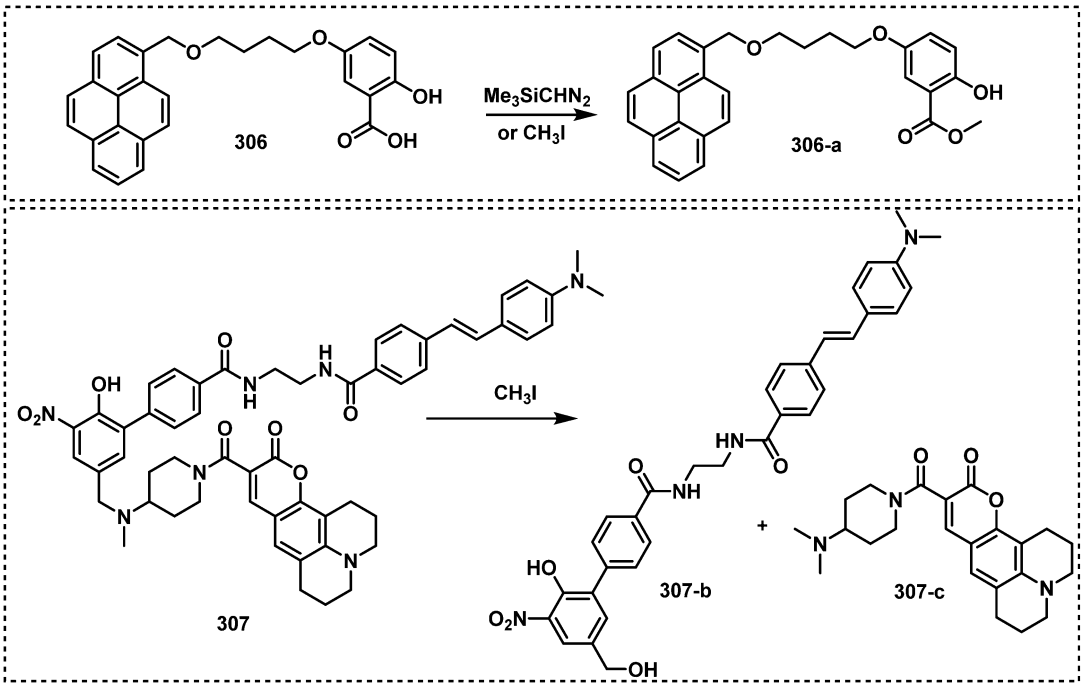

Fig. 51 Structures of fluorescent alkylating agent probes **306** and **307**.

60 min. This probe was used to visualize malononitrile in living HeLa cells. In 2021, Gong *et al.* designed and synthesized the ratiometric fluorescent probe **HBTA** (**304**) for malononitrile detection.[299] A decrease in fluorescence at 529 nm was observed, while a new fluorescence emission signal at 645 nm emerged. This probe exhibited an LOD of 27 nM and was employed to image malononitrile in living HeLa cells and zebrafish. In 2021, the Huang group reported a Michael addition reaction-based fluorescent probe, **Hcy-DCV** (**305**), for the determination of malononitrile.[300] After treatment with malononitrile, the colour changed from yellow to colourless, while the fluorescence at 540 nm substantially decreased. This probe showed a rapid response to malononitrile (within 5 min), high sensitivity (6.92 ppb), and good water solubility. **Hcy-DCV** was further employed to visualize malononitrile in living H1975 cells and zebrafish. Although **Mal-P1** (**303**) and **HBTA** (**304**) exhibited high sensitivity and selectivity for the detection of malononitrile in aqueous samples, living cells and zebrafish. Piperidine (0.1% or 0.075% in buffer) must be added to accelerate the reaction, which limits the practical utility of these probes. **Hcy-DCV** (**305**) proved superior in terms of sensitivity and response time; however, its selectivity over cyanide and other related ions was unsatisfactory.

Alkylating agents are widely used in chemistry; in addition, vesicants are alkylating agents. In 2019, Jiang and Broome developed a pyrene-based turn-on fluorescent probe, probe **306**, for alkylating agent detection.[301] This probe reacted with various alkylating agents, including methyl iodide, iodoethane,

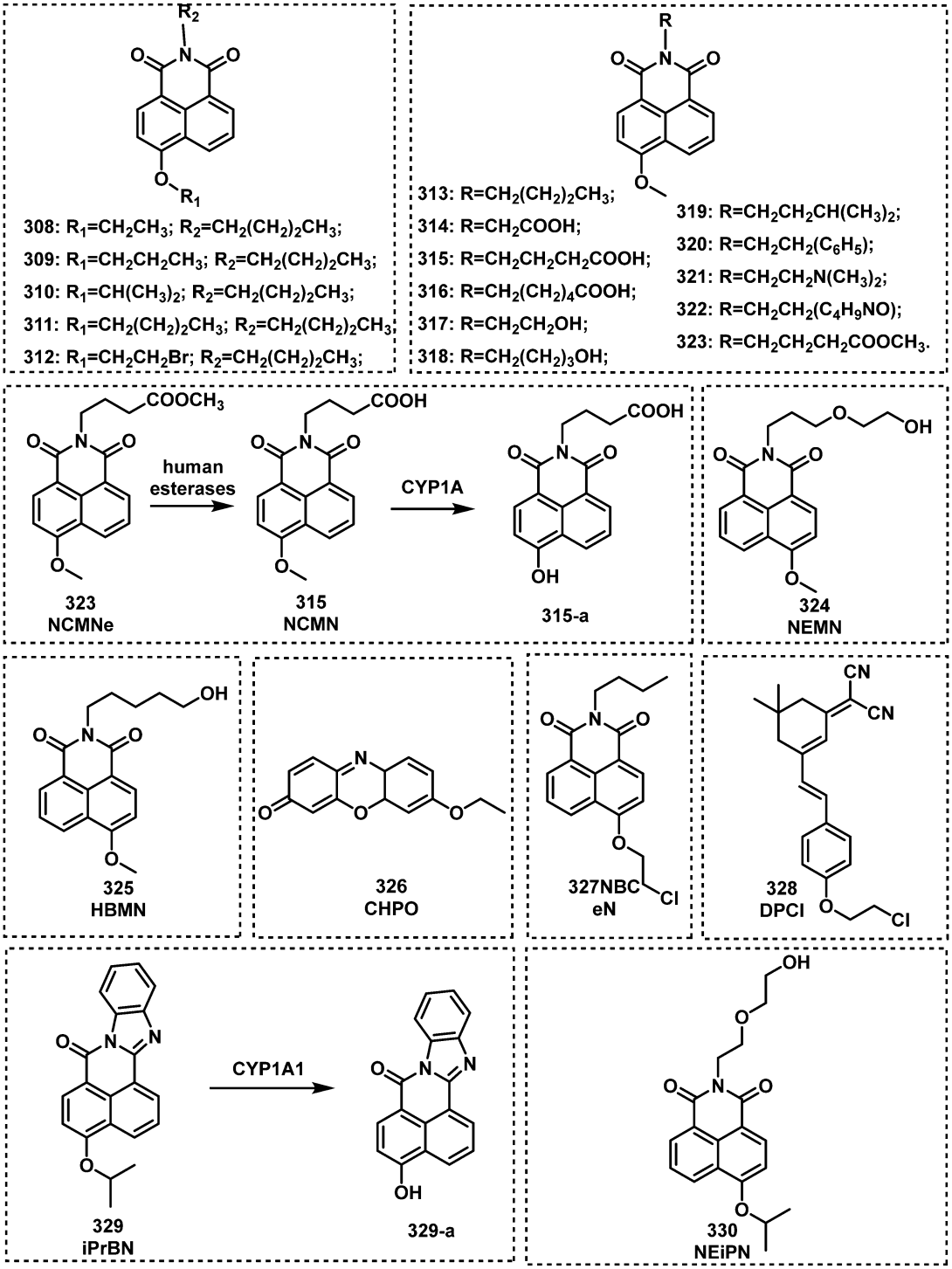

Fig. 52 Structures of fluorescent probes for the detection of CYP1A **308–330**.

bromoethane, busulfan, pipobroman, and temozolomide and showed considerable fluorescence at 475 nm after incubation. Tuo and co-workers reported a FRET probe, probe **307**, for alkylating agent detection.[302] This probe consisted of coumarin 343 as the fluorophore and DABCYL as the quencher, which was nonfluorescent, and released the fluorophore after incubation with alkylating agents. This probe could also detect numerous alkylating agents, including methyl iodide, methyl bromoacetate, and bis(chloroethyl) ether. Probes **306** and **307** represent interesting and new sensing strategies, however, both systems required long incubation times (hours) to accomplish the desired transformation. We believe these strategies may inspire researchers to explore strategies to improve the reaction rate.

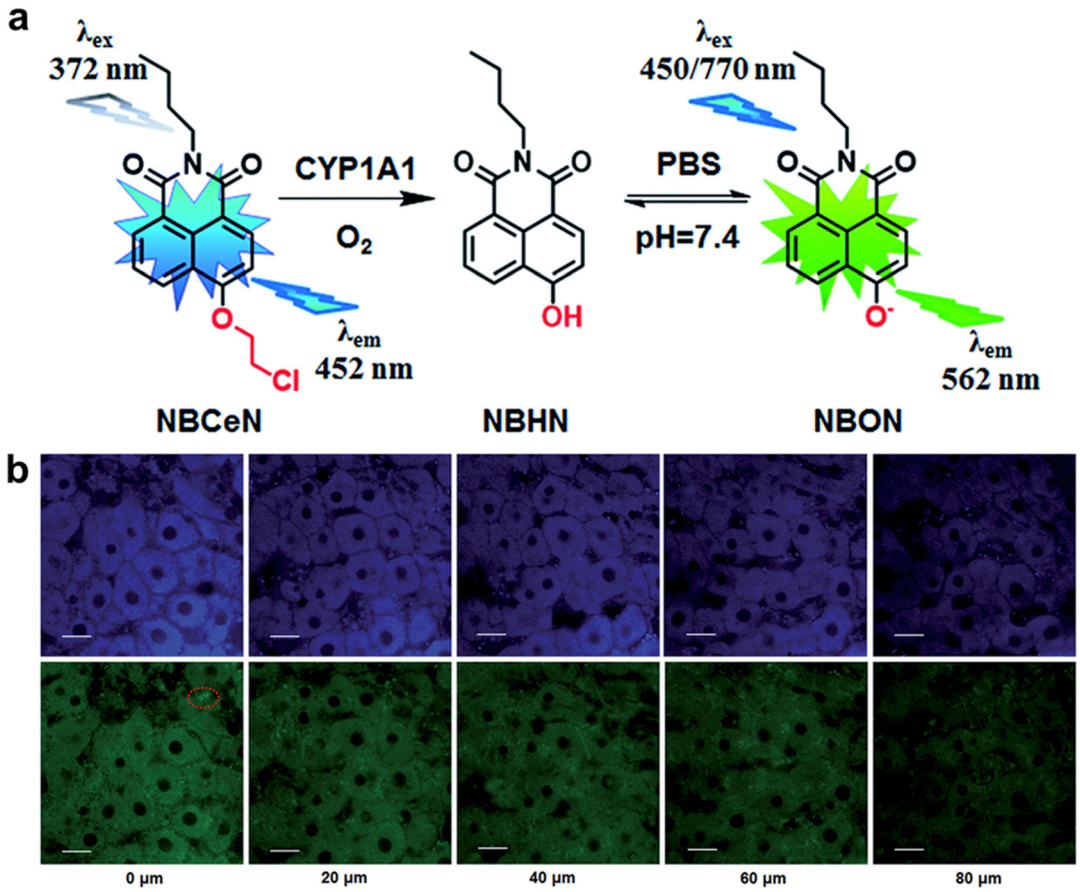

Fig. 53 (a) Structures of NBCeN and the proposed detection mechanism for CYP1A1. (b) TPM images of a fresh rat liver slice stained with NBCeN. Reproduced with permission from ref. 313. Copyright (2017) The Royal Society of Chemistry.

Cytochrome P450s (P450s) play an important role in the metabolism of endogenous and exogenous substances, including CWAs.[303] Cytochrome P450s are important targets for vesicants.[304–307] Cytochrome P450 1A (CYP1A) is one of the most important phase I drug-metabolizing enzymes in humans.[308] CYP1A catalyses the O-demethylation of melatonin to produce *N*-acetylserotonin.[309] In 2015, Dai and co-workers synthesized a series of 1,8-naphthalimide derivatives (**308–323**) to screen CYP1A fluorescent probes.[308] After screening and optimization, **315** showed the best detection performance. The probe consisted of 4-hydroxy-1,8-naphthalimide and methoxy groups. Upon reaction with CYP1A the fluorescence emission of **NCMN** shifted from 452 nm to 564 nm. This probe also exhibited a 15-fold enhancement in fluorescence and low LODs (2×10^{-5} nM for CYP1A2 and 5×10^{-5} nM for CYP1A1). **NCMN** was further employed to image endogenous CYP1A in living A549 and HepG2 cells and rat liver tissues. This group also found that a methyl ester derivative of **NCMN** (**317**) could be hydrolyzed by human esterases to release **NCMN** which exhibits improved permeability. Compound **323** also could image CYP1A in living A549 and HepG2 cells. Zhang and co-workers employed this same strategy to develop a naphthalimide-based fluorescent probe, **NEMN** (**324**), for CYP1A detection.[310] After coming into contact with CYP1A, the fluorescence emission at 552 nm notably increased and was accompanied by a reduction in fluorescence intensity at 458 nm. This probe exhibited a 20-fold fluorescence enhancement, low LODs (8.1 nM for CYP1A1 and 15.75 nM for CYP1A2) and a rapid response (10 min). **NEMN** was further employed to image CYP1A in living human cells. On the basis of a strategy similar to that for **NCMN** and **NEMN**, Li and co-workers developed the CYP1A2 fluorescent probe **HBMN** (**325**).[311] **HBMN** exhibited a 60-fold higher affinity for CYP1A2 than 7-ethoxyresorufin. As such, it was used to detect differences in CYP1A2 expression in various living human cells after induction with 2,3,7,8-tetrachlorodibenzo-*p*-dioxin (potential carcinogen). **CHPO** (**326**) is a commercial fluorescent probe for CYP1A that has been widely used for related research.[312] This probe exhibits enhanced selectivity towards CYP1A1 than CYP1A2. In 2017, Dai *et al.* developed a two-photon fluorescent probe, **NBCeN** (**327**), for the detection of CYP1A1.[313] This probe uses 4-hydroxy-1,8-naphthalimide as the fluorophore unit and an *O*-chloroethyl group as the recognition unit. Upon interacting with CYP1A, the fluorescence emission of the probe shifts from 452 nm to 562 nm while exhibiting a 32-fold fluorescence enhancement and a low LOD (2.5 nM). **NBCeN** was further employed to image CYP1A1 in living A549 cells and rat liver tissue. Based on a similar strategy to that of **NBCeN**, in 2019, Xue and co-workers developed an NIR fluorescent probe, **DPCl** (**328**), for CYP1A1 detection.[314]

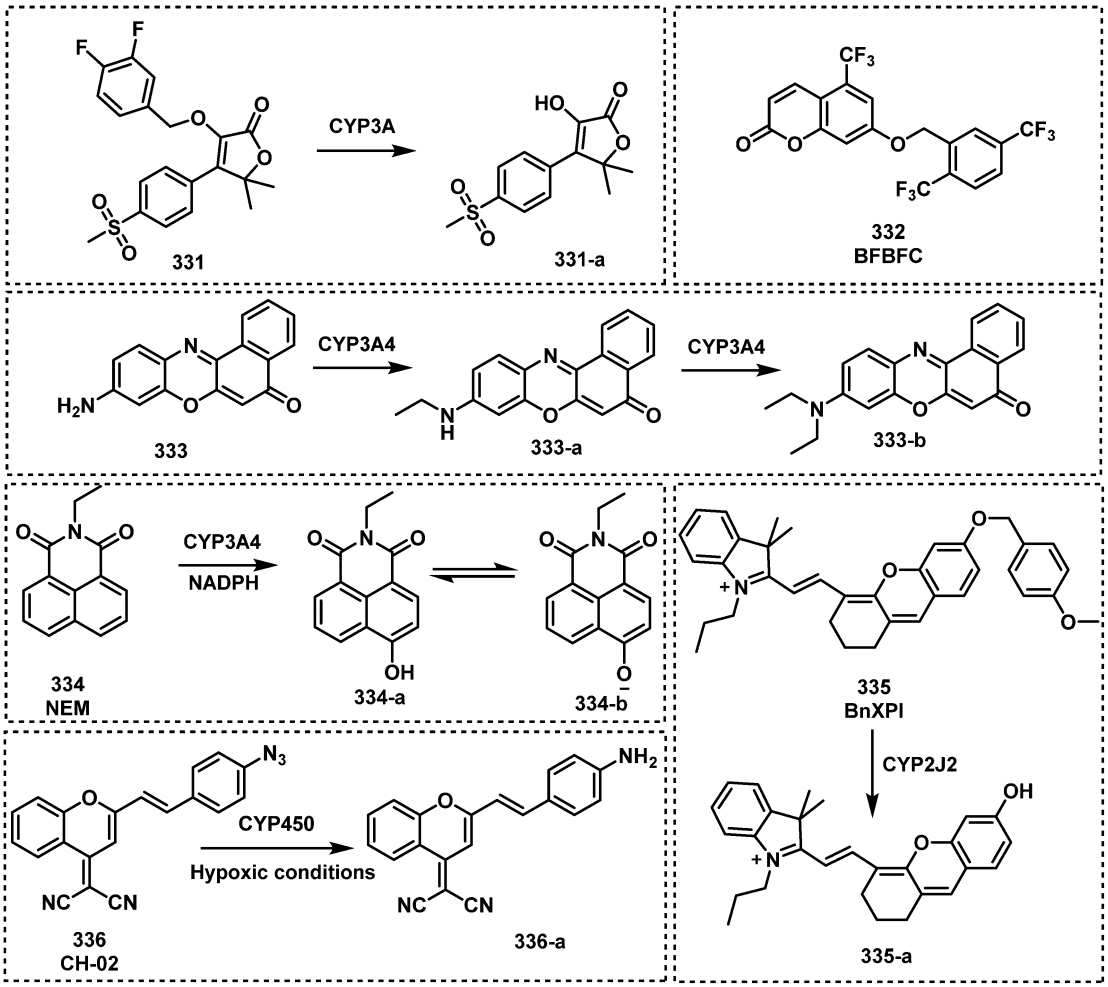

Fig. 54 Structures of fluorescent CYP450 probes **331–336**.

After reaction with CYP1A1, the fluorescence emission intensity increased at 673 nm. This probe exhibited a low LOD value of 0.026 nM. In 2018, Ning and co-workers developed a two-photon fluorescent probe, **iPrBN** (**329**), for CYP1A1 detection.[315] This probe consisted of 4-hydroxy-7*H*-benzo[*de*]benzo[4,5]imidazo[2,1-*a*] isoquinolin-7-one and an isopropyl group. **iPrBN** was almost nonfluorescent, whereas a substantial fluorescence enhancement at 525 nm was observed after the addition of CYP1A1. The LOD of **iPrBN** for CYP1A1 (0.036 nM) was almost 100-fold lower than that of the previously reported fluorescent probe, **NBCeN** (2.5 nM). **iPrBN** was used to image CYP1A1 in living cells and at the whole-organism level. In 2019, Ji and co-workers developed a naphthalimide-based fluorescent probe, **NEiPN** (**330**), for the detection of CYP1A1, which employed an isopropyl group as the recognition unit.[316] After treatment with CYP1A1 under simulated physiological conditions, the fluorescence emission decreased at 453 nm, and a new fluorescence peak emerged at 550 nm. **NEiPN** exhibited a 51-fold enhancement in fluorescence, a low LOD (0.04874 nM) and good water solubility. Finally, this probe was used to detect the activity of CYP1A1 in living human cells and zebrafish in real-time.

CYP3A4 is the main member of the CYP3A subfamily. CYP3A4 is involved in the oxidation of more than 50% of commercial drugs. Chauret and co-workers used 3-hydroxy-5,5-dimethyl-4-(4-methylsulfonylphenyl)-(5*H*)-furan-2-one as the fluorophore unit and synthesized several alkyl-substituted derivatives of this fluorophore. Among these compounds, the 3,4-difluorobenzyl substrate (**331**) was more specific for the CYP3A subfamily than the isopropyl substrate due to the CYP3A preference for substrates with larger leaving groups. In 2001, Renwick and co-workers synthesized a series of 4-trifluoromethylcoumarin derivatives as fluorescent probes for CYP3 detection,[317] and **BFBFC** (**332**) showed improved selectivity for CYP3A4. In 2008, Lampe and co-workers presented **Nile Red** (**333**), as a fluorescent probe to detect cytochrome CYP3A4.[318] **Nile Red** is metabolized by CYP3A4 to the corresponding *N*-monoethyl and *N*-desethyl products. After incubation with CYP3A4, steady-state fluorescence emission and excitation spectra, as well as excited-state lifetimes at varying Nile Red concentrations. In presence of CYP3A4 (1 μM), at low concentrations of the probe, the maximum excitation is observed at 454 nm; at higher concentrations, 585 nm. And itraconazole can competitively eliminate the Nile Red binding site of CYP3A4.

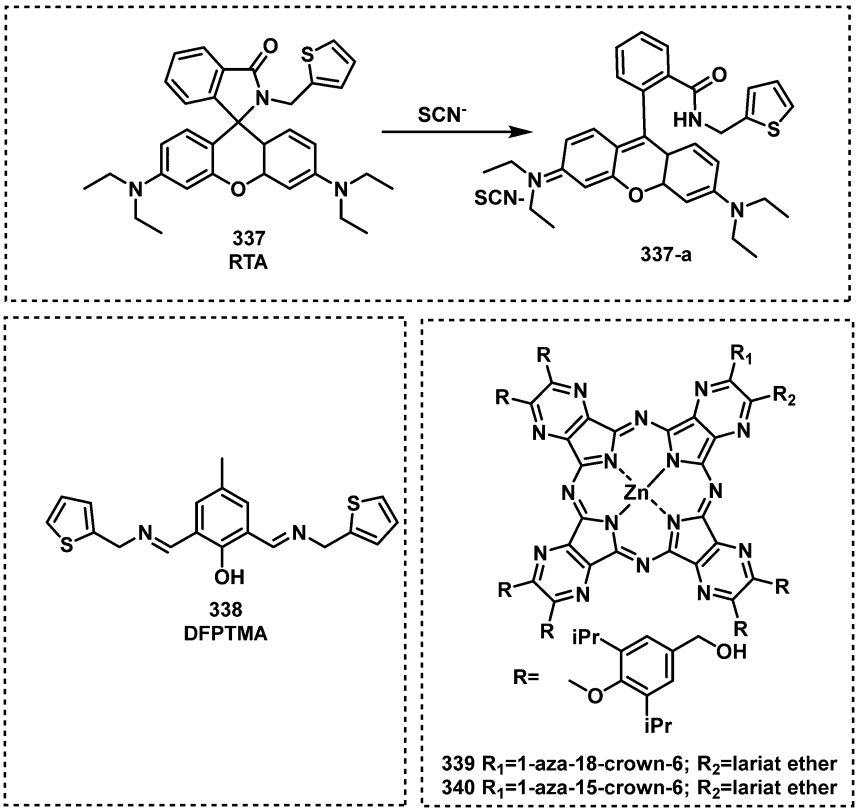

Fig. 55 Structures of fluorescent probes for the detection of thiocyanate.

In 2019, on the basis of a two-dimensional molecular design strategy, Ning and co-workers developed a fluorescent probe, **NEM** (**334**), for CYP3A4 detection.[319] Hydroxylation of **NEM** by CYP3A4 resulted in a 29-fold enhancement in fluorescence at 558 nm. Furthermore, **NEM** was successfully applied for the real-time imaging of CYP3A4 in various living systems, including living human primary hepatocytes and zebrafish. CYP2J2 also plays a key role in the oxidative metabolism of various xenobiotics and endogenous compounds. According to the structural features and substrate preferences of CYP2J2, Ning and co-workers developed a *para*-hydroxybenzyl-based fluorescent probe, **BnXPI** (**335**).[320] Upon *O*-demethylation by CYP2J2, a self-immolative reaction occurred spontaneously *via* 1,6-elimination of the *para*-hydroxybenzyl resulting in fluorescence emission at 718 nm. This probe also exhibited a low LOD (0.024 mg mL^{-1}) and was further used to image CYP2J2 in living cells, tumour tissues, and tumour-bearing animals. In 2016, O'Connor *et al.* reported an azide-containing fluorescent probe, **CH-02** (**336**), for CYP450 enzymes that operated in an oxygen-dependent manner.[321] Generally, azide-containing compounds are employed as powerful tools for click chemistry and used as recognition units for hydrogen sulfide detection. These authors confirmed that hydrogen sulfide does not react with **CH-02** by the addition of an exogenous sulfide donor or regulate the expression of cystathionine-β-synthase, whereas CYP450 reduces **CH-02** to generate fluorescence emission at 625 nm. CYP detection is not only important for understanding the metabolism of CWAs but can also improve our ability to choose the correct treatments for CWA poisoning. Although fluorescent probes **308–326** and **332–334** enabled the detection of CYP 1A and 3A4, it difficult to achieve specificity for CYP1A2, 2B6 and 3A5.

As a major cyanide metabolite, thiocyanate (SCN^-) is the most common indirect marker of cyanide exposure.[322] SCN^- is normally present in human blood at concentrations ranging from 1.7–290 μM.[323,324] In 2013, Banerjee and co-workers reported a rhodamine-based fluorescent probe, **RTA** (**337**), for SCN^- detection.[325] This probe was nonfluorescent by itself, but in the presence of SCN^-, a 90-fold fluorescence enhancement at 540 nm was observed. **RTA** exhibits an LOD of 0.01 μM and was used for SCN^- detection in living cells and sheep blood serum. In 2015, Das *et al.* developed a SCN^- selective fluorescent probe, **DFPTMA** (**338**).[326] In the presence of SCN^-, the fluorescence emission of **DFPTMA** at 540 nm was considerably enhanced, probably *via* the formation of hydrogen bonds. In 2019, Lochman *et al.* reported a series of red-emitting fluorescent probes for metal cations.[327] These probes derived from tetrapyrazinoporphyrazines (TPyzPzs) with a recogntion unit that consists of an aza-crown and supporting substituents. Among these probes, **339** and **340** exhibited high selectivity toward SCN^-, which was explained by a unique sensing mechanism combining size-fit recognition of cation, coordination of SCN^- with central zinc cation, and chaotropic ability of SCN^- allowing desolvation of cation. In the presence of SCN^-, a substantial fluorescence enhancement at 580 nm was observed. These probes exhibited

low LODs (approximately 7 μM) and could be used to detect SCN^- in saliva (3.31 ± 0.07 mM). These probes were further applied to visualize SCN^- in living HeLa cells.

As seen throughout this review, fluorescence spectrometery and fluorescence laser scanning confocal microscopy are frequently used for performance assessment of fluorescent probes in solution and in cells, respectively. However, a test paper-coated with a fluorescent probe is the simplest way for the on-demand sensing of CWAs. A major hurdle for these technologies is the instability of the test paper. For these reasons, we believe test paper is only useful for the qualitative detection of CWAs at relatively high concentrations. More recently, researchers embedded CWAs probes onto more advanced materials such as electrospun fibers to achieve better sensitivity.[155] These systems are generally superior to test papers and solution-based sensing.[155] In addition, probes embedded onto materials are amenable for incorporation into portable detectors. Such technologies have enabled on-site detection and quantitative analysis.[328] Portable detectors for on-site detection typically consist of an air pump, an integrated optical system (including optical source, light path system, and image recorder), an image processing module (which translates the fluorescence into an electrical signal), a power supply circuit, an LCD screen, linked to the cloud platform.[328] While these smart detectors exhibit advantages in terms of sensing accuracy and automation, miniaturization is an essential element that should be considered for the future development of the field.

8. Conclusion and outlook

CWAs are hazardous chemical substances that need to be studied in greater detail. Significant advances have been made in the field of CWA detection with fluorescent probes now developed that possess high sensitivity, and good selectivity. These new technologies are essential for environmental detection, as well as for use in chemical biology. The ability to non-invasively investigate the dynamic processes of CWAs *in vitro* and *in vivo*, is crucial to improve our understanding on the mechanisms of CWAs in living systems. However, several challenges remain with the design of an effective CWA probes, these include faster response times, enhanced responses, improved selectivity, and higher sensitivity. Limited numbers of fluorescent probes are available for blister agent detection (*e.g.*, SM). Moreover, fluorescent probes for the detection of divinyl sulfone, a highly toxic metabolite of SM, should also be developed. No fluorescent probes are currently available to detect this toxic species. Regarding nerve agent detection, several effective fluorescent probes exist, however, a greater focus should be directed to imaging the enzyme AChE. While many blood-agent probes have been developed, probes for the metabolites of these blood agents such as thiocyanate and 2-aminothiazoline-4-carboxylic acid are needed. The detection of these metabolites is crucial for the diagnosis of blood agent poisoning. An attractive strategy that should be further explored is the design and synthesis of fluorescent probes that permit the simultaneous detection of multiple types of CWAs. Only a few examples currently exist. Finally, with the continued growth in chemistry and synthetic biology, many new highly toxic chemicals such as saxitoxin, aflatoxin B1, and trichothecenes have appeared, which might be potential CWAs. Developing fluorescent probes for the detection of these potential CWAs are therefore required. For practical application, device portability while maintaining function and high sensitivity is a particularly important topic for translation of these detection methods into practical applications.[329]

Abbreviations

AChE	Acetylcholinesterase
AEGLs	Acute exposure guideline levels
AIE	Aggregation-induced emission
APD	Advanced portable chemical agent detector
CAM	Chemical warfare agent monitor
CEES	2-Chloroethyl ethyl sulfide
ClCN	Cyanogen chloride
CS	*o*-Chlorobenzylidene malonitrile
CTAB	Cetyltrimethylammonium bromide
CWAs	Chemical warfare agents
CWC	Chemical weapons convention
CYP1A	Cytochrome P450 1A
D–A	Donor–acceptor
DCP	Diethyl chlorophosphate
DECP	Diehtyl cyanophosphate
DFP	Diisopropyl fluorphosphate
DMMP	Dimethyl methylphosphonate
DMMP	Diisopropyl methylphosphonate
D–π–A	Donor–π–acceptor
ESIPT	Excited-state intramolecular proton transfer
FID	Flame ionization detector
FPDs	Flame photometric detectors
FRET	Förster resonance energy transfer
GA	Tabun
GB	Sarin
GD	Soman
GF	Cyclosarin
HBT	2-(2′-Hydroxyphenyl)benzothiazole
HCN	Hydrogen cyanide
HCN	Hydrogen cyanide
HLCT	Hybridized local and charge-transfer excited state
HN1	Bis-(2-chloroethyl)ethylamine
HN2	Mechlorethamine
HN3	Tris-(2-chloroethyl)amine
HYDROM	Hydromorphine
ICT	Intramolecular charge transfer
IDA	The indicator displacement assay
IDLH	Immediate danger to life and health
IMS	Ion mobility spectrometry
IR	Infra-red
JCAD	The joint chemical agent detector
JCSD	Joint contaminated surface detector
JSLSCAD	The joint service lightweight standoff chemical agent detector

LCD	Lightweight chemical detector
LOD	The limit of detection
NaCN	Sodium cyanide
NAT2	*N*-Acetyltransferases
NBD	7-Nitro-2,1,3-benzoxadiazole
OPCW	Organization for the prohibition of chemical warfare
PeT	Photoinduced electron transfer
PID	Photoionization ionization detector
PVS	Poly(vinylsulfonate)
RAID-M	Rapid alarm and identification device-monitor
SAWs	Surface acoustic waves
SCN^-	Thiocyanate
SM	Sulfur mustard
UV	Ultraviolet
WWI	World war I
2-PAM	Pralidoxime

Conflicts of interest

There are no conflicts to declare.

Acknowledgements

W. Q. M. thanks the National Natural Science Foundation of China (No. 82271916 and 81801869). K. X. thanks the National Natural Science Foundation of China (81871521). W. Q. M also wishes to thank Shanghai Municipal Health Commission-Outstanding Youth Foundation of Public Health (GWV-10.2-YQ18). X. P. H. thanks the National Natural Science Foundation of China (No. 91853201) and the Fundamental Research Funds for the Central Universities (222201717003) for financial support. TDJ wishes to thank the Royal Society for a Wolfson Research Merit Award and the Open Research Fund of the School of Chemistry and Chemical Engineering, Henan Normal University for support (2020ZD01). J. Y. thanks to the National Research Foundation of Korea (NRF) grant funded by the Korea government (MSIT) (No. 2022R1A2C3005420). M. X. S. thanks the National Natural Science Foundation of China (82103885). A. C. S. would like to thank the Glasstone Research fellowship (University of Oxford) and the major research grant from Jesus College, Oxford for support.

References

1 D. Steindl, W. Boehmerle, R. Körner, D. Praeger, M. Haug, J. Nee, A. Schreiber, F. Scheibe, K. Demin, P. Jacoby, R. Tauber, S. Hartwig, M. Endres and K. U. Eckardt, *Lancet*, 2021, **397**, 249–252.
2 R. Stone, *Science*, 2018, **359**, 1314–1315.
3 P. A. Lombardo, *Nature*, 2017, **541**, 154–155.
4 D. Dons, *Science*, 2013, **341**, 1051.
5 G. R. Ciottone, *N. Engl. J. Med.*, 2018, **378**, 1611–1620.
6 L. Szinicz, *Toxicology*, 2005, **214**, 167–181.
7 A. Mangerich and C. Esser, *Arch. Toxicol.*, 2014, **88**, 1909–1911.
8 L. E. Llewellyn, *Nat. Prod. Rep.*, 2006, **23**, 200–222.
9 D. Butler, *Nature*, 2018, **556**, 285–286.
10 E. J. Hulse, J. D. Haslam, S. R. Emmett and T. Woolley, *Br. J. Anaesth*, 2019, **123**, 457–463.
11 M. Schwenk, *Toxicol. Lett.*, 2018, **293**, 253–263.
12 P. D. Anderson, *J. Pharm. Pract.*, 2012, **25**, 61–68.
13 H. Committee to Review the Health Effects in Vietnam Veterans of Exposure to, P. Board on the Health of Select and M. Institute of, in Veterans and Agent Orange: Update 2012, National Academies Press (US) Copyright 2014 by the National Academy of Sciences. All rights reserved., Washington (DC), 2014, DOI: 10.17226/18395.
14 A. T. Kirk, A. Bohnhorst, C. R. Raddatz, M. Allers and S. Zimmermann, *Anal. Bioanal. Chem.*, 2019, **411**, 6229–6246.
15 L. Chen, D. Wu and J. Yoon, *ACS Sens.*, 2018, **3**, 27–43.
16 R. Zhu, J. M. Azzarelli and T. M. Swager, *Angew. Chem., Int. Ed.*, 2016, **55**, 9662–9666.
17 Y. Sun and K. Y. Ong, *Detection Technologies for Chemical Warfare Agents and Toxic Vapors*, CRC Press, 2004.
18 H. H. Hill and G. Simpson, *Field Anal. Chem. Technol.*, 1997, **1**, 119–134.
19 R. Sferopoulos, *A Review of Chemical Warfare Agent (CWA) Detector Technologies and Commercial-Off-The-Shelf Items*, 2008.
20 M. E. Kosal, *The basic of chemical and biological weapons detectors*, 2003.
21 S. H. Park, N. Kwon, J. H. Lee, J. Yoon and I. Shin, *Chem. Soc. Rev.*, 2020, **49**, 143–179.
22 B. Thomas, K. C. Yan, X. L. Hu, M. Donnier-Maréchal, G. R. Chen, X. P. He and S. Vidal, *Chem. Soc. Rev.*, 2020, **49**, 593–641.
23 D. Wu, A. C. Sedgwick, T. Gunnlaugsson, E. U. Akkaya, J. Yoon and T. D. James, *Chem. Soc. Rev.*, 2017, **46**, 7105–7123.
24 J. Zhang, X. Chai, X. P. He, H. J. Kim, J. Yoon and H. Tian, *Chem. Soc. Rev.*, 2019, **48**, 683–722.
25 K. Kim, O. G. Tsay, D. A. Atwood and D. G. Churchill, *Chem. Rev.*, 2011, **111**, 5345–5403.
26 Y. J. Jang, K. Kim, O. G. Tsay, D. A. Atwood and D. G. Churchill, *Chem. Rev.*, 2015, **115**, Pr1–76.
27 X. Zhou, S. Lee, Z. Xu and J. Yoon, *Chem. Rev.*, 2015, **115**, 7944–8000.
28 L. Chen, D. Wu and J. Yoon, *ACS Sens.*, 2018, **3**, 27–43.
29 Z. Xu, X. Chen, H. N. Kim and J. Yoon, *Chem. Soc. Rev.*, 2010, **39**, 127–137.
30 J. A. Ma and P. K. Dasgupta, *Anal. Chim. Acta*, 2010, **673**, 117–125.
31 F. Wang, L. Wang, X. Chen and J. Yoon, *Chem. Soc. Rev.*, 2014, **43**, 4312–4324.
32 E. P. Randviir and C. E. Banks, *Trac, Trends Anal. Chem.*, 2015, **64**, 75–85.
33 P. B. Pati, *Sens. Actuators, B*, 2016, **222**, 374–390.
34 D. Udhayakumari, *Sens. Actuators, B*, 2018, **259**, 1022–1057.
35 C. C. Liu, S. L. Liu, H. L. Xi, H. L. Yu, S. K. Zhou, G. L. Huang, L. H. Liang and J. Q. Liu, *J. Chromatogr. A*, 2017, **1492**, 41–48.

36 S. Sezigen, R. K. Eyison, E. Kilic and L. Kenar, *Clin. Toxicol.*, 2020, **58**, 36–44.
37 X. Cheng, C. Liu, Y. Yang, L. Liang, B. Chen, H. Yu, J. Xia, S. Liu and Y. Li, *Toxicol. Lett.*, 2021, **344**, 46–57.
38 J. McManus and K. Huebner, *Crit. Care Clin.*, 2005, **21**, 707–718, vi.
39 D. G. Lam, P. Rice and R. F. Brown, *Burns*, 2002, **28**, 19–25.
40 K. Weibrecht, S. Rhyee, M. E. Manuell, C. Longo, E. W. Boyer and E. Brush, *Ann. Emergency Med.*, 2012, **59**, 70–74.
41 M. Chen, X. Dong, H. Deng, F. Ye, Y. Zhao, J. Cheng, G. Dan, J. Zhao, Y. Sai, X. Bian and Z. Zou, *Signal Transduction Targeted Ther.*, 2021, **6**, 29.
42 S. Inturi, N. Tewari-Singh, C. Agarwal, C. W. White and R. Agarwal, *Mutat. Res.*, 2014, **763–764**, 53–63.
43 C. Lage, M. de Pádula, T. A. M. de Alencar, S. R. D. F. Gonçalves, L. D. S. Vidal, J. Cabral-Neto and A. C. Leitão, *Mutat. Res., Rev. Mutat. Res.*, 2003, **544**, 143–157.
44 V. Kumar and E. V. Anslyn, *J. Am. Chem. Soc.*, 2013, **135**, 6338–6344.
45 V. Kumar and E. V. Anslyn, *Chem. Sci.*, 2013, **4**, 4292–4297.
46 V. Kumar and H. Rana, *RSC Adv.*, 2015, **5**, 91946–91950.
47 G. D. Raghavender, A. K. Purohit, V. Tak, D. K. Dubey, P. Kumar and D. Pardasani, *Chem. Commun.*, 2014, **50**, 12363–12366.
48 V. Kumar, H. Rana, G. Raviraju and A. K. Gupta, *Anal. Chem.*, 2018, **90**, 1417–1422.
49 H. Wang, J. Guan, X. Han, S.-W. Chen, T. Li, Y. Zhang, M.-S. Yuan and J. Wang, *Talanta*, 2018, **189**, 39–44.
50 W. Meng, H. Zhang, L. Xiao, X. Chen, M. Sun, Q. Xu, Y. Cao, K. Xiao and Z. Li, *Sens. Actuators, B*, 2019, **296**, 126678.
51 W. Meng, M. Sun, Q. Xu, J. Cen, Y. Cao, Z. Li and K. Xiao, *ACS Sens.*, 2019, **4**, 2794–2801.
52 D. Li, H. Xi, S. Han and S. Zhao, *Anal. Methods*, 2021, **13**, 484–490.
53 W. Feng, H. Li, M. J. Xue, Q. L. Zhang, S. L. Liu and Q. H. Song, *Anal. Chim. Acta*, 2021, **1159**, 338440.
54 M.-J. Xue, X.-Z. Wei, W. Feng, Z.-F. Xing, S.-L. Liu and Q.-H. Song, *J. Hazard. Mater.*, 2021, **416**, 125789.
55 D.-H. Lee, D.-N. Lee and J.-I. Hong, *New J. Chem.*, 2016, **40**, 9021–9024.
56 A. C. Sedgwick, J. T. Brewster, T. Wu, X. Feng, S. D. Bull, X. Qian, J. L. Sessler, T. D. James, E. V. Anslyn and X. Sun, *Chem. Soc. Rev.*, 2021, **50**, 9–38.
57 M. J. Xue, X. Z. Wei, W. Feng, Z. F. Xing, S. L. Liu and Q. H. Song, *J. Hazard. Mater.*, 2021, **416**, 125789.
58 R. Stone, *Science*, 2018, **359**, 23.
59 H. John and H. Thiermann, *J. Mass Spectrom. Adv. Clin. Lab*, 2021, **19**, 20–31.
60 N. Amend, J. Langgartner, M. Siegert, T. Kranawetvogl, M. Koller, H. John, C. Pflügler, C. Mögele-Schmid, F. Worek, H. Thiermann and T. Wille, *Arch. Toxicol.*, 2020, **94**, 2239–2247.
61 Z. Kovarik, N. Maček Hrvat, M. Katalinić, R. K. Sit, A. Paradyse, S. Žunec, K. Musilek, V. V. Fokin, P. Taylor and Z. Radić, *Chem. Res. Toxicol.*, 2015, **28**, 1036–1044.
62 A. Fidder, A. G. Hulst, D. Noort, R. de Ruiter, M. J. van der Schans, H. P. Benschop and J. P. Langenberg, *Chem. Res. Toxicol.*, 2002, **15**, 582–590.
63 V. Aroniadou-Anderjaska, J. P. Apland, T. H. Figueiredo, M. De Araujo Furtado and M. F. Braga, *Neuropharmacology*, 2020, **181**, 108298.
64 A. N. Bigley, C. Xu, T. J. Henderson, S. P. Harvey and F. M. Raushel, *J. Am. Chem. Soc.*, 2013, **135**, 10426–10432.
65 K. A. Van Houten, D. C. Heath and R. S. Pilato, *J. Am. Chem. Soc.*, 1998, **120**, 12359–12360.
66 E. P. Lloyd, R. S. Pilato and K. A. Van Houten, *ACS Omega*, 2018, **3**, 16028–16034.
67 S. W. Zhang and T. M. Swager, *J. Am. Chem. Soc.*, 2003, **125**, 3420–3421.
68 T. J. Dale and J. Rebek, *J. Am. Chem. Soc.*, 2006, **128**, 4500–4501.
69 R. Gotor, A. M. Costero, P. Gaviña and S. Gil, *Dyes Pigm.*, 2014, **108**, 76–83.
70 R. Gotor, P. Gaviña, L. E. Ochando, K. Chulvi, A. Lorente, R. Martínez-Máñez and A. M. Costero, *RSC Adv.*, 2014, **4**, 15975–15982.
71 A. Barba-Bon, A. M. Costero, S. Gil, A. Harriman and F. Sancenon, *Chem. – Eur. J.*, 2014, **20**, 6339–6347.
72 Z. Wu, X. Wu, Y. Yang, T. B. Wen and S. Han, *Bioorg. Med. Chem. Lett.*, 2012, **22**, 6358–6361.
73 X. Wu, Z. Wu and S. Han, *Chem. Commun.*, 2011, **47**, 11468–11470.
74 S. Han, Z. Xue, Z. Wang and T. B. Wen, *Chem. Commun.*, 2010, **46**, 8413–8415.
75 G. Heo, R. Manivannan, H. Kim and Y.-A. Son, *Dyes Pigm.*, 2019, **171**, 107712.
76 H. S. Sarkar, A. Ghosh, S. Das, P. K. Maiti, S. Maitra, S. Mandal and P. Sahoo, *Sci. Rep.*, 2018, **8**, 3402.
77 S. S. Li, Y. C. Zheng, W. Q. Chen, M. L. Zheng, H. Zheng, Z. Zhang, Y. Cui, J. Y. Zhong and C. L. Zhao, *Molecules*, 2019, **24**, 827.
78 Y. J. Jang, S. V. Mulay, Y. Kim, P. Jorayev and D. G. Churchill, *New J. Chem.*, 2017, **41**, 1653–1658.
79 X. X. Hu, Y. T. Su, Y. W. Ma, X. Q. Zhan, H. Zheng and Y. B. Jiang, *Chem. Commun.*, 2015, **51**, 15118–15121.
80 Z. Lei and Y. Yang, *J. Am. Chem. Soc.*, 2014, **136**, 6594–6597.
81 A. K. Mahapatra, K. Maiti, S. K. Manna, R. Maji, S. Mondal, C. Das Mukhopadhyay, P. Sahoo and D. Mandal, *Chem. Commun.*, 2015, **51**, 9729–9732.
82 S. S. Ali, A. Gangopadhyay, K. Maiti, S. Mondal, A. K. Pramanik, U. N. Guria, M. R. Uddin, S. Mandal, D. Mandal and A. K. Mahapatra, *Org. Biomol. Chem.*, 2017, **15**, 5959–5967.
83 S. S. Ali, A. Gangopadhyay, A. K. Pramanik, S. K. Samanta, U. N. Guria, S. Manna and A. K. Mahapatra, *Analyst*, 2018, **143**, 4171–4179.
84 R. Puglisi, A. Pappalardo, A. Gulino and G. T. Sfrazzetto, *ACS Omega*, 2019, **4**, 7550–7555.
85 H. Liu, Y. Y. Fu, A. Liu, Y. G. Yu, Q. G. He, H. M. Cao and J. G. Cheng, *Anal. Methods*, 2018, **10**, 1709–1714.
86 T. I. Kim, S. B. Maity, J. Bouffard and Y. Kim, *Anal. Chem.*, 2016, **88**, 9259–9263.
87 Z. L. Lu, W. L. Fan, X. M. Shi, C. A. Black, C. H. Fan and F. F. Wang, *Sens. Actuators, B*, 2018, **255**, 176–182.
88 W. Xuan, Y. Cao, J. Zhou and W. Wang, *Chem. Commun.*, 2013, **49**, 10474–10476.

89 L. Wu, C. Huang, B. P. Emery, A. C. Sedgwick, S. D. Bull, X. P. He, H. Tian, J. Yoon, J. L. Sessler and T. D. James, *Chem. Soc. Rev.*, 2020, **49**, 5110–5139.
90 Y. Jung and D. Kim, *Materials*, 2019, **12**, 2943.
91 S. Kundu, S. Saha and P. Sahoo, *Results Chem.*, 2019, **1**, 100014.
92 X. Hu, H. Zeng, T. Chen, H.-Q. Yuan, L. Zeng and G.-M. Bao, *Sens. Actuators, B*, 2020, **319**, 128282–128287.
93 X. Feng, Y. Wang, W. Feng and Y. Peng, *Chin. Chem. Lett.*, 2020, **31**, 2960–2964.
94 F. W. Dagnaw, W. Feng and Q.-H. Song, *Sens. Actuators, B*, 2020, **318**, 127937.
95 S. Zhang, C. Zhou, B. Yang, Y. Zhao, L. Wang, B. Yuan and H. Li, *New J. Chem.*, 2021, **45**, 7564–7570.
96 K. J. Wallace, J. Morey, V. M. Lynch and E. V. Anslyn, *New J. Chem.*, 2005, **29**, 1469–1474.
97 K. J. Wallace, R. I. Fagbemi, F. J. Folmer-Andersen, J. Morey, V. M. Lynth and E. V. Anslyn, *Chem. Commun.*, 2006, 3886–3888, DOI: **10.1039/B609861D**.
98 H. S. Hewage, K. J. Wallace and E. V. Anslyn, *Chem. Commun.*, 2007, 3909–3911, DOI: **10.1039/B706624D**.
99 T. J. Dale and J. Rebek, *Angew. Chem., Int. Ed.*, 2009, **48**, 7850–7852.
100 C. K. Maurya, U. Pathak and P. K. Gupta, *Anal. Bioanal. Chem.*, 2021, **413**, 4501–4509.
101 S. S. Ali, A. Gangopadhyay, A. K. Pramanik, U. N. Guria, S. K. Samanta and A. K. Mahapatra, *Dyes Pigm.*, 2019, **170**, 107585.
102 B. L. Huo, M. Du, A. Shen, M. W. Li, Y. R. Lai, X. Bai, A. J. Gong and Y. X. Yang, *Anal. Chem.*, 2019, **91**, 10979–10983.
103 Y. J. Jang, O. G. Tsay, D. P. Murale, J. A. Jeong, A. Segev and D. G. Churchill, *Chem. Commun.*, 2014, **50**, 7531–7534.
104 Y. Kim, Y. J. Jang, S. V. Mulay, T. T. T. Nguyen and D. G. Churchill, *Chem. – Eur. J.*, 2017, **23**, 7785–7790.
105 H. Lee and H. J. Kim, *Tetrahedron*, 2014, **70**, 2966–2970.
106 J. Y. Lee, Y. H. Lee and Y. G. Byun, *Phosphorus, Sulfur Silicon Relat. Elem.*, 2012, **187**, 641–649.
107 Y. C. Cai, C. Li and Q. H. Song, *J. Mater. Chem. C*, 2017, **5**, 7337–7343.
108 T. Y. Qin, Y. Y. Huang, K. N. Zhu, J. H. Wang, C. J. Pan, B. Liu and L. Wang, *Anal. Chim. Acta*, 2019, **1076**, 125–130.
109 L. Chen, H. Oh, D. Wu, M. H. Kim and J. Yoon, *Chem. Commun.*, 2018, **54**, 2276–2279.
110 S.-S. Li, Y.-C. Zheng, X.-M. Zhu, H.-B. Wang, L.-H. Liang, X.-Z. Wang, L. Yuan, F.-H. Zhang, H. Zheng and C.-L. Zhao, *Sens. Actuators, B*, 2021, **337**, 129804–129812.
111 M. S. J. Khan, Y. W. Wang, M. O. Senge and Y. Peng, *J. Hazard. Mater.*, 2018, **342**, 10–19.
112 L. Patra, P. Ghosh, S. Das, S. Gharami, N. Murmu and T. K. Mondal, *J. Photochem. Photobiol., A*, 2020, **388**, 112188.
113 S. Royo, A. M. Costero, M. Parra, S. Gil, R. Martínez-Máñez and F. Sancenon, *Chem. – Eur. J.*, 2011, **17**, 6931–6934.
114 H. Xu, H. Zhang, L. Zhao, C. Peng, G. Liu and T. Cheng, *New J. Chem.*, 2020, **44**, 10713–10718.
115 B. D. Diaz de Greñu, D. Moreno, T. Torroba, A. Berg, J. Gunnars, T. Nilsson, R. Nyman, M. Persson, J. Pettersson, I. Eklind and P. Wästerby, *J. Am. Chem. Soc.*, 2014, **136**, 4125–4128.
116 C. Sun, W. Xiong, W. Ye, Y. Zheng, R. Duan, Y. Che and J. Zhao, *Anal. Chem.*, 2018, **90**, 7131–7134.
117 S. Gharami, K. Aich, S. Das, L. Patra and T. K. Mondal, *New J. Chem.*, 2019, **43**, 8627–8633.
118 J. Yao, Y. Fu, W. Xu, T. Fan, Y. Gao, Q. He, D. Zhu, H. Cao and J. Cheng, *Anal. Chem.*, 2016, **88**, 2497–2501.
119 A. C. Sedgwick, K. C. Yan, D. N. Mangel, Y. Shang, A. Steinbrueck, H. H. Han, J. T. Brewster, 2nd, X. L. Hu, D. W. Snelson, V. M. Lynch, H. Tian, X. P. He and J. L. Sessler, *J. Am. Chem. Soc.*, 2021, **143**, 1278–1283.
120 J. Li, J. Wang, H. Li, N. Song, D. Wang and B. Z. Tang, *Chem. Soc. Rev.*, 2020, **49**, 1144–1172.
121 S. Huang, Y. Wu, F. Zeng, L. Sun and S. Wu, *J. Mater. Chem. C*, 2016, **4**, 10105–10110.
122 Y. Kim, Y. J. Jang, D. Lee, B. S. Kim and D. G. Churchill, *Sens. Actuators, B*, 2017, **238**, 145–149.
123 Y. C. Cai, C. Li and Q. H. Song, *ACS Sens.*, 2017, **2**, 834–841.
124 L. Yao, S. Zhang, R. Wang, W. Li, F. Shen, B. Yang and Y. Ma, *Angew. Chem., Int. Ed.*, 2014, **53**, 2119–2123.
125 X. B. Li, Y. N. Lv, S. Y. Chang, H. Q. Liu, W. Q. Mo, H. W. Ma, C. J. Zhou, S. T. Zhang and B. Yang, *Anal. Chem.*, 2019, **91**, 10927–10931.
126 C. Yan, Z. Guo, W. Chi, W. Fu, S. A. A. Abedi, X. Liu, H. Tian and W.-H. Zhu, *Nat. Commun.*, 2021, **12**, 3869.
127 S. Goswami, A. Manna and S. Paul, *RSC Adv.*, 2014, **4**, 21984–21988.
128 M. Gupta and H. I. Lee, *Sens. Actuators, B*, 2017, **242**, 977–982.
129 Y. Y. Fu, J. P. Yu, K. X. Wang, H. Liu, Y. G. Yu, A. Liu, X. Peng, Q. G. He, H. M. Cao and J. G. Cheng, *ACS Sens.*, 2018, **3**, 1445–1450.
130 M. Sathiyaraj and V. Thiagarajan, *RSC Adv.*, 2020, **10**, 25848–25855.
131 P. Zheng, Z. Cui, H. Liu, W. Cao, F. Li and M. Zhang, *J. Hazard. Mater.*, 2021, **415**, 125619.
132 D. Knapton, M. Burnworth, S. J. Rowan and C. Weder, *Angew. Chem., Int. Ed.*, 2006, **45**, 5825–5829.
133 S. Sarkar, A. Mondal, A. K. Tiwari and R. Shunmugam, *Chem. Commun.*, 2012, **48**, 4223–4225.
134 A. Barba-Bon, A. M. Costero, S. Gil, F. Sancenón and R. Martínez-Máñez, *Chem. Commun.*, 2014, **50**, 13289–13291.
135 L. Ordronneau, A. Carella, M. Pohanka and J. P. Simonato, *Chem. Commun.*, 2013, **49**, 8946–8948.
136 K. Gupta and A. K. Patra, *ACS Sens.*, 2020, **5**, 1268–1272.
137 W. A. Maza, C. M. Vetromile, C. Kim, X. Xu, X. P. Zhang and R. W. Larsen, *J. Phys. Chem. A*, 2013, **117**, 11308–11315.
138 S. K. Sheet, B. Sen and S. Khatua, *Inorg. Chem.*, 2019, **58**, 3635–3645.
139 P. Raj and N. Singh, *Chemistryselect*, 2017, **2**, 4725–4732.
140 N. Singh, K. Kumar, N. Srivastav, R. Singh, V. Kaur, J. P. Jasinski and R. J. Butcher, *New J. Chem.*, 2018, **42**, 8756–8764.
141 X. Sun, D. Shabat, S. T. Phillips and E. V. Anslyn, *J. Phys. Org. Chem.*, 2018, **31**, e3827.

142 V. Kumar and H. Rana, *Chem. Commun.*, 2015, **51**, 16490–16493.
143 X. Sun, J. F. Reuther, S. T. Phillips and E. V. Anslyn, *Chem. -- Eur. J.*, 2017, **23**, 3903–3909.
144 X. Sun, S. Dahlhauser and E. V. Anslyn, *J. Am. Chem. Soc.*, 2017, **139**, 4635–4638.
145 X. Sun and E. V. Anslyn, *Angew. Chem., Int. Ed.*, 2017, **56**, 9522–9526.
146 X. L. Sun, A. A. Boulgakov, L. N. Smith, P. Metola, E. M. Marcotte and E. V. Anslyn, *ACS Cent. Sci.*, 2018, **4**, 854–861.
147 D. H. Lee, S. A. Valenzuela, M. N. Dominguez, M. Otsuka, D. J. Milliron and E. V. Anslyn, *Cell Rep. Phys. Sci.*, 2021, **2**, 100552.
148 W. Weihui, S. Shaohui, L. Jian, Z. Liang, L. Dan, X. Yanhua, W. Lianyuan, Z. Haiyan, S. Yonglin and J. Zhigang, *Analyst*, 2020, **145**, 5425–5429.
149 H. Xu, H. Zhang, C. Wang, K. Chen, G. Liu, C. Tan and T. Cheng, *Dyes Pigm.*, 2021, **186**, 109007.
150 A. K. Das, S. Goswami, C. K. Quah and H. K. Fun, *RSC Adv.*, 2016, **6**, 18711–18717.
151 T. Zellner and F. Eyer, *Toxicol. Lett.*, 2020, **320**, 73–79.
152 G. J. Fitzgerald, *Am. J. Public Health*, 2008, **98**, 611–625.
153 X. Zhou, Y. Zeng, C. Liyan, X. Wu and J. Yoon, *Angew. Chem., Int. Ed.*, 2016, **55**, 4729–4733.
154 L. T. Zeng, H. Y. Zeng, L. R. Jiang, S. Wang, J. T. Hou and J. Yoon, *Anal. Chem.*, 2019, **91**, 12070–12076.
155 Y. Hu, L. Chen, H. Jung, Y. Y. Zeng, S. Lee, K. M. K. Swamy, X. Zhou, M. H. Kim and J. Yoon, *ACS Appl. Mater. Interfaces*, 2016, **8**, 22246–22252.
156 H. C. Xia, X. H. Xu and Q. H. Song, *ACS Sens.*, 2017, **2**, 178–182.
157 H.-C. Xia, X.-H. Xu and Q.-H. Song, *Anal. Chem.*, 2017, **89**, 4192–4197.
158 S.-L. Wang, L. Zhong and Q.-H. Song, *Chem. Commun.*, 2017, **53**, 1530–1533.
159 H. Xie, Y. Wu, F. Zeng, J. Chen and S. Wu, *Chem. Commun.*, 2017, **53**, 9813–9816.
160 H. Zhang and D. M. Rudkevich, *Chem. Commun.*, 2007, 1238–1239, DOI: **10.1039/b614725a**.
161 L. Chen, D. Wu, J.-M. Kim and J. Yoon, *Anal. Chem.*, 2017, **89**, 12596–12601.
162 Y. Hu, X. Zhou, H. Jung, S. J. Nam, M. H. Kim and J. Yoon, *Anal. Chem.*, 2018, **90**, 3382–3386.
163 X. Wu, Z. Wu, Y. Yang and S. Han, *Chem. Commun.*, 2012, **48**, 1895–1897.
164 Y. Zhang, A. Peng, X. Jie, Y. Lv, X. Wang and Z. Tian, *ACS Appl. Mater. Interfaces*, 2017, **9**, 13920–13927.
165 P. L. Liu, N. Liu, C. L. Liu, Y. M. Jia, L. P. Huang, G. H. Zhou, C. P. Li and S. Wang, *Dyes Pigm.*, 2019, **163**, 489–495.
166 W.-Q. Zhang, K. Cheng, X. Yang, Q.-Y. Li, H. Zhang, Z. Ma, H. Lu, H. Wu and X.-J. Wang, *Org. Chem. Front.*, 2017, **4**, 1719–1725.
167 S. L. Wang, L. Zhong and Q. H. Song, *Chem. – Eur. J.*, 2018, **24**, 5652–5658.
168 W. Feng, S. Gong, E. Zhou, X. Yin and G. Feng, *Anal. Chim. Acta*, 2018, **1029**, 97–103.
169 W. Zhou, Q. Chen, A. Wu, Y. Zhang and W. Yu, *J. Chin. Chem. Soc.*, 2020, **67**, 1213–1218.
170 K. Cheng, N. Yang, Q.-Y. Li, X.-W. Gao and X.-J. Wang, *ACS Omega*, 2019, **4**, 22557–22561.
171 Q. Hu, Q. Huang, K. Liang, Y. Wang, Y. Mao, Q. Yin and H. Wang, *Dyes Pigm.*, 2020, **176**, 108229.
172 L. Yang, F. Wang, Z. Sun, X. Kong and Y. Kong, *Anal. Methods*, 2020, **12**, 3123–3129.
173 F. Zeng, G. Bao, B. Zhou and Y. Han, *New J. Chem.*, 2021, **45**, 5631–5636.
174 L. Yang, F. Wang, J. Zhao, X. Kong, K. Lu, M. Yang, J. Zhang, Z. Sun and J. You, *Talanta*, 2021, **221**, 121477.
175 L. Patra, K. Aich, S. Gharami and T. K. Mondal, *Sens. Actuators, B*, 2021, **326**, 128837.
176 Z. Guo, C. Yan and W. H. Zhu, *Angew. Chem., Int. Ed.*, 2020, **59**, 9812–9825.
177 Q. Hu, T. Gong, Y. Mao, Q. Yin, Y. Wang and H. Wang, *Spectrochim. Acta, Part A*, 2021, **253**, 119589.
178 M. Sayar, E. Karakus, T. Guner, B. Yildiz, U. H. Yildiz and M. Emrullahoglu, *Chem. – Eur. J.*, 2018, **24**, 3136–3140.
179 T. Cao, D. Gong, L. Zheng, J. Wang, J. Qian, W. Liu, Y. Cao, K. Iqbal, W. Qin and A. Iqbal, *Anal. Chim. Acta*, 2019, **1078**, 168–175.
180 S.-L. Wang, C.-L. Zhang and Q.-H. Song, *J. Mater. Chem. C*, 2019, **7**, 1510–1517.
181 J. Tan, Z. Li, W. Yao, Z. Ji, Z. Sun and J. You, *Dyes Pigm.*, 2021, **187**, 109138.
182 L. Yang, Z. Sun, Z. Li, X. Kong, F. Wang, X. Liu, J. Tang, M. Ping and J. You, *Anal. Methods*, 2019, **11**, 4600–4608.
183 A. Gangopadhyay and A. K. Mahapatra, *New J. Chem.*, 2019, **43**, 14991–14996.
184 P. Kundu and K. C. Hwang, *Anal. Chem.*, 2012, **84**, 4594–4597.
185 Q. Hu, C. Duan, J. Wu, D. Su, L. Zeng and R. Sheng, *Anal. Chem.*, 2018, **90**, 8686–8691.
186 C. Wu, H. Xu, Y. Li, R. Xie, P. Li, X. Pang, Z. Zhou, B. Gu, H. Li and Y. Zhang, *Talanta*, 2019, **200**, 78–83.
187 A. Gangopadhyay and A. K. Mahapatra, *New J. Chem.*, 2019, **43**, 11743–11748.
188 L. Zeng, H. Zeng, S. Wang, S. Wang, J.-T. Hou and J. Yoon, *Chem. Commun.*, 2019, **55**, 13753–13756.
189 S. Wang, B. Zhu, B. Wang, P. Fan, Y. Jiu, M. Zhang, L. Jiang and J.-T. Hou, *Dyes Pigm.*, 2020, **173**, 107933.
190 T. Chen, L. Jiang, J.-T. Hou, W. Wang, L. Zeng and G.-M. Bao, *J. Mater. Chem. A*, 2020, **8**, 24695–24702.
191 Z.-J. Li, W.-J. Zhang, W.-Z. Bi, Q.-J. Ma, S.-X. Feng, X.-L. Chen and L.-B. Qu, *RSC Adv.*, 2021, **11**, 10836–10841.
192 T.-I. Kim, D. Kim, J. Bouffard and Y. Kim, *Sens. Actuators, B*, 2019, **283**, 458–462.
193 X. Z. Wei, Y. L. Fu, M. J. Xue and Q. H. Song, *Org. Lett.*, 2019, **21**, 9497–9501.
194 M. Du, B. Huo, J. Liu, M. Li, A. Shen, X. Bai, Y. Lai, L. Fang and Y. Yang, *J. Mater. Chem. C*, 2018, **6**, 10472–10479.
195 A. Gangopadhyay, S. S. Ali and A. K. Mahapatra, *Chemistryselect*, 2019, **4**, 8968–8972.
196 T.-I. Kim, B. Hwang, J. Bouffard and Y. Kim, *Anal. Chem.*, 2017, **89**, 12837–12842.

197 L. Bai, W. Feng and G. Feng, *Dyes Pigm.*, 2019, **163**, 483–488.
198 A. C. Sedgwick, L. Wu, H.-H. Han, S. D. Bull, X.-P. He, T. D. James, J. L. Sessler, B. Z. Tang, H. Tian and J. Yoon, *Chem. Soc. Rev.*, 2018, **47**, 8842–8880.
199 K. Maiti, D. Ghosh, R. Maiti, V. Vyas, P. Datta, D. Mandal and D. K. Maiti, *J. Mater. Chem. A*, 2019, **7**, 1756–1767.
200 B. Ma, X. Wang, S. Gao, L. Qi, Y. Xu, J. Yang and G. Zuo, *Dyes Pigm.*, 2020, **177**, 108279.
201 S. Paul, P. Ghosh and P. Roy, *New J. Chem.*, 2020, **44**, 5784–5791.
202 Y.-L. Huang, W. Ye, Y.-T. Su, Z.-Y. Wu and H. Zheng, *Dyes Pigm.*, 2020, **173**, 107854.
203 J. Zhu, X. Mu, S. Zhang, L. Yan and X. Wu, *Spectrochim. Acta, Part A*, 2021, **251**, 119485.
204 J. P. Collman, R. Boulatov, C. J. Sunderland and L. Fu, *Chem. Rev.*, 2004, **104**, 561–588.
205 F. M. Henretig, M. A. Kirk and C. A. McKay, Jr, *N. Engl. J. Med.*, 2019, **380**, 1638–1655.
206 V. M. Luque-Almagro, C. Moreno-Vivian and M. D. Roldan, *Curr. Opin. Biotechnol.*, 2016, **38**, 9–13.
207 L. Long, M. Huang, N. Wang, Y. Wu, K. Wang, A. Gong, Z. Zhang and J. L. Sessler, *J. Am. Chem. Soc.*, 2018, **140**, 1870–1875.
208 W. Sun, S. Guo, C. Hu, J. Fan and X. Peng, *Chem. Rev.*, 2016, **116**, 7768–7817.
209 M. Tomasulo and F. M. Raymo, *Org. Lett.*, 2005, **7**, 4633–4636.
210 M. Tomasulo, S. Sortino, A. J. P. White and F. M. Raymo, *J. Org. Chem.*, 2006, **71**, 744–753.
211 S. Pattaweepaiboon, W. Kongmon, T. Thaweechai, N. Kaewchangwat, E. Thanayupong, K. Suttisintong and W. Sirisaksoontorn, *Dyes Pigm.*, 2020, **173**, 108005.
212 N. Maurya and A. K. Singh, *Inorg. Chim. Acta*, 2020, **499**, 119156.
213 Z. M. Dong, H. Ren, J. N. Wang, J. B. Chao and Y. Wang, *Spectrochim. Acta, Part A*, 2019, **217**, 27–34.
214 L. Zhu, J. Nie, Q. Li, J. Du, X. Fan, F. Bai, Q. Yang, Y. Shan and Y. Li, *J. Lumin.*, 2019, **215**, 116620.
215 H. Pan, Y. J. Liu, S. Z. Liu, Z. P. Ou, H. B. Chen and H. M. Li, *Talanta*, 2019, **202**, 329–335.
216 L. Li, M. H. Zan, X. W. Qie, P. Miao, J. Yue, Z. M. Chang, Z. Wang, F. Q. Bai, H. X. Zhang, J. K. Ferri and W. F. Dong, *Talanta*, 2018, **185**, 1–6.
217 M. J. Peng, Y. Guo, X. F. Yang, L. Y. Wang and J. An, *Dyes Pigm.*, 2013, **98**, 327–332.
218 M. Sun, S. Wang, Q. Yang, X. Fei, Y. Li and Y. Li, *RSC Adv.*, 2014, **4**, 8295–8299.
219 Y. Wang, J. Wang and Q. Xian, *Talanta*, 2018, **190**, 487–491.
220 L. Hou, F. Li, J. Guo, X. Zhang, X. Kong, X. T. Cui, C. Dong, Y. Wang and S. Shuang, *J. Mater. Chem. B*, 2019, **7**, 4620–4629.
221 B. Zhai, Z. Hu, C. Peng, B. Liu, W. Li and C. Gao, *Spectrochim. Acta, Part A*, 2020, **224**, 117409.
222 S. Erdemir and S. Malkondu, *Talanta*, 2021, **221**, 121639.
223 L. Long, Y. Han, X. Yuan, S. Cao, W. Liu, Q. Chen, K. Wang and Z. Han, *Food Chem.*, 2020, **331**, 127359.
224 P. S. Kumar, P. R. Lakshmi and K. P. Elango, *Spectrochim. Acta, Part A*, 2019, **221**, 117172.
225 J. M. Jung, D. Yun, H. Lee, K.-T. Kim and C. Kim, *Sens. Actuators, B*, 2019, **297**, 126814.
226 S. T. Wang, Y. W. Sie, C. F. Wan and A. T. Wu, *J. Lumin.*, 2016, **173**, 25–29.
227 L. Wan, Q. H. Shu, J. P. Zhu, S. H. Jin, N. Li, X. Chen and S. S. Chen, *Talanta*, 2016, **152**, 39–44.
228 W.-J. Qu, T.-B. Wei, Q. Lin, W.-T. Li, J.-X. Su, G.-Y. Liang and Y.-M. Zhang, *Sens. Actuators, B*, 2016, **232**, 115–124.
229 Q. Wu, S. Wang, E. Hao and L. Jiao, *Spectrochim. Acta, Part A*, 2021, **247**, 119102.
230 Y. Wu, W.-M. Ding, J. Li, G. Guo, S.-Z. Zhang, H.-R. Jia and Y.-X. Sun, *J. Fluoresc.*, 2021, **31**, 437–446.
231 M. S. Kim, D. Yun, J. B. Chae, H. So, H. Lee, K.-T. Kim, M. Kim, M. H. Lim and C. Kim, *Sensors*, 2019, **19**, 5458.
232 S.-J. Hong, J. Yoo, S.-H. Kim, J. S. Kim, J. Yoon and C.-H. Lee, *Chem. Commun.*, 2009, 189–191, DOI: **10.1039/b815326d**.
233 C. H. Lee, H. J. Yoon, J. S. Shim and W. D. Jang, *Chem. – Eur. J.*, 2012, **18**, 4513–4516.
234 Y. Zhang, D. Li, Y. Li and J. Yu, *Chem. Sci.*, 2014, **5**, 2710–2716.
235 W. Chen, Z. Zhang, X. Li, H. Agren and J. Su, *RSC Adv.*, 2015, **5**, 12191–12201.
236 Y. X. Hua, Y. L. Shao, Y. W. Wang and Y. Peng, *J. Org. Chem.*, 2017, **82**, 6259–6267.
237 Q. Niu, L. Lan, T. Li, Z. Guo, T. Jiang, Z. Zhao, Z. Feng and J. Xi, *Sens. Actuators, B*, 2018, **276**, 13–22.
238 S. Suganya, E. Ravindran, M. K. Mahato and E. Prasad, *Sens. Actuators, B*, 2019, **291**, 426–432.
239 K. Deng, L. Wang, Q. Xia, R. Liu and J. Qu, *Sens. Actuators, B*, 2019, **296**, 126645.
240 B. Aydiner, *J. Photochem. Photobiol., A*, 2019, **382**, 111916.
241 S. Mu, H. Gao, C. Li, S. Li, Y. Wang, Y. Zhang, C. Ma, H. Zhang and X. Liu, *Talanta*, 2021, **221**, 121606.
242 W.-C. Lin, S.-K. Fang, J.-W. Hu, H.-Y. Tsai and K.-Y. Chen, *Anal. Chem.*, 2014, **86**, 4648–4652.
243 Y.-D. Lin, Y.-S. Peng, W. Su, C.-H. Tu, C.-H. Sun and T. J. Chow, *Tetrahedron*, 2012, **68**, 2523–2526.
244 G.-L. Fu and C.-H. Zhao, *Tetrahedron*, 2013, **69**, 1700–1704.
245 Y. Qu, B. Jin, Y. Liu, Y. Wu, L. Yang, J. Wu and J. Hua, *Tetrahedron Lett.*, 2013, **54**, 4942–4944.
246 Z. Liu, X. Wang, Z. Yang and W. He, *J. Org. Chem.*, 2011, **76**, 10286–10290.
247 P. B. Pati and S. S. Zade, *RSC Adv.*, 2013, **3**, 13457–13462.
248 S. Park and H. J. Kim, *Chem. Commun.*, 2010, **46**, 9197–9199.
249 L. Yuan, W. Y. Lin, Y. T. Yang, J. Z. Song and J. L. Wang, *Org. Lett.*, 2011, **13**, 3730–3733.
250 Y. Sun, Y. Wang, D. Cao, H. Chen, Z. Liu and Q. Fang, *Sens. Actuators, B*, 2012, **174**, 500–505.
251 H. Lee and H.-J. Kim, *Tetrahedron Lett.*, 2012, **53**, 5455–5457.
252 Q. Zou, F. Tao, Z. Xu, Y. Ding, Y. Tian and Y. Cui, *Anal. Methods*, 2019, **11**, 5553–5561.

253 Y. Zhu, K. Wang, W. Song, B. Dong, S. Zhao, R. Guan, Z. Li, Y. Sun, D. Cao and W. Lin, *Sens. Actuators, B*, 2019, **294**, 283–290.
254 T. Gomez, D. Moreno, B. D. de Grenu, A. C. Fernandez, T. Rodriguez, J. Rojo, J. V. Cuevas and T. Torroba, *Chem. – Asian J.*, 2013, **8**, 1271–1278.
255 J. Chao, Z. Li, Y. Zhang, F. Huo, C. Yin, Y. Liu, Y. Li and J. Wang, *J. Mater. Chem. B*, 2016, **4**, 3703–3712.
256 S. Erdemir and S. Malkondu, *Talanta*, 2020, **207**, 120278.
257 N. Assadollahnejad, M. Kargar, H. R. Darabi, N. Abouali, S. Jamshidi, A. Sharifi, K. Aghapoor and H. Sayahi, *New J. Chem.*, 2019, **43**, 13001–13009.
258 P. Anand, A. B. Kunnumakkara, R. A. Newman and B. B. Aggarwal, *Mol. Pharm.*, 2007, **4**, 807–818.
259 Y. M. Hijji, A. G. Elsafy, H. S. Al-Easa, B. Attili, M. Abdelrasoul, N. Mohamed and G. K. Nasrallah, *Anal. Methods*, 2019, **11**, 5169–5176.
260 S. Malkondu, S. Erdemir and S. Karakurt, *Dyes Pigm.*, 2020, **174**, 108019.
261 C. Nandhini, P. S. Kumar, K. Poongodi, R. Shanmugapriya and K. P. Elango, *J. Mol. Liq.*, 2021, **327**, 114833.
262 C. L. Chen, Y. H. Chen, C. Y. Chen and S. S. Sun, *Org. Lett.*, 2006, **8**, 5053–5056.
263 H.-T. Niu, D. Su, X. Jiang, W. Yang, Z. Yin, J. He and J.-P. Cheng, *Org. Biomol. Chem.*, 2008, **6**, 3038–3040.
264 H.-T. Niu, X. Jiang, J. He and J.-P. Cheng, *Tetrahedron Lett.*, 2008, **49**, 6521–6524.
265 Z. Ekmekci, M. D. Yilmaz and E. U. Akkaya, *Org. Lett.*, 2008, **10**, 461–464.
266 X. Lv, J. Liu, Y. L. Liu, Y. Zhao, M. L. Chen, P. Wang and W. Guo, *Sens. Actuators, B*, 2011, **158**, 405–410.
267 Y. Hao, N. Khac Hong, Y. Zhang, G. Zhang, S. Fan, F. Li, C. Guo, Y. Lu, X. Song, P. Qu, Y.-N. Liu and M. Xu, *Talanta*, 2018, **176**, 234–241.
268 Y. H. Jeong, C. H. Lee and W. D. Jang, *Chem. – Asian J.*, 2012, **7**, 1562–1566.
269 B.-B. Wang, Y. Wang, W.-N. Wu, Z.-H. Xu, X.-L. Zhao, Z.-Q. Xu and Y.-C. Fan, *Inorg. Chem. Commun.*, 2020, **122**, 108245.
270 K. S. Lee, H. J. Kim, G. H. Kim, I. Shin and J. I. Hong, *Org. Lett.*, 2008, **10**, 49–51.
271 S. K. Kwon, S. Kou, H. N. Kim, X. Chen, H. Hwang, S.-W. Nam, S. H. Kim, K. M. K. Swamy, S. Park and J. Yoon, *Tetrahedron Lett.*, 2008, **49**, 4102–4105.
272 P. B. Pati and S. S. Zade, *Eur. J. Org. Chem.*, 2012, 6555–6561.
273 J. Jo, A. Olasz, C. H. Chen and D. Lee, *J. Am. Chem. Soc.*, 2013, **135**, 3620–3632.
274 S. Goswami, A. Manna, S. Paul, A. K. Das, K. Aich and P. K. Nandi, *Chem. Commun.*, 2013, **49**, 2912–2914.
275 M. K. Bera, C. Chakraborty, P. K. Singh, C. Sahu, K. Sen, S. Maji, A. K. Das and S. Malik, *J. Mater. Chem. B*, 2014, **2**, 4733–4739.
276 J. H. Lee, J. H. Jang, N. Velusamy, H. S. Jung, S. Bhuniya and J. S. Kim, *Chem. Commun.*, 2015, **51**, 7709–7712.
277 R. Sukato, N. Sangpetch, T. Palaga, S. Jantra, V. Vchirawongkwin, C. Jongwohan, M. Sukwattanasinitt and S. Wacharasindhu, *J. Hazard. Mater.*, 2016, **314**, 277–285.
278 L. Wang, L. Li and D. Cao, *Sens. Actuators, B*, 2016, **228**, 347–359.
279 Y. Kim, H. S. Huh, M. H. Lee, I. L. Lenov, H. Y. Zhao and F. P. Gabbai, *Chem. – Eur. J.*, 2011, **17**, 2057–2062.
280 A. Dvivedi, S. Kumar and M. Ravikanth, *Sens. Actuators, B*, 2016, **224**, 364–371.
281 F. Wu, H. Liu, C. Zhong and L. Zhu, *Tetrahedron Lett.*, 2016, **57**, 5120–5123.
282 C. Fu, Z. Wang, C. Rao, Z. Li, L. Chen, T. Zhu, F. Yi, Z.-J. Yao and C. Liu, *Dyes Pigm.*, 2019, **170**, 107598.
283 X. Chen, S.-W. Nam, G.-H. Kim, N. Song, Y. Jeong, I. Shin, S. K. Kim, J. Kim, S. Park and J. Yoon, *Chem. Commun.*, 2010, **46**, 8953–8955.
284 F. Zelder and L. Tivana, *Org. Biomol. Chem.*, 2015, **13**, 14–17.
285 L.-Z. Liu, L. Wang, M. Yu, Q. Zhao, Y. Zhang, Y.-X. Sun and W.-K. Dong, *Spectrochim. Acta, Part A*, 2019, **222**, 117209.
286 P. Ravichandiran, A. Boguszewska-Czubara, M. Maslyk, A. P. Bella, P. M. Johnson, S. A. Subramaniyan, K. S. Shim and D. J. Yoo, *Dyes Pigm.*, 2020, **172**, 107828.
287 S. Khoshsoroor, A. Mohammadi, B. Khalili and S. Mohammadi, *J. Photochem. Photobiol., A*, 2020, **388**, 112208.
288 E. J. Hulse, J. D. Haslam, S. R. Emmett and T. Woolley, *Br. J. Anaesth.*, 2019, **123**, 457–463.
289 Y. Zhong, J. Zhan, G. Xu, Y. Chen, Q. Qin, X. Liao, S. Ma, Z. Yang and Y. Cai, *Angew. Chem., Int. Ed.*, 2021, **60**, 8121–8129.
290 J. Chen, D. Liao, Y. Wang, H. Zhou, W. Li and C. Yu, *Org. Lett.*, 2013, **15**, 2132–2135.
291 Y. Wu, Y. Sun, F. Xiao, Z. Wu and R. Yu, *Talanta*, 2017, **162**, 174–179.
292 X. Wang, P. Li, Q. Ding, C. Wu, W. Zhang and B. Tang, *J. Am. Chem. Soc.*, 2019, **141**, 2061–2068.
293 J. Ma, T. Si, C. Yan, Y. Li, Q. Li, X. Lu and Y. Guo, *ACS Sens.*, 2020, **5**, 83–92.
294 N. He, L. Yu, M. Xu, Y. Huang, X. Wang, L. Chen and S. Yue, *J. Mater. Chem. B*, 2021, **9**, 2623–2630.
295 X. Wu, J. M. An, J. Shang, E. Huh, S. Qi, E. Lee, H. Li, G. Kim, H. Ma, M. S. Oh, D. Kim and J. Yoon, *Chem. Sci.*, 2020, **11**, 11285–11292.
296 W. Meng, Z. Pei, Y. Wang, M. Sun, Q. Xu, J. Cen, K. Guo, K. Xiao and Z. Li, *J. Hazard. Mater.*, 2021, **410**, 124811.
297 F. T. Fraunfelder, *BMJ*, 2000, **320**, 458–459.
298 Y. Jung, N. K. Park, S. Kang, Y. Huh, J. Jung, J. K. Hur and D. Kim, *Anal. Chim. Acta*, 2020, **1095**, 154–161.
299 Y. Gong, X. Guo, B. Teng, Q. Zhang, P. Zhang and C. Ding, *Dyes Pigm.*, 2021, **184**, 108859.
300 L. Tu, J. Liu, Z. Zhang, Q. Qi, S. Yao and W. Huang, *Analyst*, 2021, **146**, 2221–2228.
301 Y. L. Jiang and A.-M. Broome, *ACS Sens.*, 2019, **4**, 1791–1797.
302 W. Tuo, J. Bouquet, F. Taran and T. Le Gall, *Chem. Commun.*, 2019, **55**, 8655–8658.
303 F. P. Guengerich, M. R. Waterman and M. Egli, *Trends Pharmacol. Sci.*, 2016, **37**, 625–640.

304 A. Tsoutsoulopoulos, S. Brockmoller, H. Thiermann and D. Steinritz, *Toxicol. Lett.*, 2020, **321**, 69–72.
305 J. P. Gray, V. Mishin, D. E. Heck, D. L. Laskin and J. D. Laskin, *Toxicol. Appl. Pharmacol.*, 2010, **247**, 76–82.
306 F. Pons, J. H. Calvet, M. Haag, V. Raeppel, T. Keravis and N. Frossard, *Pharmacol. Toxicol.*, 2001, **88**, 40–44.
307 A. A. Brimfield, A. M. Mancebo, R. P. Mason, J. J. Jiang, A. G. Siraki and M. J. Novak, *Toxicol. Appl. Pharmacol.*, 2009, **234**, 128–134.
308 Z.-R. Dai, G.-B. Ge, L. Feng, J. Ning, L.-H. Hu, Q. Jin, D.-D. Wang, X. Lv, T.-Y. Dou, J.-N. Cui and L. Yang, *J. Am. Chem. Soc.*, 2015, **137**, 14488–14495.
309 X. Ma, J. R. Idle, K. W. Krausz and F. J. Gonzalez, *Drug Metab. Dispos.*, 2005, **33**, 489–494.
310 X. Zhang, Y. Zhou, X. Gu, Y. Cheng, M. Hong, L. Yan, F. Ma and Z. Qi, *Talanta*, 2018, **186**, 413–420.
311 L. Shangguan, Y. Wei, K. Wang, Y. Zhang and S. Liu, *Anal. Chim. Acta*, 2019, **1046**, 179–184.
312 E. A. Roberts, Z. W. Xie, S. Yang and J. Lipa, *Drug Metab. Dispos.*, 1993, **21**, 56–61.
313 Z.-R. Dai, L. Feng, Q. Jin, H. Cheng, Y. Li, J. Ning, Y. Yu, G.-B. Ge, J.-N. Cui and L. Yang, *Chem. Sci.*, 2017, **8**, 2795–2803.
314 T. Xue, Y. Dai, X. Zhang, Y. Cheng, X. Gu, H. Ji, S. Misal and Z. Qi, *Sens. Actuators, B*, 2019, **293**, 265–272.
315 J. Ning, Z. Tian, B. Wang, G. Ge, Y. An, J. Hou, C. Wang, X. Zhao, Y. Li, X. Tian, Z. Yu, X. Huo, C. Sun, L. Feng, J. Cui and X. Ma, *Mater. Chem. Front.*, 2018, **2**, 2013–2020.
316 H. Ji, X. Zhang, Y. Dai, T. Xue, S. Misal and Z. Qi, *Analyst*, 2019, **144**, 7390–7397.
317 A. B. Renwick, D. F. V. Lewis, S. Fulford, D. Surry, B. Williams, P. D. Worboys, X. Cai, R. W. Wang, R. J. Price, B. G. Lake and D. C. Evans, *Xenobiotica*, 2001, **31**, 187–204.
318 J. N. Lampe, C. Fernandez, A. Nath and W. M. Atkins, *Biochemistry*, 2008, **47**, 509–516.
319 J. Ning, W. Wang, G. Ge, P. Chu, F. Long, Y. Yang, Y. Peng, L. Feng, X. Ma and T. D. James, *Angew. Chem., Int. Ed.*, 2019, **58**, 9959–9963.
320 J. Ning, T. Liu, P. Dong, W. Wang, G. Ge, B. Wang, Z. Yu, L. Shi, X. Tian, X. Huo, L. Feng, C. Wang, C. Sun, J. Cui, T. D. James and X. Ma, *J. Am. Chem. Soc.*, 2019, **141**, 1126–1134.
321 L. J. O'Connor, I. N. Mistry, S. L. Collins, L. K. Folkes, G. Brown, S. J. Conway and E. M. Hammond, *ACS Cent. Sci.*, 2017, **3**, 20–30.
322 S. I. Baskin, I. Petrikovics, G. E. Platoff, G. A. Rockwood and B. A. Logue, *Toxicol. Mech. Methods*, 2006, **16**, 339–345.
323 K. Minakata, H. Nozawa, K. Gonmori, I. Yamagishi, M. Suzuki, K. Hasegawa, K. Watanabe and O. Suzuki, *Anal. Bioanal. Chem.*, 2011, **400**, 1945–1951.
324 C. V. Vinnakota, N. S. Peetha, M. G. Perrizo, D. G. Ferris, R. P. Oda, G. A. Rockwood and B. A. Logue, *Biomarkers*, 2012, **17**, 625–633.
325 A. Banerjee, A. Sahana, S. Lohar, I. Hauli, S. K. Mukhopadhyay, D. A. Safin, M. G. Babashkina, M. Bolte, Y. Garcia and D. Das, *Chem. Commun.*, 2013, **49**, 2527–2529.
326 S. Das, S. Lohar, J. Sanmartin Matalobos and D. Das, *Chin. J. Chem.*, 2015, **33**, 1173–1177.
327 L. Lochman, M. Machacek, M. Miletin, Š. Uhlířová, K. Lang, K. Kirakci, P. Zimcik and V. Novakova, *ACS Sens.*, 2019, **4**, 1552–1559.
328 Y. Ke, Y. Liu, B. Zu, D. Lei, G. Wang, J. Li, W. Ren and X. Dou, *Angew. Chem., Int. Ed.*, 2022, **61**, e202203358.
329 W.-T. Dou, H.-H. Han, A. C. Sedgwick, G.-B. Zhu, Y. Zang, X.-R. Yang, J. Yoon, T. D. James, J. Li and X.-P. He, *Sci. Bull.*, 2022, **67**, 853–878.

